Self-organisation of auxin transport in plant cells

Mathematical modelling of auxin/proton dynamics
at a single cell level

Arno Steinacher

Submitted in partial fulfilment of the requirements for the degree of
Doctor of Philosophy

Department of Computer Science
University of Sheffield
July 2011

Declaration

I declare that this thesis was composed by myself, that the work contained herein is my own except where explicitly stated otherwise in the text. This work has not been submitted for any other degree or professional qualification except as specified.

Arno Steinacher , Sheffield, 20/07/2011

Articles and presentations arising from this thesis

Journal articles

Garnett, P., Steinacher, A., Stepney, S., Clayton, R., and Leyser, O. Computer simulation: the imaginary friend of auxin transport biology. Bioessays 32, 9 (2010), 828-835.

Steinacher, A., Leyser, O., and Clayton, R. A computational model of auxin and pH dynamics in a single plant cell. Journal of Theoretical Biology (accepted).

Conference contributions

Steinacher, A., Clayton, R., and Leyser, O. Modelling self-organisation of polar auxin transport on a single cell level. 2010 GARNet Meeting, Durham (Poster).

Modelling self-organisation of polar auxin transport in plant cells. Second Workshop Dynamical Systems Applied to Biology and Natural Sciences 2011, CMAF, University of Lisboa (Talk)

Abstract

The phytohormone auxin plays a key role in many plant developmental processes. Its polar cell-to-cell transport is linked to and dependent on auxin efflux transporters and their polar localisation in cell membranes. This relies on feedback loops between auxin and its transport on many levels. Hypotheses brought forward in auxin biology, trying to elucidate the nature of these feedbacks, such as the canalisation hypothesis, depend on mechanisms by which auxin transport is established and maintained on specific routes through tissues. Auxin transport canalisation is based on a proposed feedback between auxin flux and auxin transport polarisation, with the result that auxin transport is directed by the strength of auxin fluxes. Despite this phenomenon being well described in biology, its underlying mechanisms are largely unknown. Many of them are occurring at the cell level, justifying a focus on cells in elucidating the nature of this feedback. In this thesis, computational modelling of self-organising mechanisms potentially leading to such phenomena at a cell level has been accomplished. While many auxin transport models are already available at tissue and whole plant scales, such a single cell model is a novel contribution. With the main focus on auxin/proton interactions grounded on the results of biological experiments, a feedback by which auxin influences its own transport by the activation of plasma membrane-bound proton pumps is described. In simulations, it is shown to lead to increased allocation of auxin in cells as well as to enhancement of all auxin transport fluxes over the membrane, and in due course to the establishment of canalisation-type polarisation patterns, without polarised transporter localisation. The results point towards a functional redundancy of polarisation in auxin transport and lead to hypotheses on differential energisation of auxin transporters, which may play a role in auxin transport polarisation events.

Acknowledgements

Even though my declaration that this thesis is my own piece of work holds true, it would definitely not have been possible without the input, help and support of many people, whom I want to thank at this point.

Let's start with my supervisors.
Richard, your calm and reassuring guidance helped me a lot, especially in the beginning of the project, to get into the for me hitherto rather unknown field of computational modelling. While your line of research did not include questions of auxin biology before, your interest in the subject, your encouragement, your help in methodological questions and your scientific advice were always deeply appreciated. Thank you for your supervision!
Ottoline, thank you for your contagious enthusiasm and engagement in all sorts of questions of plant development. Your input on the biology side of things was of immense help to get to grips with understanding the (to me still often confusing) paths of auxin action. It was great to meet your lab in York and to feel fully integrated, despite working in Sheffield on a somewhat isolated project.
Many thanks also to Susan - my trips to our regular modelling meetings in York with you and Ottoline were always a pleasure, and I learned a lot from our discussions. Thanks also to the other participants of these meetings, especially to Philip, Genevieve and Gemma, whose work and ideas on higher level auxin models helped me a lot to put my own work into context. Thanks to the members of my PhD panel in Sheffield, Dawn and Georg, for their valuable comments on earlier drafts of this work.

Thanks to the organisers and participants of summer schools and workshops I went to, often generously sponsored. I especially enjoyed the discussions with Daniel and Shai on the DTU summer school on mathematical modelling in Copenhagen in 2010,

which were great impulses for my interest in dynamical systems. Many thanks also to the often extremely valuable feedback coming from the audience of presentations I gave at several occasions, as well as from referees of manuscripts arising from within the scope of this thesis.

These were turbulent and busy three years in Sheffield. Thanks go to my colleagues and friends whom I met in Sheffield, who cheered me up when I got stuck, but also made my life in Sheffield generally a very nice and enjoyable experience apart from work. Thank you, Jan, Patrick, Mark S., Amy, Robin, Birgit, Mark B. - for your unforgettable barbecue parties, great discussions, cooking, coming along on walks in the Peak District, willingness to lure me into stop searching for bugs in my code and instead going out together, and for everything else.

I want to thank my wife Mirja for her support and understanding over the last years. You and our little daughter Ina have been a wonderful counterweight in the work/life balance during my PhD, enabling me to equilibrate and reminding me that life is more than science. Mirja, thank you for being who you are. As I am writing this, Ina sits on my knees, asking me to stop writing and play - this often helped me a lot, though I sometimes reluctantly accepted it, too focused on my apparently inbuilt to-do lists. Many ideas for my work came on the playground, thank you for taking me there. Thanks also to all the people who supported us with childcare, especially to Lars and Christina.

Thanks go also to my 'older' friends, for being constants in my life, for a tremendous support from all around the world, and for all the rest. Thank you, Andrzej, Georg, Bernhard, Nikola, Markus, Martina, Per, Jürgen, Wolfgang...

Not least I want to thank the White Rose University Consortium which supported my work with a scholarship. Many thanks for everyone behind this support, down to the many residents of the UK who with their taxes enable people like me to be free to work in research, which I consider a great privilege.

Contents

Declaration iii

Articles and presentations arising from this thesis v

Abstract vii

Acknowledgements ix

List of Tables xiv

List of Figures xv

List of Abbreviations xix

1 Introduction 1

1.1 Aim and focus of this thesis 1

1.2 Structure of this thesis 2

2 Auxin biology 5

2.1 A brief history of auxin biology 5

2.2 The many roles of auxin 7

2.3 Routes of auxin transport 12

2.3.1 The cellular mechanisms underlying auxin transport 13

2.3.2 Auxin transport canalisation 15

3 Computer models in auxin biology 17

3.1 Computational modelling in biology 18

3.2 Auxin transport models 19

3.2.1 Canalisation Models 20

3.2.2 Phyllotaxis models 22
3.2.3 Unified models 24
3.2.4 Whole plant models 25
3.3 PIN polarisation in auxin transport models 26
3.4 Concluding remarks 27

4 A single cell model prototype for PIN polarisation 29
4.1 Assumptions and model topology 30
4.2 Mathematical formulation 31
4.3 Computational model 34
4.4 Computer simulation 39
4.5 Results 42
4.6 Discussion 44

5 Auxin and protons 49
5.1 Maintenance of pH in plant cells 51
5.2 Auxin/pH interactions 52
5.2.1 Effect of pH on auxin 53
5.2.2 Auxin effects on pH 54
5.3 Auxin/pH dynamics and pH homeostasis in previous computational models 57

6 AP-10: A kinetic model of auxin and proton interactions 59
6.1 Model description 59
6.1.1 General assumptions underlying AP-10 60
6.1.2 Submodel 1: pH homeostasis 60
6.1.3 Submodel 2: Auxin transport and dissociation 63
6.1.4 Submodel 3: Auxin-induced apoplastic acidification (AAA) 64
6.1.5 The unified model 66
6.1.6 Computer simulation 66
6.2 Results 66
6.2.1 pH homeostasis 67
6.2.2 Auxin/pH dose-response curves 67
6.2.3 General model behaviour 69

6.2.4 Influence of pH homeostasis settings on model behaviour 71
6.3 Discussion 76
6.3.1 Modelling of pH homeostasis 76
6.3.2 Linking auxin transport to protons 77
6.3.3 Auxin influence on proton pumps 78

7 Minimised auxin/pH models: From AP-10 to AP-2 79
7.1 4-component minimal model (AP-4) 81
7.2 2-component minimal model (AP-2) 86
7.3 A comparison of AP-10 with minimal models 90

8 SAP-2: A spatio-temporal model of auxin/proton dynamics 93
8.1 Assumptions of the SAP-2 model 94
8.2 Extending AP-2 to a continuous reaction-diffusion system 96
8.3 Numerical solution 98
8.3.1 Solving using fixed point iteration 100
8.3.2 IMEX schemes: 1-SBDF and 2-SBDF 100
8.4 Results 101
8.4.1 Reproduction of core AP model findings in SAP-2 105
8.4.2 Time scale of AAA in SAP-2 105
8.4.3 Heterogeneity in the PMF due to AAA 106
8.4.4 Net auxin fluxes over the plasma membrane due to AAA 107
8.4.5 Parameter sensitivity 110
8.4.6 Auxin and proton dynamics in a file of 3 cells 115
8.5 Discussion 116

9 Conclusion and Outlook 121

A Model Parameters, Initial Conditions, Equations 127

Bibliography 137

List of Tables

6.1 Kinetic reactions for the pH homeostasis model (submodel 1). 61
6.2 Kinetic reactions for the auxin transport/dissociation model (submodel 2) . 63
6.3 Kinetic reactions for the AAA submodel. 64

7.1 Variables and components in the AP-10 model, the 4-component minimal model (AP-4) and the 2-component minimal model (AP-2). 80
7.2 An overview of all reactions in the auxin/pH model and the way they are treated in AP-10 and minimised implementations. 81

A.1 List of parameters in the PIN polarisation model, described in chapter 4 . . 127
A.2 List of all parameters in the unified auxin/pH model, AP-10 128
A.3 Initial conditions in the AP-10 model 129
A.4 List of all parameters used in the 4-component minimal model, AP-4 130
A.5 Initial conditions in the AP-4 model 130
A.6 List of all parameters in the 2-component minimal model, AP-2 131
A.7 Initial conditions in the AP-2 model 132
A.8 List of all parameters in the spatiotemporal auxin/pH model, SAP-2 132

List of Figures

2.1 The chemical structure of auxins 6
2.2 A scheme of the route of polar auxin transport in plants. 12
2.3 The chemiosmotic hypothesis of auxin transport 13

3.1 Auxin transport canalisation. 21
3.2 Up-the-gradient transport mechanism of auxin. 23
3.3 Subcellular events of PIN dynamics, as employed in auxin transport models. 27

4.1 Topology of the PIN polarisation model. 31
4.2 Spatial Finite Difference discretisation 34
4.3 Stencil in the FDM-discretisation of the PIN polarisation model 36
4.4 Sparse matrix of the model environment for the PIN polarisation model . . . 38
4.5 PIN polarisation results 41
4.6 Auxin concentration in cells with two different boundary conditions for auxin concentration. 43
4.7 Two different polarisation scenarios in the PIN polarisation model prototype. 44
4.8 Parameter sensitivity analysis of the PIN polarisation model. 45

5.1 Feedbacks between auxin and pH 53
5.2 Dissociation curve for auxin. 54
5.3 ABP_{57} -mediated proton pump activation. 56

6.1 A simplified structure of submodel 1 - pH homeostasis 61
6.2 Diagram of the AP-10 model 65
6.3 Behaviour of the pH homeostasis submodel as result to changes in external pH (pH stress experiments) 67

6.4 Dose-response experiments of auxin-induced apoplastic acidification in the AP-10 model and in biological experiments. 68
6.5 Apoplastic acidification peak changes due to alterations of parameters K_{ABP} and V_{ABP} 69
6.6 Auxin fluxes and allocation as a result of auxin-induced apoplastic acidification 70
6.7 The influence of changes of single auxin transport parameters on the shape of the AAA peak in dose-response simulations, as obtained after a simulation time of 2 hours. Reducing the value of α (upper), β (middle) or γ (lower) by an order of magnitude (dashed lines) or increasing it by an order of magnitude (dotted lines) resulted in shifts of onset and offset of the AAA peak, but did not qualitatively change the AAA peak otherwise. 72
6.8 pH-dependent membrane permeabilities for H^+/OH^- 73
6.9 pH stress experiments with different settings for pH-dependent permeabilities. 74
6.10 Auxin-induced apoplastic acidification under the assumptions of constant vs. pH-dependent membrane permeabilities for H^+/OH^- 75
6.11 Auxin fluxes and allocation under the assumptions of constant vs. pH-dependent membrane permeabilities for H^+/OH^- 75

7.1 Gaussian curve fitted to AAA strengths from biological dose-response experiments 84
7.2 Comparison between AP-10 and minimised models. 91

8.1 Comparison between simulations employing the 1-SBDF and 2-SBDF scheme for a numerical solution, using different time step sizes. 102
8.2 Auxin concentrations in the SAP-2 model after 8 hours of simulation time. . 103
8.3 Auxin-induced apoplastic acidification and its effects on auxin transport fluxes and cytosolic auxin allocation in SAP-2. 104
8.4 Time scale of auxin allocation and AAA in SAP-2. 106
8.5 Proton gradient heterogeneities over the plasma membrane in SAP-2. . . . 107
8.6 Proton fluxes and gradients in the proton motive force with AAA in effect. . 108
8.7 Auxin fluxes in SAP-2 with and without AAA in effect. 109
8.8 The relationship between passive and active auxin import. 110

8.9 Active vs. passive transport as a function of AAA and auxin source concentration. 111
8.10 Auxin transport parameters α and γ and their influence on simulation outcomes. 112
8.11 Auxin transport parameters α and β and their respective influence on auxin allocation in cells. 113
8.12 Auxin transport parameters α and β and their respective influence on the strength of AAA during simulations. 113
8.13 Maximum and minimum net auxin fluxes over the membrane as a function of auxin transport parameters α and β during simulations. 114
8.14 Auxin distribution in a simulation involving 3 cells in a row. 115
8.15 Auxin concentrations and pH evolution in a simulation involving 3 cells in a file. 116
8.16 Net fluxes and PMF heterogeneities over cell membranes in a simulation involving 3 cells in a file. 117

List of Abbreviations

1-SBDF	First Order Semi-implicit Backwards Differentiation (numerical scheme)
2,4,5-T	2,4,5-Trichlorophenoxyacetic acid, a synthetic auxin
2,4-D	2,4-Dichlorophenoxyacetic acid, a synthetic auxin
2-SBDF	Second Order Semi-implicit Backwards Differentiation (numerical scheme)
AAA	Auxin-induced Apoplastic Acidification
ABCB	ATP-Binding Cassette B proteins
ABP1	Auxin Binding Protein 1
ABP_{57}	Auxin Binding Protein 57
AP-10	Auxin/proton model with 10 components
AP-2	Auxin/proton model with 2 components
AP-4	Auxin/proton model with 4 components
ARF	Auxin Responsive Factor
ATP	Adenosine triphosphate
AUX1	Auxin import carrier protein
AuxRE	Auxin Response Elements
Aux/IAA	Auxin/Indole-3-acetic acid inducible genes
AVP1	H^+-pyrophosphatase in *Arabidopsis*
BTCS	Backward Time Centered Space Scheme (numerics)
FDM	Finite Difference Method (numerics)
FTCS	Forward Time Centered Space Scheme (numerics)

GFP	Green Fluorescent Protein
IAA	Indole-3-acetic acid, an endogenous auxin
IAA^-	Anionic (polar) auxin
IAAH	Undissociated (non-polar) auxin
IMEX	Implicit-Explicit Method
LAX	Auxin import carrier proteins (*Like AUX1*)
NAA	1-Naphthaleneacetic acid, a synthetic auxin
ODE	Ordinary Differential Equation
PATS	Polar Auxin Transport Stream
PDE	Partial Differential Equation
PGP	P-glycoproteins
pH	Negative decimal logarithm of proton concentration
PIN	Auxin efflux transporter protein, named after the pin-formed phenotype of *pin1* mutants in *Arabidopsis*
PINOID	A protein kinase, catalysing PIN phosphorylation
pK_a	Negative decimal logarithm of the acid dissociation constant K_a
PM	Plasma Membrane
PMF	Proton Motive Force
PP	Pyrophosphate
RAM	Root Apical Meristem
SAM	Shoot Apical Meristem
SAP-2	Spatio-temporal auxin/proton model with 2 components
SCF	Skp, Cullin and F-box containing complex
TP	Tonoplast (vacuolar membrane)

CHAPTER 1

Introduction

In this thesis, self-organising aspects in the cell-to-cell transport of the plant growth hormone auxin are investigated by the formulation of mathematical models and their implementation in computer simulation. Feedback between auxin and protons at a cell scale, which are partly well known from biology, have been implemented and integrated in the context of auxin transport. Computational modelling allowed for an exploration of the systems behaviour with implications for future biological experiments.

1.1 Aim and focus of this thesis

The aim of the work presented in this thesis is to explore dynamics of several feedbacks between the plant hormone auxin and its transport from cell to cell in plant tissues, which are vital for the establishment of specific accumulation patterns during auxin transport, some of which are critical to plant development. While some of these feedback mechanisms are well known from biology, much remains still unclear, partly because it is difficult to measure auxin concentration in living plant tissue, but partly also due to the complexity of regulatory networks in which auxin is involved. There is evidence of a feedback between auxin and protons, with some experimental data available in previously published studies, but to my knowledge this feedback mechanism has not gained enough consideration so far to elucidate its implications for auxin transport. The work in this thesis is an attempt to address some of the questions concerned with such an investigation by the formulation of a theoretical model of auxin

transport at a single cell level, using a continuous deterministic approach with ordinary differential equations (ODEs). The main focus of the work presented here was on self-organising mechanisms leading to ordered cell-to-cell transport of auxin, and on proposing and testing hypotheses about mechanisms that could not be directly addressed by experiments alone. This thesis does not contain biological experiments for model validation, however the theoretical models described have been evaluated using existing data from the literature. Moreover, the models are testable using wet experiments, and their predictions (especially changes in pH due to auxin transport and the formation of pH gradient patterns over the cell membrane) are targeted towards biological experiments for validation.

1.2 Structure of this thesis

The thesis consists of the following sections:

Chapter 2: Auxin biology. This chapter gives the necessary biological background to the reader. The field of auxin biology is reviewed by presenting the importance of auxin in plant development. The concept of polar auxin transport is introduced and the cellular basis of polar auxin transport are explained.

Chapter 3: Computer models in auxin biology. Since computational modelling has already been used intensively in auxin biology and since the thesis presents several models of auxin transport, this chapter gives an overview of the models that have been published already, their scope and their assumptions. Key achievements and open questions in those models are discussed. Some of the material in this chapter has been published in an article where I was co-author [63].

Chapter 4: A single cell model prototype for PIN polarisation. In this chapter, a model prototype is presented: an auxin transport model on a single cell level, capable of auxin transport polarisation due to PIN polar targeting and resulting in canalisation-driven transport. It was implemented in Matlab and the results are described in this chapter.

Chapter 5: Auxin and protons. Since the model prototype did not include sufficient detail, it did not give further insights in the open questions that were intended to be targeted within this work. The relationship between auxin and protons was considered to be a next step in examining auxin transport at a cell level that has not been explored in previous auxin models. In this chapter, the current knowledge about auxin/proton interactions is reviewed.

Chapter 6: AP-10: A kinetic model of auxin and proton interactions. Based on the biological data available, a model of auxin and proton interactions is proposed and described. Its implementation first as a set of submodels, then as a unified model is documented. Simulations were undertaken with the modelling package COPASI and the results are presented in this chapter. Parts of this chapter have been submitted towards publication.

Chapter 7: Minimised auxin/pH models: From AP-10 to AP-2. With the next aim to put the core model of the last chapter into a spatial context, the core model is minimised mathematically to reduce its complexity towards a level that is more easily implementable in a numerical solution of such a model. The equivalence of the minimal models with the original core model is verified.

Chapter 8: SAP-2: A spatio-temporal model of auxin/proton dynamics. The minimised core model is extended towards a reaction diffusion model. Issues in the numerical solution of this set of equations are addressed and eventually solved. The results of this computer simulation, written in Python, are presented and discussed.

Chapter 9: Conclusion and Outlook. This chapter gives a short summary of the key findings of this thesis and puts them into context of what has been presented as a literature review in chapters 2 and 3. As well, interesting open questions are mentioned at the end of this chapter.

CHAPTER 2

Auxin biology

Auxin is a plant hormone involved in a remarkably wide range of processes. The name *auxin* is derived from the greek word *auxein* - 'to grow', pointing to its role as a facilitator of growth during plant development. In this chapter, a general overview of auxin biology and a short historic outline of auxin discovery are given. As well, the phenomenon of polar auxin transport and current ideas about its underlying mechanisms are reviewed.

2.1 A brief history of auxin biology

In 1880, Charles and Francis Darwin published a book on *The Power of Movement in Plants* [36]. Among many other experiments, they described the bending of coleoptiles in several plant species (the coleoptile is a sheath covering embryonic leaves and the shoot tip in grasses [11]) towards a unidirectional source of light. While the coleoptile would usually bend towards the light, this reaction did not happen when the tip of the coleoptile was covered with tin foil or if the tip was cut off. Their conclusion was that

> '[...] it is a general rule with seedling plants that the illumination of the upper part determines the curvature of the lower part. [...] These results seem to imply the presence of some matter in the upper part which is acted on by light, and which transmits its effects to the lower part. (p. 484 ff.)'

While the chemical substance auxin (indole-3-acetic acid, IAA) was already known by that time [46, 191], it took nearly 50 years until Darwin's idea of a hypothetical signal, transmitted from the coleoptile tips to lower parts of the plant and promoting growth, could be linked to this substance. In 1926, Fritz Went successfully isolated auxin from *Avena* coleoptiles [244], after experiments in which he placed agar blocks under coleoptile tips and subsequently was able to induce growth in decapitated coleoptiles by placement of the agar. The transmitted growth-inducing substance that was captured in these agar blocks was a few years later named *auxin* by Kögl [99]. In the following years, a few synthetic auxins like 2,4-D (2,4-dichlorophenoxyacetic acid) have been synthesized and been applied as herbicides in agriculture [26, 238]. While IAA is the most abundant naturally occurring auxin, apart from synthetic auxins there are also other substances with a close structural similarity to auxin, showing similar effects on plant physiology and development. The chemical structures of two prominent auxins are shown in figure 2.1.

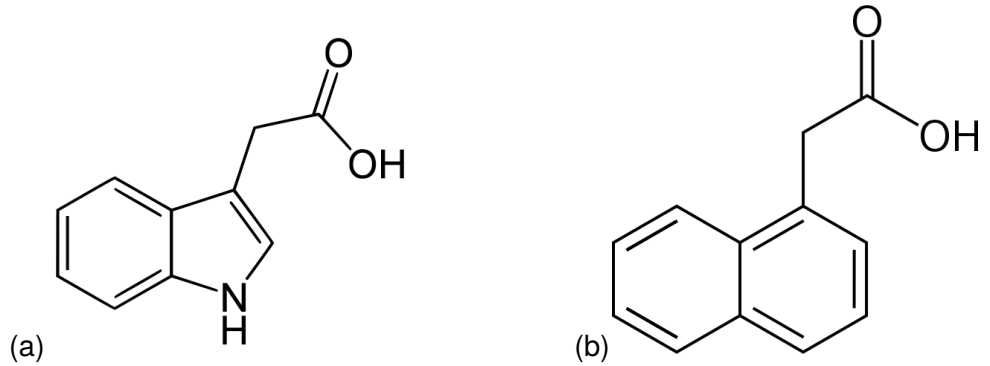

Figure 2.1: The chemical structure of auxins. *Left:* The structure of indole-3-acetic acid (IAA) , the most abundant endogenous auxin. *Right:* The chemical structure of 1-naphthaleneacetic acid (NAA), a prominent synthetic auxin. This figure is reproduced from [63].

A very famous appearance of auxin in non-scientific history was the wide application of auxins as defoliants during the Vietnam war under the name of *Agent Orange*, which is a mixture of 2,4-D with another synthetic auxin, 2,4,5-trichlorophenoxyacetic acid (2,4,5-T). The use of auxin as herbicide shows how powerful this substance really is for plants - while large amounts of auxin can kill them, and absence of auxin impairs growth [75, 158], it seems that just the right amount of auxin enables plants to thrive. But what is the right amount, how is this amount regulated over time in different parts of the plant and by which mechanisms does auxin control growth?

2.2 The many roles of auxin

Before trying to outline some of the answers that biologists provided to these questions over the last decades, it might be useful to remember two quite obvious, yet very important aspects of plant biology at this point. First, plants are sessile organisms, which means that they are not free to move, and second, plant development is a continuous process going on through a plant's life span [11]. As long as a plant lives, it usually grows and develops new organs, such as leaves or roots. In contrast to animal systems, plants show a more close connection between tissue establishment and reaction to environmental inputs, resulting in adaptive growth and ongoing adaptation of the adult body plan to changing environmental situations. On these grounds, adaptive growth in plants can be viewed as somewhat equivalent to behavioural responses in animals [118], allowing them to react flexibly to changing environments despite being sessile. Moreover, the organisational structure of plants is less hierarchical than in animals, resulting in more distributed control systems and emphasizing the role of communication between single plant cells to establish coordinated developmental responses at tissue and whole plant levels [118, 153]. Plant hormones play a vital role in this network of intercellular communication. There are several known plant hormones, such as abscisic acid, cytokinin, ethylene, gibberellins and strigolactone, but among these, auxin is often considered to play a leading role [13, 220, 248].

The following sections provide a short overview of the most prominent processes in which auxin is involved as a regulator. Auxin action is not easy to track down and the regulatory pathways by which it affects plant development are arranged in highly complex and self-organising networks involving many positive and negative feedback loops [18, 117, 118]. This overview does not intend to be exhaustive, but aims rather to present a taste of some prominent aspects of this intricate auxin regulatory network, providing a contextual background for the computational modelling study presented later in this thesis. In what follows, two aspects will often be mentioned: polar auxin transport and the feedback between auxin and its transport proteins. These mechanisms are further elucidated in section 2.3. Since the work presented in this thesis focusses on the lower-level mechanistic basis of auxin action rather than on higher-level developmental processes, these higher-level features of auxin biology are presented first in order to give the necessary biological background information.

Cell elongation and cell division. The mechanism by which coleoptiles bend towards the light is due to a differential growth rate in cells below the coleoptile tips [220]. Cell columns on the shaded side elongate at a higher rate than cell columns on the illuminated side. This cell elongation is one of the mechanisms triggered by auxin. Based on numerous experiments involving different amounts of auxin present versus elongation length of tissues during a given time, growth-response curves for certain auxin levels could be established, showing that increase of auxin concentrations in tissues are generally causing an increased growth of these tissues, but higher levels of auxin inhibit growth, leading to bell-shaped curves of growth response to auxin [75, 91, 93, 150, 203, 176]. These growth responses to auxin can result from changes in cell division, cell elongation, or both [163]. Auxin can regulate the transcription of cell-cycle related genes, which presumably influences cell cycle progression [236], leading to cell division and replication. The elongation of cells is hindered by the rigidity of cell walls. Here, biochemical wall loosening and osmotic uptake of water are both necessary to enable elongation [220]. In this context, the acid-growth hypothesis states that auxin-induced acidification of the apoplast (the cell wall space outside the plasma membrane) results in wall loosening [76, 175], which is promoted by the activation of pH-dependent proteins called expansins [34, 44].

Auxin signalling. Much of the complexity of how auxin is perceived in cells and how auxin triggers cellular processes is still not fully understood. However, insights into auxin signalling have been gained over the last decades and should be mentioned very briefly in this overview. Auxin causes changes in expression of many genes, such as the *Aux/IAA*s (Auxin/Indole-3-acetic acid inducible genes) and some *ARF*s (auxin responsive factors) [115, 144]. ARFs bind to the promoters of auxin-induced genes with promoters carrying Auxin Response Elements (AuxREs). Aux/IAA and ARFs dimerize at low levels of auxin, bringing the Aux/IAA proteins to the promoters, where they act as repressors of transcription. Increasing auxin levels lead to binding of auxin to the F-box protein TIR1 in SCF^{TIR1} (SCF stands for *Skp, Cullin, F-box containing complex* and is a multi-protein ubiquitin-ligase), resulting in recruiting of the Aux/IAA proteins, forming a complex which attaches ubiquitin to the Aux/IAA proteins. This ubiquitination leads to the degradation of Aux/IAA proteins. Once Aux/IAAs are degraded, the ARFs on the promoters of auxin-responsive genes are able to homodimerize and sub-

sequently stimulate gene transcription [115, 144, 228, 242]. Since Aux/IAA-ARF also represses *Aux/IAA* genes, degradation of Aux/IAA leads once more to the transcription of *Aux/IAA*s, establishing a regulatory feedback of auxin-responsive gene expression [137, 177].

Plant tropisms. The ability of plants to turn or grow towards certain environmental stimuli is often referred to as *tropism* [148]. Apart from phototropism (the growth towards light), which has already been mentioned above, there are other tropisms connected to and dependent on auxin action, mainly gravitropism, the growth in response to gravity, and thigmotropism, the growth with respect to touch [148, 220]. Gravitropism is found in most plant parts. Many aspects in this response are auxin-dependent [161], especially on the function of the auxin transport proteins AUX1 and PIN2 [15, 202, 216, 251] (see section 2.3.1 for a more detailed discussion on these and other auxin transport proteins).

Shoot branching and apical dominance. Plants are potentially able to grow throughout their life span. Of particular importance are well-defined tissue regions called meristems, containing undifferentiated cells that have the function of stem cells. Along the apical-basal axis there are apical meristems, which consist of the RAM (root apical meristem) and the SAM (shoot apical meristem). In the shoot, there are also so-called axillary meristems, which are derived from the primary SAM and located in the axils of leaves (the angle between leaf petiole and the main stem), able to establish new axes of growth [11, 133, 201, 220]. These axillary meristems are often dormant and their growth is inhibited by the apical bud, a phenomenon called *apical dominance*. A role for auxin in this process was discovered in 1933 by Thiemann and Skoog in experiments where the primary apex was removed, triggering the activation and subsequent outgrowth of the lower buds. This process could be inhibited by the application of auxin on the site of the removed shoot tip [225]. The applied auxin moves basipetally from the shoot tip towards the roots (see section 2.3), however its inhibitory effect on buds was subsequently found not to occur directly [206], and also to involve other hormones, namely cytokinin and strigolactones [133]. Cytokinin, produced in roots as well as in shoots and moving upwards towards the leaves, promotes bud outgrowth [116]. Auxin inhibits cytokinin synthesis both in shoots and roots [116], whereas cytokinin

enhances auxin synthesis and inhibits auxin transport and signalling [88, 145], which links both hormones in a regulatory feedback. Another hormone involved in auxin-controlled apical dominance is strigolactone, negatively regulating shoot branching [233] and dampening auxin transport [35], while its synthesis is up-regulated by auxin [116].

Phyllotactic patterning. The spatial arrangement of leaves, or related organs, in the growing shoot is termed *phyllotaxis*. Phyllotactic patterns have often raised interest beyond plant sciences, especially in mathematics [1], because of their highly geometrically ordered nature. A well-known example are spiral phyllotactic patterns, such as the compound flowers of sunflowers. The number of clockwise versus anti-clockwise spirals are consecutive numbers in the Fibonacci series, and the divergence angle between leaf primordia is very close to the the golden angle [107]. There is a body of evidence that auxin regulates phyllotaxis by the establishment of regular distribution patterns of auxin maxima in the SAM [180], which themselves are the product of an interplay between auxin and its cellular transporters that is still not fully understood ~~to date~~ [108, 178, 196].

Vascular tissue formation. Vascular tissue is the conductive tissue in higher plants, consisting of bundles of cells with the function of providing supporting structure for the plant as well as transporting substances between leaves and root [39]. The vascular bundle consists of two conducting tissue types: the xylem which mainly conducts water and mineral nutrients from the root towards the leaves, consisting of dead cells that underwent apoptosis, and the phloem, conducting sucrose and other substances and consisting of living tissue [11]. The development of vascular tissue to connect newly formed organs such as leaves to the already existing transport system of the plant has been shown to be regulated by auxin to a high extent [39, 131, 194]. Auxin transport is usually basipetal in the shoot, which means directed from the site of its production, mainly young expanding leaves, towards the root of the plant. The canalisation hypothesis describes how during cell-to-cell transport auxin flow canalises to form narrow files of auxin transporting cells by a feedback between auxin, its flux, and its transporters [189]. The cells through which these distinct paths of auxin lead may subsequently differentiate to vascular tissue [39]. The movement of auxin in leaves and the induction

of leaf venation patterning has been found to rely on the same mechanism of auxin transport canalisation [184, 185]. During the following sections, the current mechanistic explanations of both the main polar auxin transport stream and the canalisation hypothesis will be discussed in more detail.

Root patterning and development. Similar to the involvement of auxin in regulating growth and branching in shoots, there is also evidence that growth and patterning in roots is maintained and regulated by auxin and auxin transport dynamics. In the RAM of the root tip, auxin maxima occur and are steadily maintained [73] and auxin levels are correlated with the expression of *PLETHORA (PLT)* genes which control stem cell activity [2, 60], however the exact mechanism of the interaction between auxin and PLT remains elusive and possibly includes several intermediate signals [41, 42]. The formation of lateral roots also relies on auxin action. Application of auxin triggers lateral root development, while treatment with the auxin transport inhibitor NPA results in arrested lateral root development, with auxin being redistributed towards the root tip [29]. Since lateral roots originate from deeper layers of the parental root, auxin may also be involved in remodelling the cell wall structures towards outer layers of root tissue to enable lateral root outgrowth [213]. Other factors involved in auxin-controlled lateral root formation include elevation of auxin levels by physical stresses due to root bending and curvature [112] and interactions with the plant hormone ethylene [85], which is also an important factor in plant root growth and has been found to up-regulate auxin synthesis in roots [217], while auxin itself is able to promote ethylene synthesis [14].

Other involvements of auxin. Apart from these prominent aspects of auxin action in development, auxin is also involved in other notable processes, such as the establishment of the embryonic axis of polarity [59, 243], fruit development and ripening [157, 229] and regulation of leaf senescence [120, 156]. Auxin also participates in metabolic reactions to tissue wounding by stimulating several factors involved in wound healing [223].

2.3 Routes of auxin transport

Auxin is produced mainly in young developing leaves [122, 123], but also in other parts of the plant [30]. Many alternative and genetically redundant routes lead to auxin production and are still not fully understood to date, however some pathways have been elucidated over the last years, which are mostly dependent on a tryptophan (Trp) precursor [5, 224, 249]. The routes of auxin transport through higher plants have a directionality from the shoot tip towards the roots, a phenomenon often referred to as polar auxin transport stream (PATS). In the roots, this transport stream is reversed at the tips in a fountain-like manner, directing auxin back upwards in outer cell layers [12, 166] (see figure 2.2). Since these directed routes in PATS are established by a concerted cell-to-cell transport of auxin through tissues [149], this mechanism is driven by the interplay of auxin and its transporters at the cell level. Therefore, the following sections focus on the cellular basis of auxin transport and the feedbacks between auxin and its transporters, leading to such an ordered phenomenon as PAT, and thereby linking short-range with long-range signalling.

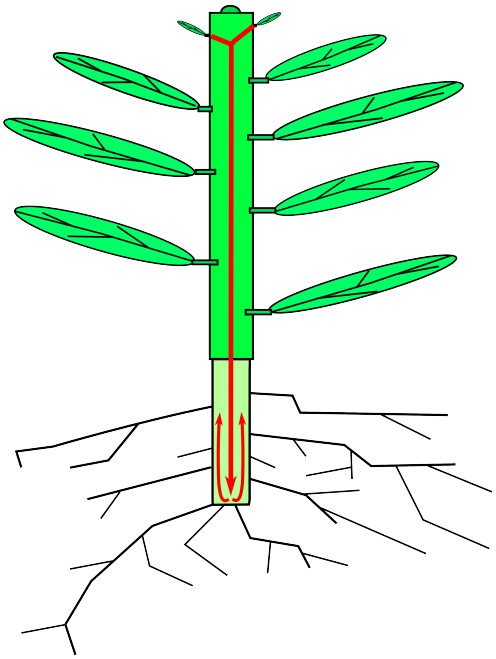

Figure 2.2: A scheme of the route of polar auxin transport in plants. Auxin is mainly produced in young leaves near the shoot apical meristem (located at the shoot tip) and then transported basipetally towards the root tips, where its transport directionality is reversed (red arrows).

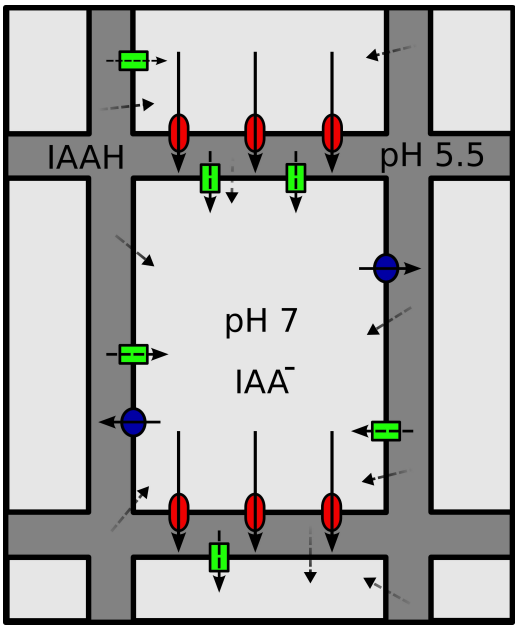

Figure 2.3: The chemiosmotic hypothesis of auxin transport. Cell wall compartments (dark grey) have a pH around 5.5, while the cytosol is nearly neutral in pH. In the cell wall, part of the auxin is protonated (IAAH), while in the cytosol virtually all auxin appears in its anionic form (IAA^-). Arrows indicate the routes of auxin transport over cellular membranes. Auxin in its protonated form is able to enter the cell unaided (bare dotted arrows). Transporter proteins in this figure include importers of the AUX1/LAX family (green), and exporters of the PIN (red) and ABCB families (blue), acting on anionic auxin. This figure is reproduced from [63].

2.3.1 The cellular mechanisms underlying auxin transport

The chemiosmotic hypothesis of auxin transport describes how auxin is transported across the cell membrane [186]. Auxin is a weak acid, with a pK_a of 4.75 [220]. The pK_a is the negative decimal logarithm of the acid dissociation constant K_a and indicating at which pH a monoprotic acid such as auxin is half dissociated. Dissociation is the reversible process by which an acid separates in water. In the case of auxin, due to this mechanism the proton is split off from the auxin molecule (IAAH) and added to one water molecule (H_2O). As a result, the water molecule is turned into a hydronium ion (H_3O^+) and the protonated auxin (IAAH) is turned into its anionic (or ionised) form (IAA^-). In the acidic extracellular space (apoplast, or cell wall space), auxin is dissociated to a much lower extent, compared with the near-neutral cytosol (the intracellular fluid), in which nearly all auxin is ionised. The plasma membrane shows a higher permeability for protonated auxin due to its lipophilic nature, whereas the permeability for anionic auxin is much lower, and so anionic auxin is virtually unable to leave the cell unaided. This poses a mechanism by which auxin is trapped in cells, unless specific transporters facilitate its efflux (see figure 2.3). The chemiosmotic hypothesis predicts a polarised auxin transporter abundance in cells in order to establish the directed flow of the PATS [174, 186].

Many auxin transporters have been described during the last years. Among the auxin efflux transporters there are two prominent families: PINs and ABCBs (or PGPs).

Transporters of the PIN family are named after the pin-formed phenotype of *pin1* mutants in *Arabidopsis*, indicating that PINs play a crucial role in plant development, such as phyllotactic patterning, which is responsible for the formation of new leaves [21, 101, 167]. A very prominent member of the PIN family is PIN1, a transport protein consisting of two sets of five transmembrane regions, separated by a hydrophilic loop [61]. It is one of the so-called canonical 'long' PINs (PIN1-4, PIN7) that are often found to be polarised in cells, which means that they are often asymmetrically distributed on the plasma membrane [221, 255]. Directed auxin flux has been found to occur in tissues with polarised PIN distribution, where the direction of the auxin flow through a tissue is determined by the polar localisation of PINs [247]. Other members of the PIN family (PIN5, PIN6, PIN8) are termed 'short' PINs and lack parts of the central hydrophilic loop. They are found in endosomal compartments, giving rise to the hypothesis that they might be involved in auxin homeostasis within cells [147]. One striking feature of long PINs is that they are not statically inserted in membranes, but rather undergo redistribution between the plasma membrane and endosomal compartments, often referred to as PIN cycling: PIN insertion into the plasma membrane, followed by PIN endocytic recycling [53, 57], dependent on vesicle transport proteins (PIN endocytic recycling is clathrin-dependent), which are transported to endosomes along microtubules [132, 162]. Some factors have been found to play a role in the directionality of PIN accumulation, such as an exchange factor for ARF GTPases (ARF-GEFs), called GNOM in *Arabidopsis* [67, 222] or the protein kinase PINOID, which catalyses PIN phosphorylation and regulates PIN polarisation [98, 136]. While these factors seem to be required in PIN polar targeting, there is still little knowledge of the exact mechanism behind PIN polarisation. Auxin is able to up-regulate the transcription of *PINOID* and of *PIN*s [117, 237], and also influences the stability of PINs on the membrane by inhibiting PIN endocytosis, thereby stabilising PINs at the membrane [159]. While the effect of auxin on transcription is dependent on the TIR1/AFB, Aux/IAA-ARF pathway described in section 2.2, its effect on endocytosis is regulated by other means, maybe through the detection of extracellular auxin by ABP1, an auxin binding protein [195].

Transporters of the ATP-binding cassette B family (ABCBs), or P-glycoproteins (PGP), are also involved in auxin efflux and have been found to stabilize PINs at the membrane

and sometimes co-localize with PINs [20, 226]. Some studies suggest that ABCBs are important for the effectiveness of PIN-dependent polar auxin transport [146]. ABCBs seem primarily to regulate long-distance auxin transport and are not required to establish routes of auxin transport, or for organogenesis [226].

A prominent family of auxin influx transport proteins, called AUX1/LAX (like AUX), is also critical in auxin transport [15, 28, 101, 251], and is involved in the regulation of root gravitropism, phyllotaxis, lateral root formation and root growth [8, 15, 166]. The *Arabidopsis* mutant *aux1* is defective in carrier-mediated auxin uptake and AUX1/LAX proteins are important for the creation of auxin sinks [127], however, loss of AUX1 function does not seem to have obvious effects on the phenotype, beyond defective root gravitropism [255].

There are two additional mechanisms that could account for auxin transport from cell to cell. One idea proposes a neurotransmitter-like transport of auxin from cell to cell [9]. Since PINs are cycling between endosomes and cell membranes in vesicles, it is possible that auxin uptake takes place into vesicles already in the cell, which are later fused with the plasma membrane thereby releasing auxin into the extracellular space by a neurotransmitter-like secretion. Another hypothesis concerns the possibility of auxin transport from cell to cell through plasmodesmata, which are cytoplasmic bridges between cells, and which are connected to the endoplasmic reticulum [6, 187]. Neither hypothesis is well supported by biological findings [24].

2.3.2 Auxin transport canalisation

The auxin transport canalisation hypothesis has been proposed by Sachs in 1981 [189], stating that initial auxin fluxes between cells are reinforced by a feedback between auxin and its transporters, eventually leading to distinct routes (canals) of strong auxin flux. This hypothesis has been useful in understanding the formation of vascular tissue, including leaf veins, where auxin and its transport routes lay out the path for subsequent tissue differentiation [184]. Since PINs are important in establishing auxin flux directionality, this idea would imply a feedback between auxin and PINs, causing PINs to accumulate where the auxin flux is highest and polarise in the direction of the flux. This source-sink PIN polarisation pattern can indeed be observed using imaging techniques involving GFP-tagged PINs [21, 160]. However, there are still many gaps

in understanding the mechanistic basis of auxin transport canalisation, with an often posed question towards how cells could sense auxin flux in order to polarise efflux transporters in the direction of flux [117]. As well, the notion that auxin forms maxima in the SAM during the process of phyllotaxis, inferred from the indirect observation that the synthetic DR5 auxin response reporter is activated at the sites of incipient leaf formation [235], seems to contradict the canalisation hypothesis, since the formation of auxin maxima would require PIN polarisation towards higher auxin instead of lower auxin. It has to be noted, however, that DR5 reporters do not respond to auxin concentration directly, but to auxin dependent gene expression.

With these open questions in mind, and the difficulty of measuring auxin concentration directly, the use of computer models to formulate and test hypotheses underlying auxin transport dynamics is useful and has indeed helped to understand better some of the complex aspects in PAT [63, 106, 232]. Therefore, the following chapter has its focus on this theoretical approach. During the next chapter, computer models of auxin transport that have already been published are reviewed and their assumptions and the impact that they have on our current understanding of auxin biology are discussed in detail.

CHAPTER 3

Computer models in auxin biology

In auxin biology there are, despite many advances over the last decades, still many open questions. In the last chapter, some of these advances have been presented. The integration of auxin transport with auxin signalling, leading to the regulation of physiological and developmental processes, and the interplay of auxin with other hormones such as cytokinin, strigolactones or ethylene, have been reviewed. We already saw that auxin transport plays a crucial role within this complex network of intertwined processes, since it ensures that auxin is available at places where its action is necessary, that auxin is depleted from parts of tissues in order to produce concentration gradients (as is the case in phyllotactic patterning in the SAM), and it allows information to be transmitted from one place to another.

Some of these open questions are: how is regulated auxin transport from cell to cell established in plant tissues, resulting in specific transport patterns such as in the establishment of maxima in the root and shoot meristems, or in distinct canals of auxin transport in the context of canalisation? How are such transport patterns established in cells? We saw that the chemiosmotic hypothesis of auxin transport, now widely accepted and refined by the discovery of several auxin carriers [47, 58], hints towards the dependency of auxin transport on the interplay and polarisation of auxin transport proteins. On the other hand, the last chapter also discussed mechanisms by which auxin regulates its transporters, both on transcriptional and post-translational levels (see section 2.3.1). How can these regulation mechanisms arrive at sometimes different results, especially at flux-oriented (canalisation) versus up-the-gradient auxin

transport (as in phyllotaxis)? How do cells 'know' where to transport auxin and how does concerted transport between cells in a tissue emerge? And how do the dynamics of auxin transport within tissues influence higher level features such as shoot or root branching? There are also problems on a methodological level: it is, for instance, extremely difficult to measure auxin content in living cells or cell compartments. However, there are methods to infer auxin gradients in tissues from the visualisation using *DR5:GFP*, an auxin responsive promoter element fused to the *Green Fluorescent Protein (GFP)* gene [151]. Still, precise quantifications of auxin concentrations are not possible with these methods, since DR5 does not report auxin concentrations directly, but responds to auxin dependent downstream gene expression.

As a response in order to understand better the dynamics and underlying processes of auxin transport, many computer models have been developed over the last years, targeting these open questions mainly at the tissue and whole plant scales. This chapter gives a review of the progress and implications of these models to date and discusses important knowledge gaps in auxin transport modelling that lead to the development of a new model of auxin transport dynamics at a single cell level, which will be described in the following chapters.

3.1 Computational modelling in biology

Computational modelling is a powerful tool to broaden our understanding of complex processes by formulating, quantifying, simulating and testing the mechanistic rules (such as the relationship between chemical or biological entities) upon which the behaviour of the whole system of interest hypothetically rests. While modelling does not prove a mechanism, it potentially increases the strength of an explanation by exploring the consequences of one or several mechanisms and the importance of underlying assumptions, thereby guiding future empirical experiments, the results of which then can feed back into the modelling process [170], an integration of theoretical and experimental approaches in biology that is often referred to as systems biology [96]. Mathematical and comptuational modelling are often distinguished, because mathematical modelling explicitly defines the relationship entities, thereby unambiguously characterizing the system of interest formally, while computational modelling provides executable models based on algorithms which simulate how the system progresses

from one time step to the next [25, 55]. However, computational models are often implementations of explicit mathematical models.

In biology, theoretical modelling approaches have been very fruitful over the last decades, for example in the use of mathematical models in physiology, such as the Hodkin-Huxley model of action potential formation in nerve cells [82], in population ecology, such as the Lotka-Volterra model of predator-prey dynamics [69], or in developmental biology, with the prominent example of Turing's reaction-diffusion models of morphogenesis [231]. Apart from deterministic mathematical approaches, stochastic model approaches are now also widely used in systems biology, especially if the model deals with a system involving only a small number of agents (molecules, genes) that do not allow for formulating an average agent behaviour with continuous equations.

There are many modelling techniques available and have been used extensively in biology with stochastic, deterministic or hybrid approaches, such as modelling using ODEs (ordinary differential equations), time series analysis, SDEs (stochastic differential equations), agent based modelling, L-systems, Boolean networks or cellular automata, each of them with their own strengths and limitations. A variety of these methods has already been used in auxin-related modelling to date (for further reviews on different methodologies in plant models and comparisons between them, see [106, 121, 143, 183, 232]).

3.2 Auxin transport models

Most models of auxin transport are at a tissue or whole plant scale. The regulation of transport is mainly established by means of auxin feedback on its transporters, especially on PIN proteins [106], leading to auxin transport polarisation. These models can be categorised into the following groups: (a) phyllotaxis models, (b) canalisation-type models, and (c) unified models, integrating the mechanisms leading to (a) and (b). Whole plant models are mostly concerned with the establishment of branching patterns. The following sections give an overview of auxin transport models published to date.

3.2.1 Canalisation Models

In canalisation models, the formation of auxin canals due to the feedback between auxin transport and auxin transporter allocation is examined. Early models have been established by Mitchison [140, 141, 142], based on biological experiments of Tsvi Sachs [189]. Sachs showed in a series of experiments with pea stems that vascular tissue formation occurs between auxin sources (for example, applied exogenous auxin) and sinks (for example, existing vasculature which removes auxin from a tissue). Mitchison also considered the predictions of the chemiosmotic hypothesis of auxin transport, namely that transporter polarity in cells accounts for polar auxin transport, since otherwise auxin would be trapped in cells [70]. Two possible mechanisms were employed in Mitchisons models: facilitated diffusion [141] and transporter polarisation. In the facilitated diffusion model, auxin diffusion increases with flux, which remains controversial because a mechanistic explanation of this diffusion enhancement remains elusive [185]. However, Mitchison makes it clear in his article that this increase in diffusion might be an emergent property of underlying mechanisms in a similar manner as the increase of conductance of electrical currents in gas as the temperature rises. It has also to be noted that 'facilitated diffusion' does not mean diffusion in the strict sense of Brownian motion of molecules, eventually leading to the dissipation of concentration gradients in a given fluid, but this term also includes trans-membrane movement of substance by carriers, as long as the substance is not transported against a chemical gradient.

In his polar transport model [142], auxin fluxes directed the insertion of transporters into the membrane, such that higher fluxes between two cells resulted in a stronger abundance of transporters between them. Cell wall space was not explicitly considered in this model, instead transport occurred directly from cell to cell, which is a common abstraction in auxin models [102]. This model was able to reproduce canal formation between auxin sources and sinks, and even could account for the formation of more complex loops in leaf venation [142]. Both models, facilitated diffusion and polar transport, were dependent on the square of auxin flux, such that a non-linear relationship between auxin flux and the flux enhancement mechanism is needed for the formation of stable canals. An example of canalisation in a 2D grid of cells is shown in figure 3.1.

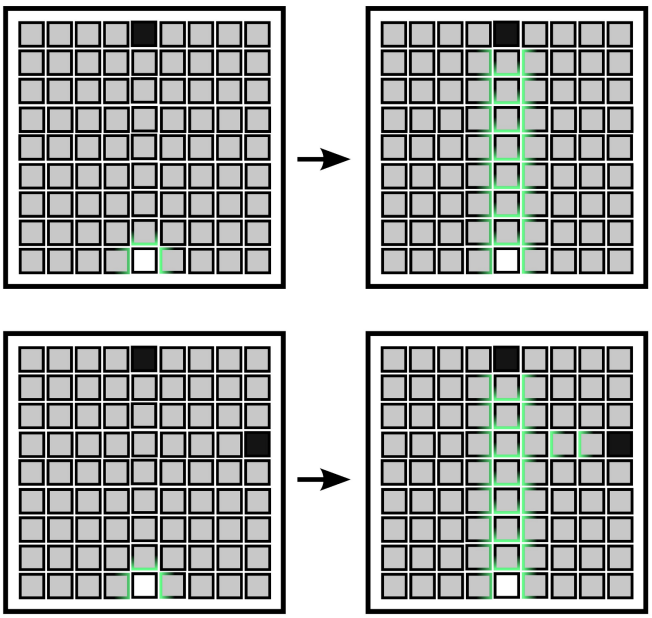

Figure 3.1: Auxin transport canalisation. A schematic tissue is drawn as a two dimensional grid of square cells. Cells acting as auxin sources are black; auxin sinks are white. PIN localisation in the membrane (green) shows the direction of auxin efflux and thus the direction of overall auxin transport through the tissue. Initial fluxes of auxin (upper left) are reinforced and lead to the development of auxin transport canals between source and sink (upper right). Lower left and lower right: The situation with two source cells. One possible result could be a branching pattern where both canals drain into the same sink. In both situations, auxin is drained from surrounding tissues (grey cells). This figure is reproduced from [63].

A prediction of Mitchison's canalisation model was that the canals exhibit high auxin flux and low auxin concentration, contrary to the results obtained by indirect visualisation techniques using the DR5 auxin responsive element [194], indicating high concentration in auxin canals. In a more recent model, Kramer could show that these canals with high auxin concentration could be reproduced when including auxin influx carriers in canal-forming cells, which were able to deplete the surrounding tissue from auxin [101]. Similarly, if parts of the membrane compete for the allocation of auxin efflux transporters, such canals with high flux and high concentration of auxin could also be established, with the result of reproduction of branched vein patterns, but no closed loops [54]. A more recently presented canalisation model [239] has been able to reproduce both high flux, high concentration canals, and several leaf venation patterns, such as closed loops, with the underlying mechanism of auxin flux enhancement depending on the inhibition of PIN endocytosis (relocation of PINs towards endosomal compartments) by a signal from a slowly diffusing apoplastic auxin-receptor. The

canalisation mechanism relies on the competition between cell membranes for free diffusing auxin receptors, however it requires the sudden immobilisation of receptors once they are bound to auxin. While it is indeed unlikely that a receptor molecule such as auxin binding protein 1 (ABP1, the putative candidate for this receptor molecule as suggested by the authors) would change its diffusion coefficient in such a drastic way by binding to auxin, which has only around 1.5 % of the molecular weight of ABP1 [50, 99], this is in fact an approximation to the receptor-auxin complex binding at the cell membrane which is nearest to where the complex formed. This model was also able to reproduce canalisation in the context of bud outgrowth competition due to apical dominance with the same mechanistic assumptions of cells competing for an extracellular auxin receptor.

A minimal canalisation model for PIN polarisation in a file of cells has been proposed by Alim and Frey [4], predicting an excitable polarisation front which is able to trigger PIN polarisation within cells. The model is implemented in 1D, it does not consider apoplastic space and it is notably solved analytically, thus it is a pure mathematical model not relying on computer simulation. It is able to reproduce bipolar cells, which could account for the occurrence of closed vein loops in leaf vein patterning. The feedback between auxin flux and auxin transport involves a mechanism by which the endocytosis rate of PINs from the membrane into the endosomal compartments is reduced in membrane parts exhibiting high flux.

3.2.2 Phyllotaxis models

There is substantial evidence that in the shoot apical meristem (SAM) geometrically distributed auxin maxima are formed which can account for phyllotactic patterning (see section 2.2). Inhibition field models of primordium formation go back to Hofmeister [83], who proposed the hypothesis that a developing leaf primordium P_i would inhibit the formation of new primordia $P_{(i+n)}$, an inhibition that weakens with increasing distance to P_i. Based on several possible signals including activating or inhibiting signals or both, which could act in such a way, a wide range of commonly found phyllotactic patterns could be reproduced in computer simulations [208]. One of these signals has been proposed to be auxin and its polar transport patterns in the SAM, based on biological results which indicate that auxin maxima are formed, depleting the surrounding

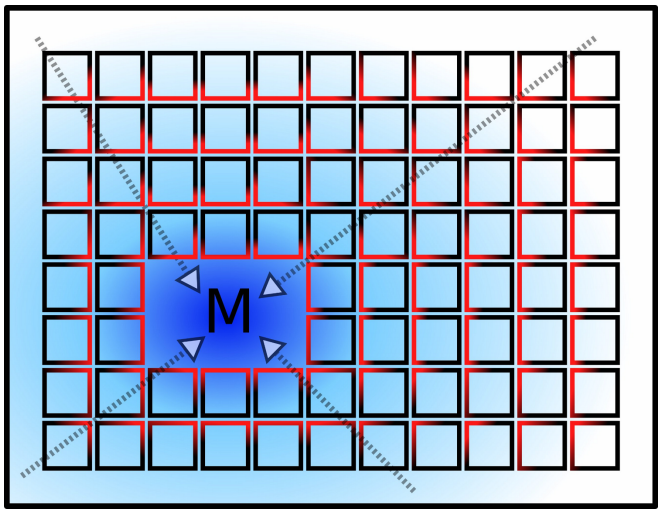

Figure 3.2: Up-the-gradient transport mechanism of auxin. In phyllotaxy models, auxin is often hypothesised to accumulate at local maxima (M) that precede organ initiation. To illustrate typical PIN polarisation patterns around an auxin maximum, the picture shows a schematic tissue of square cells (red: high concentration of PINs in the membrane, black: low PIN concentration, blue: auxin concentration). Arrows represent the direction of auxin transport. This figure is reproduced from [63].

tissue of auxin [178, 179]. In auxin transport models attempting to unveil the dynamics of auxin maxima formation in the SAM, the polar transport is therefore preferentially taking place towards the neighbour with higher auxin concentration. This apparently relies on a feedback of auxin transport polarisation towards higher auxin concentration, which is sometimes also referred to as 'up-the-gradient' as opposed to 'with-the-flux' [10]. An illustration of this mechanism is given in figure 3.2.

In these models, an initial condition with heterogeneous auxin distribution in cells leads to the polarisation of PINs towards cells with more auxin [89, 207]. The mechanism behind this is unknown, but one study proposed a hypothetical signalling mechanism by which a cell is informed about the auxin content of its neighbour cells as a driver for PIN polarisation [89], a mechanism which has also the potential of pattern formation beyond phyllotactic patterning, such as peaks, stripes and reentrant peaks with different wavelengths, and that these patterns also occurred when the PIN stability on the membranes was altered explicitly by the hypothetical signal [190]. The process of auxin maximum establishment takes part in the uppermost layer of the SAM, the epidermal layer [207]. The so-called reverse fountain model suggests that once a stable auxin maximum is established, a primordium forms at this position. Following the initiation of

organ development, auxin is then transported down into subepidermal layers towards the nearest auxin sink to form a canal connecting the new organ with already existing vascular tissue [214]. Therefore, an auxin maximum is apparently established by up-the-gradient polarisation of auxin transport, but then the tissue with an auxin maximum apparently switches to a flux-driven polarisation. In the reversed fountain model, phyllotactic patterning and canalisation meet and are linked, despite being seemingly antagonistic processes because of opposing polarisation mechanisms. How do cells switch from one regime to the other, or is there in fact an unified mechanism?

3.2.3 Unified models

There are several models that attempted to shed light on this transition mechanism. One of them introduced the hypothesis of travelling waves, where auxin maxima, once formed by up-the-gradient driven PIN polarisation, move around the tissue, thus establishing canals behind them, consisting of cells that remain polarised [134]. While interesting, this underlying mechanism for moving maxima is, at least up to now, not corroborated by any biological evidence that could explain such a behaviour.

Another proposed unifying model was able to produce phyllotactic patterning and canalisation both on flux-driven PIN polarisation [211]. The resulting polarisation of auxin transport was up-the-gradient, if auxin sinks were weak, while strong auxin sinks led to canalisation of auxin flow. Initially the simulation only contained weak sinks, causing the formation of auxin maxima, whereupon, after a threshold of concentration is reached in the cell containing the auxin maximum, the cell switches its identity from being an epidermal cell to being a primordial cell. Such a developmental switch could account for the transition to PIN polarisation towards strong sinks in sub-epidermal layers. Another attempt to unify canalisation with phyllotaxis mechanisms in auxin transport has been presented by Bayer et al. [10]. The switch between the polarisation scenarios in their model is dependent on the auxin concentration in cells, which leads to a gradual transition from up-the-gradient to flux-driven polarisation with increasing auxin concentration. Additionally, their model required a hypothetical signal from the existing vascular tissue in order to establish accurate connections between the developing veins of new primordia and existing vascular strands in the stem.

3.2.4 Whole plant models

Based on previous models which were able to reproduce plant growth dynamics and branching patterns by modelling the interaction between plant subunits (modules), which are treated as entities which are 'less-than-independent component[s] of an independent whole' [33], Yang and Midmore [252] presented a simple computational model for resource allocation during plant growth and shoot branching. This model also assumes a modular nature of plant architecture and allows for competition between the modules, which are rivals for resources. This model combines photosynthetic activity, nutrient uptake from the soil (focussed on nitrogen as a critical resource), auxin and cytokinin transports and allows for growth of the shoot. The ratio between root and shoot modules is regulated by nitrogen uptake in root modules (correlated with cytokinin production) and phytosynthetic activity of the shoot modules (correlated with auxin production). Auxin concentration in a module increases the vascular connectivity of this module to the next, thereby amplifying its access to resources from roots, represented by cytokinin. On the other hand, cytokinin production is dependent on the nutrient availability and therefore limited. This model was able to reproduce apical dominance after shading (or removing) the shoot tip by self-organisation of the quasi-independent modules and their interplay.

Another whole plant model, proposed by Prusinkiewicz et al. [173], relies on the same principle of modular plant architecture and connectivity between such modules instead of including single cells, assuming that the behaviour of these modules is mirroring the behaviour of cells, and including a canalisation-type feedback mechanism between auxin and its flux from module to module. Buds (including the shoot apex) are auxin sources and the root is an auxin sink. During the simulation, buds compete for the access to the auxin sink, which leads to an auxin transport switch: If one of the buds is active, an auxin transport canal from this bud towards the sink establishes based on a feedback of flux on polarisation (each module contains an equivalent to PINs that can be allocated to the module border facing the neighbouring module). As a result, even though the main stem has high auxin flux, other buds cannot export their auxin, because of the high auxin concentration in the main auxin canal, which accounts for apical dominance. Once the active bud is removed, auxin concentration in the main stem falls, enabling lower buds to export auxin and polarise, which subsequently

activates them to grow out. By allowing for growth of the plant system, this model could reproduce a range of branching patterns occurring in nature as well as the behaviour of some auxin mutants with altered auxin transport or response.

3.3 PIN polarisation in auxin transport models

The exact mechanism of how auxin feeds back on PIN polar targeting is still unclear. However, computational models involving such feedbacks have made assumptions about the nature and directionality of such a feedback. Some of these assumptions are illustrated in figure 3.3. Here, I want to recapitulate the main assumptions of auxin feedback on auxin transporters, as made in models of auxin transport to date. An unidentified feedback between auxin flux and transporter polarisation is made in most flux-driven models [4, 54, 142, 173, 211]. There are some criticisms of that assumption, questioning that cells could possibly sense auxin flux in a way that polarisation towards flux could occur [103, 134]. However, such a mechanism could be less obscure than this argument suggests. In an agent-based model of auxin transport in a tissue, such a flux sensing mechanism has been reproduced as emergent behaviour, resulting from simple rules of single PIN molecules responding to auxin concentration [64]. If the PINs stay at the membrane as long as enough auxin is present to transport, given a constant insertion rate, this would delay PIN removal from membrane regions with stronger auxin flux, eventually leading to polarised cells (a result that is reproduced in chapter 4 in this thesis with a deterministic ODE model).

A similar mechanism, involving the feedback of auxin on the PIN removal rate from membranes, is employed in the canalisation model of Wabnik et al. [239], based on the action of an auxin receptor molecule in the cell wall. Polarisation of PINs, guided by intracellular auxin gradients and mediated by a cellular auxin receptor, has been proposed by Kramer [103], however ABP1, which has been proposed by the author to be a putative receptor for this mechanism, is very unlikely to account for this because auxin binding to ABP1 is only stable in acidic compartments, while the cytosol is neutral in pH, and there is no evidence that ABP1 is present in the cytosol [230]. In up-the-gradient models of PIN polarisation, a signalling mechanism enabling the cell to react to different auxin concentrations in its neighbour cells has been proposed [89, 190], but there are also models with no specified mechanism to inform cells of

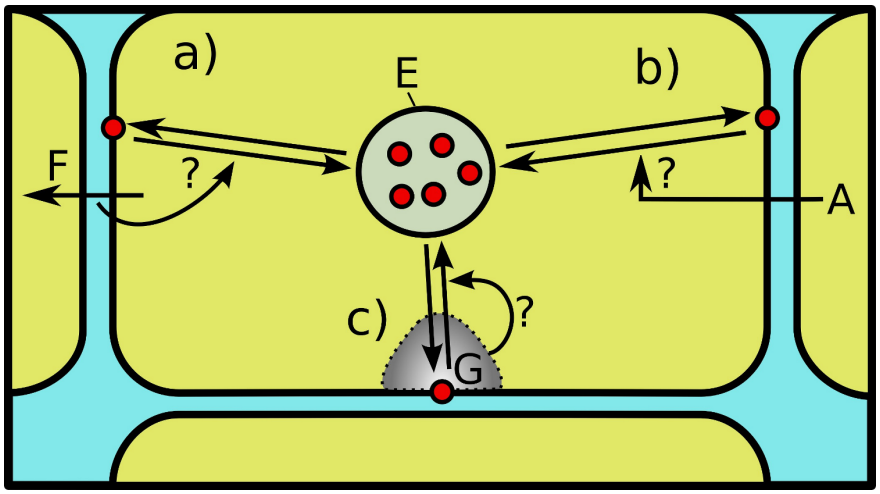

Figure 3.3: Subcellular events of PIN dynamics, as employed in auxin transport models. a) On the left, the feedback of flux (F) on PIN targeting is shown. PIN proteins (red) cycle between the membrane and endosomal compartments (E). Flux could either influence the insertion or removal of PINs from the membrane. b) The situation in up-the-gradient models: Auxin concentration in the neighbouring cell (A) feeds back on PIN cycling. c) shows the hypothetical feedback on PIN cycling driven by cytosolic auxin gradients (G) around already inserted PINs. The area G shows cytosolic auxin concentration (grey) and lower concentration near PINs (white), where auxin is depleted through active efflux. This figure is reproduced from [63].

the auxin concentration in the neighbouring cells [10, 207]. There are also alternative hypotheses for a mechanism leading towards this type of polarisation, involving the physical forces between expanding cells in the growth zone of the shoot tip [78, 152].

3.4 Concluding remarks

In chapter 2, the importance of auxin action in plant development has been reviewed on the basis of biological evidence, and it was stressed that auxin action is interlinked with auxin transport. While both are connected by several feedback loops [117], resulting in a highly complex regulatory system, auxin transport is a key aspect in this system and an important means to integrate auxin actions at different organismic levels. Computational modelling in auxin biology as an aid to understand better its dynamics has been reviewed in this section and has been shown to focus intensively on auxin transport. There are some models of auxin action available that are not explicitly focussed on auxin transport, such as a mathematical formulation of the AUX/IAA signalling mechanism in cells [137], but the majority of computer models in auxin biology

are aimed towards understanding the mechanisms underlying auxin transport, namely the nature of auxin feedback on its own transporters to establish well defined transport routes which lead to events like canalisation or phyllotactic patterning. Among those models, the vast majority have a focus on PIN polarisation on cell membranes, while there are a few exceptions that explore alternative polarisation scenarios, such as an evolutionary prototype of PIN polarisation based on the activity on 'short' PINs within cells [240].

It is quite remarkable that the obvious importance of subcellular mechanisms of auxin transport has, at least not yet, led to more attempts in focusing on auxin transport and feedback mechanisms between auxin and its transporters at a single cell level. In such a model, assumptions on the nature of such feedback mechanisms could gain much more attention than in higher-level models. As well, on the grounds that robustness in biological systems often derives from redundancy of its constituent processes [38, 241], it would be interesting to see if there are other polarisation events in auxin transport at a cell level that correspond to PIN polarisation, potentially helping to elucidate mechanistic explanations of auxin feedback on auxin transporters and the robustness and flexibility of such feedbacks.

In the next chapters of this thesis, such an attempt is made and described. First, a single cell prototype model of auxin transport is formulated and tested, and in the following extended towards a feedback mechanism that has been overlooked so far in computer models of auxin transport: the feedback between auxin and protons at a cell level. Eventually, the implications of such a feedback mechanism are tested in a spatiotemporal single cell model of auxin transport (see chapter 8).

CHAPTER 4

A single cell model prototype for PIN polarisation

From the previous chapter, it is evident that there is a need for a single-cell model of auxin transport to provide mechanistically plausible hypotheses of auxin transport and PIN polarisation on the system level of cells.

In order to estimate the scope of such a model, a 2D model prototype has been developed, including only two guiding mechanisms: (1) Auxin movement by means of diffusion within cell and apoplast, passive cellular uptake and active transport of auxin; and (2) PIN cycling dependent on auxin gradients over the membrane. The model prototype was developed to estimate and formulate the issues that could be expected from a 2D simulation of a single cell in general and, more specifically, from simulating auxin transport in that context. This chapter describes and discusses the underlying assumptions of this model, its mathematical formulation as a set of ODEs, its numerical solution by computer simulations, written in Matlab, and the results obtained. One difficulty in the model was the need to quantify polarisation in order to compare simulation results with different parameter settings. A solution for this problem has been established and is also elucidated in the following sections. The results of this model showed that PIN polarisation could be reproduced based on an auxin-gradient-driven PIN cycling mechanism, with an overall polarisation that is consistent with auxin canalisation. The scope and limitations of this model prototype are discussed at the end of

this chapter.

4.1 Assumptions and model topology

The model environment comprised one plant cell, surrounded by a cell wall and 6 boundary cells that can either act as auxin sources, auxin sinks or are inactive (neither source nor sink). The model topology is illustrated in Figure 4.1. Notable assumptions of this model are:

- The cell and its environment are represented in two dimensions.
- The cell and its vacuole are rectangular objects in this environment. The vacuole is not involved in auxin transport and allocation and is acting as a structural, inert block. It is an obstacle for auxin transport within cells
- Auxin diffuses freely within the apoplast and cytosol. The plasma membrane acts as a diffusion barrier between these two compartments. Since according to the chemiosmotic hypothesis of auxin transport cells act as 'auxin traps', it is chemically evident that auxin is *not* free to diffuse across the plasma membrane [73]. Auxin transport between apoplast and cell is dependent on three transport mechanisms in this model, (a) passive influx, (b) active influx (AUX1-mediated) and (c) active efflux (PIN1-mediated). These mechanisms will be characterized further by the following.
- PIN cycling is characterized by a symmetric insertion of PINs into the membrane at a constant rate and by a removal rate which is dependent on auxin gradients over the membrane. The pool of PINs in this model is constant and neither up-regulated by auxin on a transcriptional level nor synthesized or decaying in time.
- AUX1 importers are symmetrically distributed on the cellular membrane, and in the discretised model this is accomplished by symmetric random distribution in some membrane grid cells. It has to be noted, however, that for some root tissue cells AUX1 has also been shown to be distributed asymmetrically [215]. The rather generic model presented here does not account for this possibility, which is consistent with trying to keep the model as simple as possible.

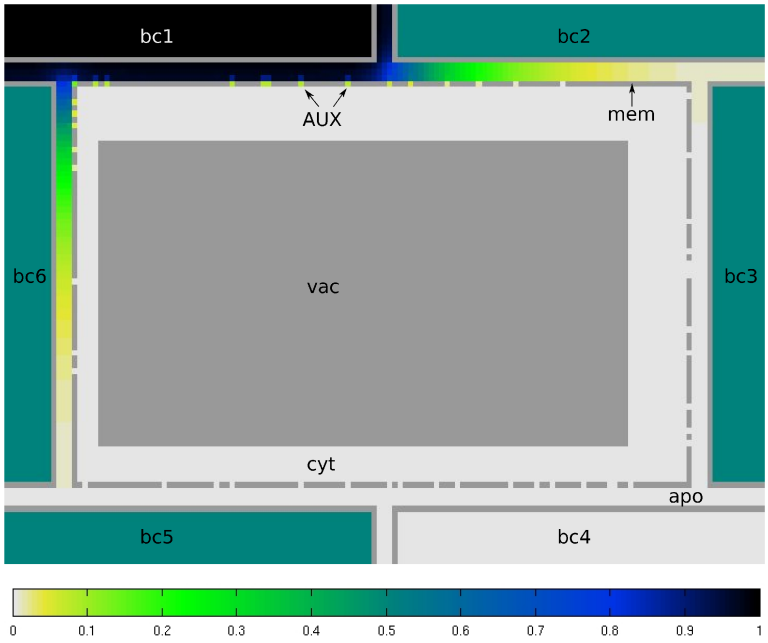

Figure 4.1: Topology of the model. A rectangular cell, bordered by a cell membrane (mem) and surrounded by 6 boundary cells (bc1 - bc6). The apoplast (apo) consists of cell wall space between the central and the boundary cells. A big vacuole (vac) is located in the cytosol (cyt) of the cell. Line breaks in the membrane symbolise the insertion sites of AUX/LAX importers (AUX). Colours represent auxin concentrations between 0 (light grey) and 1 (black), according to the colourbar, except for the cell borders, which are plotted grey for better visibility.

- The apoplast thickness is homogeneous.
- Growth is not explicitly modelled, therefore no structure in this model will expand or shrink throughout the simulation process.
- All substances occur in concentrations high enough to allow for a continuous mathematical representation of their relationships using ODEs.

4.2 Mathematical formulation

Diffusion of auxin in two dimensions is expressed by the general diffusion (heat) equation for the apoplastic compartment:

$$\frac{\partial A_{apo}}{\partial t} = D\left[\frac{\partial^2 A_{apo}}{\partial x^2} + \frac{\partial^2 A_{apo}}{\partial y^2}\right] \tag{4.1}$$

and, accordingly, for the cytosolic compartment:

$$\frac{\partial A_{cyt}}{\partial t} = D\left[\frac{\partial^2 A_{cyt}}{\partial x^2} + \frac{\partial^2 A_{cyt}}{\partial y^2}\right] \tag{4.2}$$

where A_{apo} is the amount of apoplastic auxin, A_{cyt} is the amount of cytosolic auxin and D is the diffusion constant for auxin. No diffusion takes place between the compartments apoplast and cytosol, thus the exchange of auxin between these compartments relies entirely on transport mechanisms. Movement of auxin over the cellular membrane takes place as (a) passive influx, (b) active, AUX/LAX- mediated import or (c) active, PIN-mediated export. The passive influx from apoplast to cytosol is based on the chemical affinity of apoplastic IAAH to the lipophilic cell membrane. Once in the cell, auxin dissociates due to the higher pH of the cytoplasmic environment and its affinity to the cell membrane is diminished. This reflux rate is assumed to be zero, based on the chemiosmotic model of auxin transport [186] and its indications that the amount of protonated auxin in cells is not significant, and therefore passive influx is understood as monodirectional.

The equations for auxin transport over the plasma membrane only apply for the boundary between apoplast (apo) and cytosol (cyt) in the model, such that the passive influx of auxin over the membrane (from the apoplast to the cytosol) is expressed as

$$A_{(apo \to cyt)} = \mu p A_{apo} \tag{4.3}$$

where A_{apo} is apoplastic auxin, μ is the membrane permeability for IAAH and p is the fraction of IAAH in apoplastic compartments.

Both active influx and active efflux, supported by transport proteins, are expressed as Hill functions depending on auxin concentration. Therefore, active AUX/LAX-mediated influx from apoplast to cytosol at the boundaries of these compartments is expressed by

$$A_{(apo \to cyt)} = \frac{A_{apo}^m}{K_{AUX}^m + A_{apo}^m} \tag{4.4}$$

with K_{AUX} as the saturation parameter for Auxin influx and m as the Hill coefficient for the Hill function describing a saturation equation for active influx, dependent on apoplastic auxin concentration alone.

Similar to equation 4.4, PIN-mediated active efflux from the cytosol to the apoplast at the boundaries of these compartments can be described as

$$A_{(cyt \to apo)} = \frac{A_{cyt}^n}{K_{PIN}^n + A_{cyt}^n} \tag{4.5}$$

with K_{PIN} as the saturation parameter for auxin efflux and n being the Hill coefficient for efflux.

PIN cycling. Endocytosis and recycling of PIN proteins, referred to as "PIN cycling", are based on the assumption of a pool of PINs, expressed in arbitrary units (a.u.), which is homogeneously distributed inside the cell. The total number of PINs, PIN_{tot} is constant. PINs that are near the membrane attach at an insertion rate η and rejoin the cytosolic PIN pool with an apparent drop-off rate, which is the removal rate for PINs from the membrane due to endocytosis, consisting of the background endocytosis rate k and the auxin gradient-dependent endocytosis rate g, which mirrors the strength of the auxin gradient over the plasma membrane. PIN_{frac}, the fraction of PINs near the membrane, is equal to the perimeter/area-ratio of the cytosol, under the assumption of homogeneous distribution of PINs in the cell. The amount of PINs potentially free for insertion into the membrane is $PIN_{free} = PIN_{tot} \times PIN_{frac}$. The dynamics for the PIN cycling mechanism are

$$\frac{dPIN_{ins}}{dt} = \eta PIN_{free} - (k - g) PIN_{ins} \tag{4.6}$$

$$\frac{dPIN_{free}}{dt} = -\eta PIN_{free} + (k - g) PIN_{ins} \tag{4.7}$$

where PIN_{free} is the amount of free PINs in the cytosol, PIN_{ins} is the amount of PINs inserted in the membrane, k is a basic drop-off rate for PINs inserted into the membrane and

$$g = \begin{cases} 0 & \text{if } A_{apo} \leq A_{cyt} \\ (A_{apo} - A_{cyt}) & \text{if } A_{apo} > A_{cyt} \text{ and } (A_{apo} - A_{cyt}) < k \\ k & \text{if } A_{apo} > A_{cyt} \text{ and } (A_{apo} - A_{cyt}) \geq k \end{cases}$$

The parameter g represents the feedback of auxin on the PIN drop-off rate, which is dependent on the auxin gradient over the cell membrane. If the auxin concentration in the apoplast is lower than in the cytosol, only the basic drop-off rate k determines the rate of endocytosis. If however the concentration of auxin is higher in the apoplast

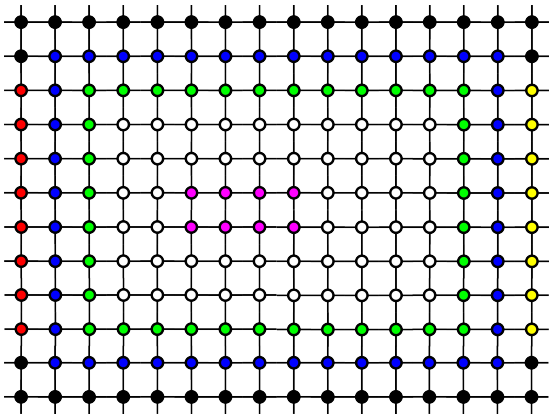

Figure 4.2: Spatial Finite Difference discretisation. As an approximation of the spatial structure of the model, the whole model environment is discretised into a 2D grid. Each grid point has a compartmental identity, represented in this figure by colours: red for auxin source, yellow for auxin sink, blue for apoplast, green for plasma membrane, white for cytosol and pink for vacuole. In the computer model, auxin transport between those grid points is evaluated (grid lines).

than in the cytosol, the endocytosis rate is diminished by the difference in auxin concentrations between the apoplast and the cytosol. The minimal rate of endocytosis is zero, such that in situations where $(A_{apo} - A_{cyt}) \geq k$, the parameter g is set to k.

4.3 Computational model

To implement the model described above in computer code, several methods have been applied and are described in the following sections: Discretisation of the model environment, implementation of the PIN cycling mechanism, definition of boundary conditions and how the computer model transports auxin at the boundary conditions and the numerical solution of the equations above.

Computational implementation of the model. The implementation of the mathematical model in computer code was based on a few further assumptions. First, the spatial information of the model has been discretised into a 2D grid order to solve the equations above numerically. The spatial discretisation of the model environment is illustrated in figure 4.2. There are several boundary conditions in this model, due to the several compartments source/sink, apoplast and cytosol involved. Thus, the transport of auxin between these compartments is defined in the following way in the computer model:

(1) While the cell in the model environment is surrounded by 6 boundary cells (see figure 4.1), exchange of auxin between the apoplast and these boundary cells only takes place if these boundary cells are defined as auxin sources or sinks. In the generic model, only one boundary cell acts as auxin source and only one boundary cell acts as auxin sink. The other boundary cells are not exchanging auxin with the apoplast.
(2) The amount of auxin in source and sink cells is fixed. Auxin transport between the source/sink cells and the apoplast takes place by diffusion.
(3) Since the model environment is spatially discretised into a set of grid points, transport of auxin between apoplast and cytosol takes place only between two neighbouring grid points if one belongs to the apoplast and the other to the cytosol.
(4) PINs are modelled as discrete units, which could be referred to as a 'pack' of molecules. The symmetric insertion of PINs into the membrane at a constant rate is implemented in the following way: First, all cytosolic grid points bordering to apoplastic grid points are numbered. These will be referred to as 'membrane' grid points in the following. At each time step that allows for PIN insertion (determined by the insertion rate η), one of these 'membrane' grid points is chosen at random. This grid point is then taking one unit of cytosolic PINs that are free to undergo PIN cycling (PIN_{free}). As long as this grid point has PIN inserted, it performs auxin efflux. The decay of PINs at these grid points (endocytosis) is evaluated at every time step. Once the PIN concentration at a 'membrane' grid point falls below a threshold (set to 0.1 in the model), the PIN unit is added to the pool of free PINs and the grid point is considered to contain no more PINs, therefore not performing auxin efflux towards the apoplast any longer. The endocytosis parameter g is evaluated locally for every 'membrane' grid point.

Explicit Method. The Finite Difference Method (FDM) was applied to discretise and solve the set of equations (4.1) to (4.7), using Matlab. A straightforward way to implement FDM is the explicit or Forward-Time-Centered-Space scheme (FTCS) [172], which was used in the first implementation of the model. Generally, with using FDM, the partial differential equations get discretised in time and space and are approximated by a set of algebraic equations [48]. The grid size was chosen to be equal both in x- and y-direction for the whole environment. Equation 4.1 can then be discretised as

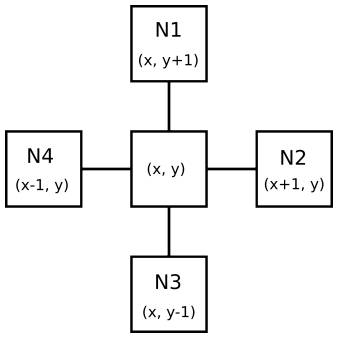

Figure 4.3: Stencil in the FDM-discretisation of the PIN polarisation model. One cell with coordinates (x, y) is connected to four neighbour cells (N1 - N4) and exchanges auxin with them. In the FDM discretisation of the whole model environment, every cell is connected to its neighbouring cells in this manner, creating a rectangular grid.

$$\frac{\Delta A(x,y)}{dt} = D\left[\frac{\Delta A(x) + \Delta A(y)}{dx^2}\right] \tag{4.8}$$

where dt is a discrete time step, dx is the chosen grid size, which is equal in direction x and y, $\Delta A(x,y)$ is a discrete change of auxin at the point (x,y), $\Delta A(x)$ is the difference of auxin concentration at point (x,y) to the neighbouring grid points in the x-direction, and $\Delta A(y)$ is the difference of auxin concentration at point (x,y) to the neighbouring grid points in the y-direction.

Using the explicit method, at each iteration point, the new auxin values on the grid point (x,y) at time $t+1$ is approximated from the values of time t, by using the values of the grid point and the surrounding grid points, which forms a so-called stencil as the unit of the whole spatial grid (see figure 4.3). Equation 4.8 can be solved explicitly as

$$\frac{A^{t+1}_{(x,y)} - A^{t}_{(x,y)}}{dt} = D\left[\frac{A^{t}_{(x-1,y)} + A^{t}_{(x+1,y)} + A^{t}_{(x,y-1)} + A^{t}_{(x,y+1)} - 4A^{t}_{(x,y)}}{dx^2}\right]$$

and, transferring all values at time t towards the right hand side,

$$A^{t+1}_{(x,y)} = A^{t}_{(x,y)} + dt \cdot D\left[\frac{A^{t}_{(x-1,y)} + A^{t}_{(x+1,y)} + A^{t}_{(x,y-1)} + A^{t}_{(x,y+1)} - 4A^{t}_{(x,y)}}{dx^2}\right]$$

Time step, grid size and diffusion constant can, for better readability, be combined to a term r, which is defined as

$$r = \frac{dt \cdot D}{dx^2}$$

and the explicit solution for equation 4.8 finally gets simplified as

$$A^{t+1}_{(x,y)} = A^{t}_{(x,y)} + r\left[A^{t}_{(x-1,y)} + A^{t}_{(x+1,y)} + A^{t}_{(x,y-1)} + A^{t}_{(x,y+1)} - 4A^{t}_{(x,y)}\right] \tag{4.9}$$

Thus, the solution of equation 4.1 using the explicit method is the evaluation of auxin at time $t+1$, according to eq. 4.9 for every grid point at every time step in the simulation. Equations 4.3 to 4.7 are processed the same way (note, however, that only 4.1 describes a two dimensional process).

Using the explicit method, one has to consider the stability criterion for r, which has to satisfy the Courant-Friedrichs-Lewy stability criterion $r \leqslant \frac{1}{4}$ [172] to reach numerical stability of the solution [48]. In order to meet this criterion, time steps had to be chosen very small. After implementation of this method it was soon clear that the solution was numerically unstable due to the diffusion term, and by choosing a sufficiently small time step, computational costs grew enormously.

To solve this instability problem, an implicit scheme for solving the diffusion equation was implemented.

Implicit method. Equation 4.8 can also be solved implicitly, using the Backward-Time-Centered-Space (BTCS) scheme [172], which leads to

$$A^{t}_{(x,y)} = A^{t+1}_{(x,y)} - r\left[A^{t+1}_{(x-1,y)} + A^{t+1}_{(x+1,y)} + A^{t+1}_{(x,y-1)} + A^{t+1}_{(x,y+1)} - 4A^{t+1}_{(x,y)}\right]$$

and further,

$$A^{t}_{(x,y)} = (1+4r)A^{t+1}_{(x,y)} - rA^{t+1}_{(x-1,y)} - rA^{t+1}_{(x+1,y)} - rA^{t+1}_{(x,y-1)} - rA^{t+1}_{(x,y+1)}$$

Auxin concentrations at time $t+1$ are now on the right hand side of the equation. If this equation is written for every point (x, y) in the modelling environment, it leads to the formulation of a system of linear equations that can be solved implicitly. The resulting system of equations has as many variables as there are grid points in the modelling environment. With this method, auxin concentrations of all grid points in the model environment at each time step are evaluated by standard matrix solving techniques. In matrix notation, this system of equations can be expressed as

$$M \cdot x = b$$

where M is the sparse band matrix representing the connectivity of all grid points in the environment, x is the vector of all grid points and b is the result vector, containing

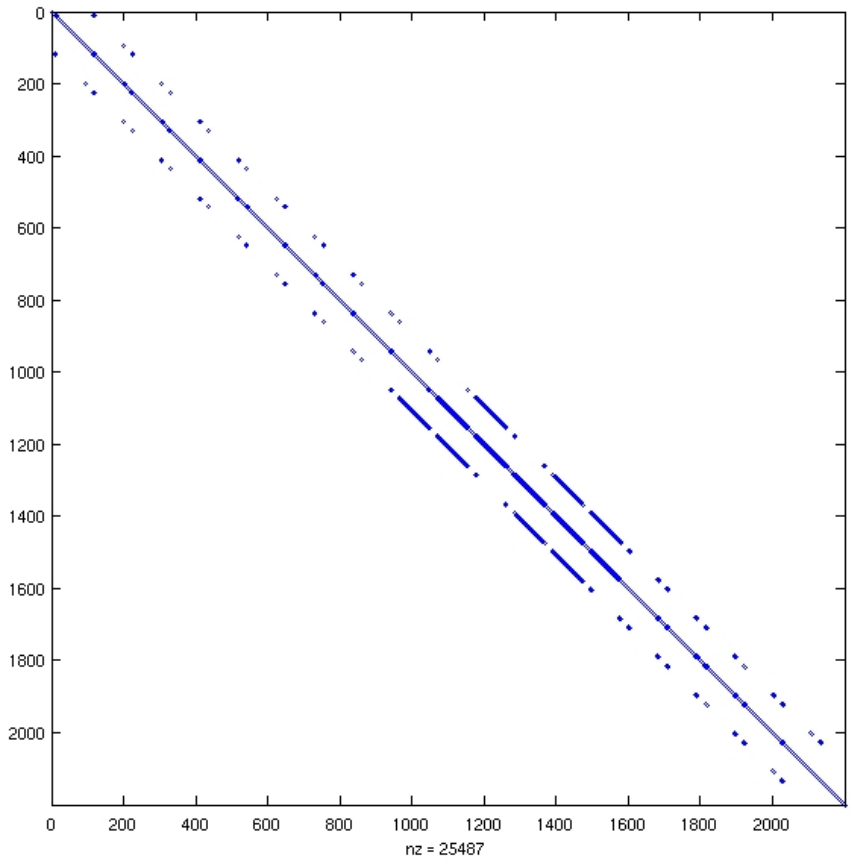

Figure 4.4: Sparse connectivity matrix of the model environment used for solving the diffusion part of the equations with an implicit method. Only the first 2200 elements of the matrix are displayed (the total matrix was of size 10004 x 10004 elements).

the auxin concentration of every grid point. Once expressed in this form, the set of linear equations can be solved using matrix methods, such as LU decomposition. For one grid cell and its 4 neighbours this would look like the following:

$$\begin{bmatrix} 1+4r & -r & -r & 0 & 0 \\ -r & 1+4r & -r & -r & 0 \\ -r & -r & 1+4r & -r & -r \\ 0 & -r & -r & 1+4r & -r \\ 0 & 0 & -r & -r & 1+4r \end{bmatrix} \times \begin{bmatrix} X_1 \\ X_2 \\ X_3 \\ X_4 \\ X_5 \end{bmatrix} = \begin{bmatrix} b0+bc1 \\ b0+bc2 \\ b0 \\ b0+bc4 \\ b0+bc5 \end{bmatrix}$$

where X_3 would be the central grid cell and X_1, X_2, X_4, X_5 the surrounding neighbours. The result vector b contains the values $b0$ (the initial condition) and bc, the boundary condition for every neighbour cell. A sparse matrix would be the extension of this example over the whole model environment. It contains the information of connectivity

between all grid points. Its number of elements is thus $n^2 \times n^2$, with n being the number of grid points. By far most entries of the sparse matrix are zero, hence its name. The sparse matrix of this model is illustrated in fig. 4.4.

One of the advantages of the implicit method over the explicit method is its unconditional stability that allows for much bigger time steps. As for the error of this method, the FTCS scheme is first order accurate in time and second order accurate in space. This means that the global error is smaller in the spatial dimension than in the time dimension [172].

4.4 Computer simulation

The model was implemented using Matlab. A list of all parameters in this model is provided in the table A.1 (appendix). Auxin diffusion was solved with the implicit method, while all other equations were solved explicitly at the same time step. Simulations, using a time step size of 0.1 seconds and an overall simulation time of 20 minutes (12000 iterations) led to accumulation of auxin in the cell and internalization of PIN proteins. Polarisation of PINs occurred within 5 minutes of the simulation time and stayed stable throughout the remaining simulation, even with longer simulation time (for a detailed description of the results see the section 4.5). However, though the polarisation of PINs was visible and easy to detect rather intuitively from the visual simulation output, this result showed an urgent need for unambiguous quantitative description. The question whether or not, and to what extent, polarisation is measurable turned out to be an important one and thus will be discussed in the following section.

Measuring polarisation

In published models of auxin transport dealing with polarisation the pattern of PIN localisation in the membrane and thus polarised cells are either input of the model, obtained from immunocytochemical labelling of PIN proteins in real plant tissue, revealing a somewhat fixed pattern of PIN localisation that does not change throughout the simulation [37, 73] - or, if polarisation is an output of the model, e.g. [10, 54, 89], it is validated by the successful reproduction of an overall polarisation pattern matching that observed in real tissue and is directly visualised. So, for instance, if the model can reproduce the formation of a new auxin canal between new leaves and already

existing vascular bundles, polarisation and subsequent direction of auxin flux can be arguably determined as to occur 'in the right way'. This kind of argumentation is sufficient because it reproduces what can be seen in plant development. In this case, polarisation is either supposed to be occurring or not, which means, leading to a final state that matches real-life outcomes or not.

These approaches, both used in models on a tissue level, make it somewhat unnecessary to define and measure polarisation quantitatively. This may explain why no previous model of PAT has provided some quantitative measurement of polarisation. This, however, seems to be important for models of single plant cells outside of a tissue context, as in this study.

PIN polarisation could be defined as (1) heterogeneous distribution, leading to clusters of inserted PIN proteins and (2) a stable directionality of the PIN cluster. It may seem redundant to mention directionality here, because polarisation as described in point (1) is no less polarisation if the cluster location changes or fluctuates in time. But from a biological perspective, directionality may be important in polarisation measurement, as we will see below. If PINs direct auxin transport, the overall auxin flux through a part of the plant tissue is the sum of all momentary polarisation directions. If PIN clusters on the membrane fluctuate over time, the resulting auxin flow through the tissue would become non-polar, or at least its polarity would be reduced by the changes of PIN localisation on the cellular level over time.

To formalise this definition, two values are introduced, the polarisation strength, p, and the centre of polarisation, pc. In the computational model, the membrane is defined as the set of cytosolic grid points that border to apoplastic grid points. The amount of all membrane grid points is denoted by m and every membrane grid point is assigned a number such that the numbering from grid point 1 to grid point m signifies the circumference of the membrane in the 2D model environment, evaluated by a clockwise count of all membrane grid points of the model environment. If the membrane is divided in equally sized sectors (in the following, we will consider the case of sectors with the length $m/2$), the polarisation sector is the sector with the highest amount of PINs inserted at each discrete time step, and therefore defines the half of the membrane $(m/2)$ with most PINs inserted. To illustrate this, a sector spanning the range

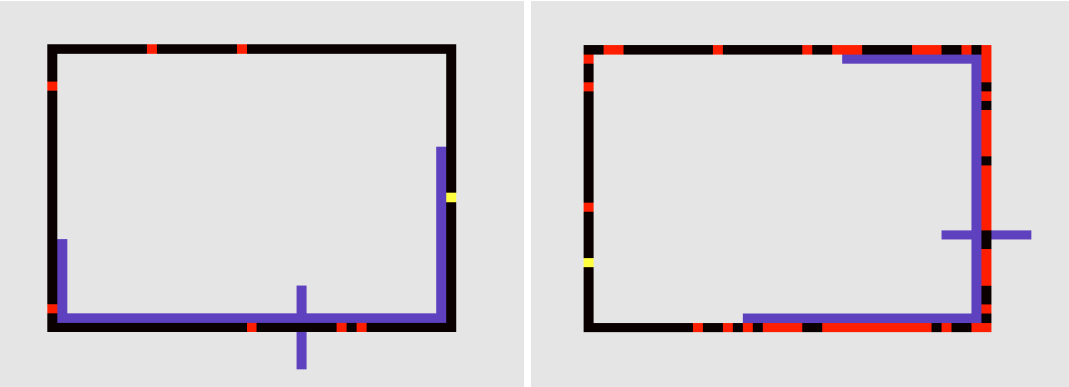

Figure 4.5: PIN polarisation at time t=90 s (left) and at time t=300 s (right) in one simulation. Inserted PINs are red dots on the cellular membrane (black). The polarisation sector is the violet line parallel to the membrane, the polarisation centre is signified by a short violet line perpendicular to the membrane. The bright yellow dots are PINs just inserting into the membrane at this time step.

from the upper left to the lower right corner of the membrane on the 2D representation of the model environment would involve all membrane grid points mg which satisfy the condition $1 \leq mg \leq m/2$. Thus, during the exhaustive search for the polarisation sector in the computational model, all m possible numbers of membrane sectors are checked for the amount of PINs inserted and the polarisation sector sct_{pol} is then defined as the vector containing all membrane grid point numbers of the section with highest amount of inserted PINs,

$$sct_{pol} = \left\{ n \ (mod \ m), n+1 \ (mod \ m), \ \ldots \ , n+\frac{m}{2} \ (mod \ m) \right\}$$

with n being the membrane grid point number at which the sector with highest amount of inserted PINs starts. The membrane grid point which is the half point of this sector is defined as the polarisation centre pc. The polarisation strength p is defined as the relative amount of PINs inserted in the polarisation sector, $PIN_{sct_{pol}}$, compared to the total amount of PINs in the membrane, PIN_{tot}.

$$p = \frac{PIN_{sct_{pol}}}{PIN_{tot}}$$

In general, we then can define polarisation as

$$P = \bar{p} \left(\frac{m - \sigma_{pc}}{m} \right) \tag{4.10}$$

where $\bar{p}$ is the mean value of polarisation strength and σ_{pc} is the standard deviation of the polarisation centre during the time course. This connects both parts of the above presented definition with each other, assuming that a weak polarisation with a stable directionality has a similar effect on directed auxin flow as a strong polarisation with unstable directionality.

An algorithm was designed, using exhaustive search to find polarisation sectors, and implemented in the model, and the values of p and pc were stored for every time step. The graphical outcome of this determination of polarisation sector and centre can be seen in fig. 4.5.

4.5 Results

The simulations had a running time of approximately 2 hours for 12000 iterations on a machine with a 3 GHz Core Duo E8400 processor and 4 GB RAM and resulted in an equilibrium of auxin gradients usually within 5 minutes simulation time. Polarisation equilibrated when auxin gradients reached their equilibrium.

Two different boundary conditions for auxin concentrations were used in the simulations: in the first, auxin source cells contained 1 arbitrary unit (a.u.) of auxin and auxin sinks contained 0 a.u. The second boundary condition that was tested defined auxin concentrations in source cells to be 0.8 a.u., as opposed to sink cells containing 0.2 a.u. Of the 6 boundary cells, those that have not been defined as source or sink cells do not exchange auxin with the apoplast (for visualisation reasons, they have been assigned the value 0.5 a.u., which can be seen in figure 4.6). The test for different auxin source and sink strengths has been undertaken to compare PIN polarisation strengths in differing strengths of apoplastic auxin gradients (see below). While the polarisation proved to be sensitive to auxin concentration gradients in the apoplast, the cytosolic auxin concentration at the end of simulations was comparable in both settings of boundary conditions for auxin, given that the other parameters k and P_{ins} were the same (see figure 4.6). Therefore, auxin gradients over the plasma membrane were found to be dependent to a high degree on the apoplastic auxin gradient. Thus, a lower apoplastic auxin gradient also brings about lower auxin gradients over the plasma membrane.

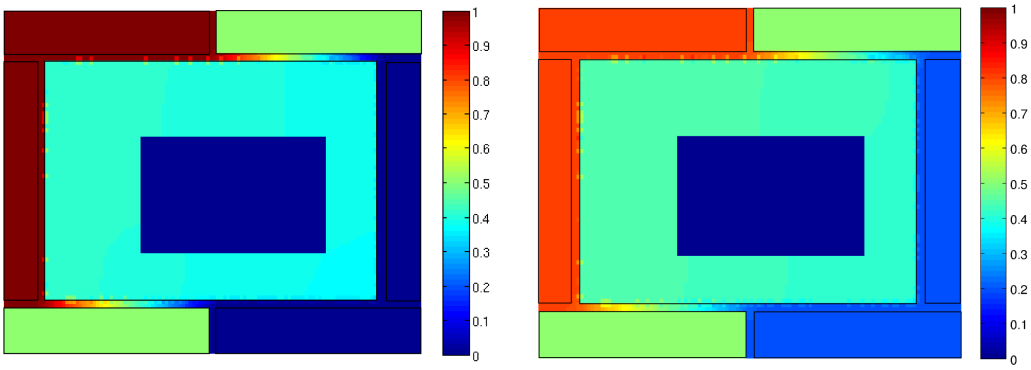

Figure 4.6: Auxin concentration in cells with two different boundary conditions for auxin concentration and the parameter settings $P_{ins} = 1$, $k = 0.01$. Polarisation direction is towards the sink boundary cells. *Left:* Auxin concentrations in the model environment at the end of 12000 iterations with boundary conditions $A_{source} = 1$ and $A_{sink} = 0$. Boundary cells containing $A = 0.5$ do neither export nor import auxin. *Right:* Auxin concentrations in the model environment at the end of 12000 iterations with boundary conditions $A_{source} = 0.8$ and $A_{sink} = 0.2$. For the topology of the model environment, refer to figure 4.1.

Stable polarisation of PIN proteins in the cell membrane was obtained mainly with $k < 0.2$ and $P_{ins} > 1$. The results from a set of simulations using different parameter values for k, P_{ins} and A_{source}/A_{sink} showed that the modelled system does not produce the same output with all parameter settings.

The resulting scenarios of PIN polarisation are pictured in fig. 4.7. The figure shows the extreme possibilities between which most outcomes occurred - between a stable centre of polarisation and fluctuating polarisation sectors. This illustrates quite well the usefulness of our definition of polarisation, as stated above.

To estimate parameter influence on polarisation, a set of simulations was run with different values of 4 selected parameters, of which two, namely the drop-off rate for PINs k and the PIN insertion rate ins have an effect on the strength of polarisation (see fig. 4.8). The size of the vacuole did not seem to change polarisation establishment and strength. As well, two settings for auxin sources and sinks were tested in order to check the influence of global auxin gradients (difference between concentrations of auxin source and sink cells) on polarisation strength. Outcomes with stronger global auxin gradient $G_A(1)$ ([Auxin(source) = 1, Auxin(sink) = 0]) were compared against the weaker gradient $G_A(0.6)$ ([Auxin(source) = 0.8, Auxin(sink) = 0.2]). The mean polarisation strength for $G_A(1)$ was $P = 0.75$, against $P = 0.67$ for $G_A(0.6)$ (with standard

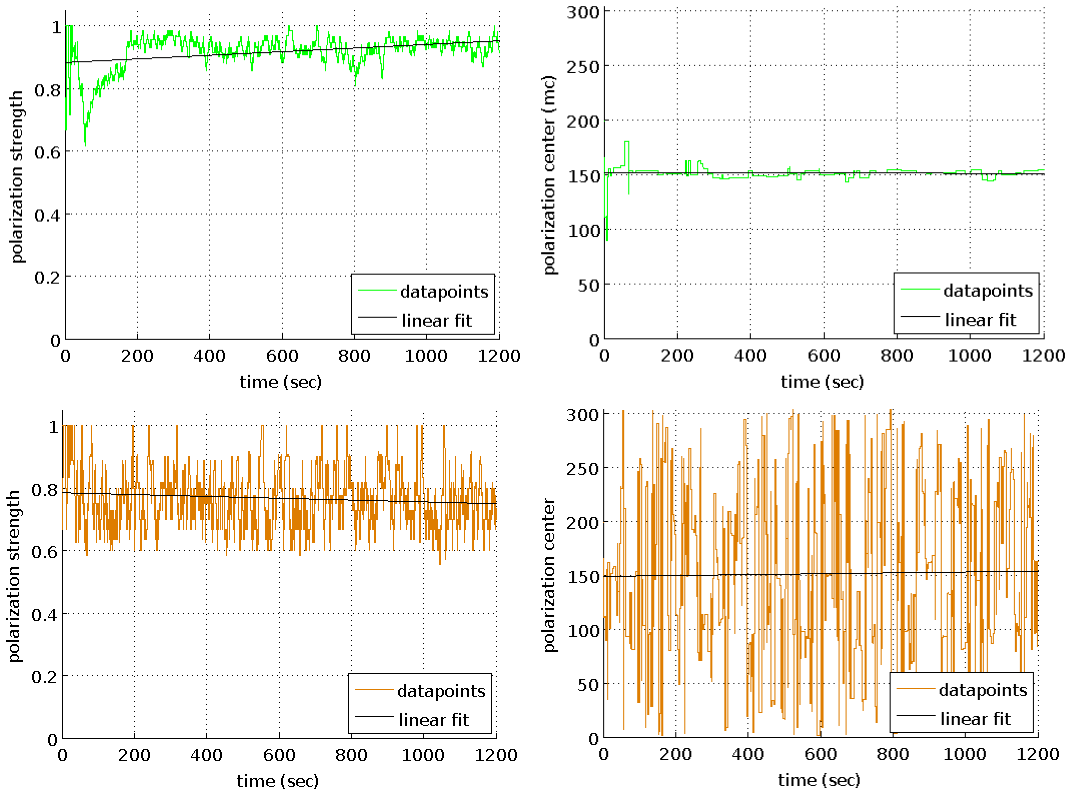

Figure 4.7: Two different polarisation scenarios. Above: High polarisation strength coupled with a stable center of polarisation (using a PIN drop-off rate of $k = -0.01$). Below: Medium polarisation coupled with fluctuating centers of polarisation (with $k = -0.2$)

deviations of 0.16 and 0.14, respectively) in the set of simulations with differing parameters for k, *ins* and the size of the vacuole. Notably, strong polarisation above $G_A(0.6)$ only occurred for the least values of k, which seems to counteract weak global auxin gradients by amplifying the response to the gradient. This result indicates that a steep apoplastic auxin gradient across the tissue is necessary for the establishment of a strong polarisation signal for PINs.

4.6 Discussion

The PIN polarisation model presented above is able to reproduce PIN polarisation events on a cellular level that are consistent with the canalisation hypothesis [189], based on a small set of assumptions. The mechanism driving PIN polarisation relies on auxin gradients over the membrane, which are assumed to alter the drop-off rate of PINs from the membrane, probably mediated by endocytosis [97]. While feedback

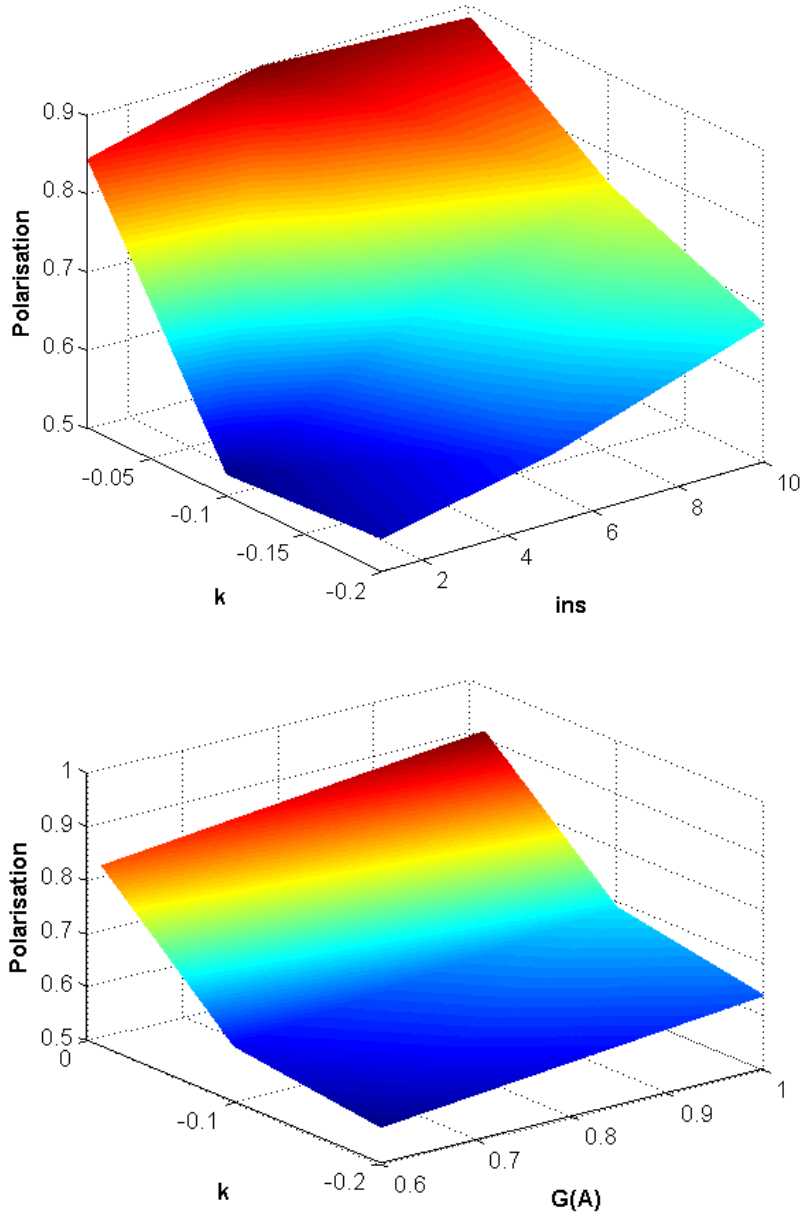

Figure 4.8: Parameter analysis: Strength of polarisation (unitless) with different parameter settings, based on linear interpolation of the results. *Upper*: Parameters *ins* versus k and their influence on polarisation strength. *ins* is the membrane insert rate of PINs per second, k is the basic drop-off rate for inserted PINs. *Lower:* Polarisation as a function of extracellular auxin gradients $G(A)$, and the influence of the PIN insertion rate k on this effect.

of auxin on PIN stability on the membrane is consistent with biological findings [40, 159], auxin gradients over the membrane might not be necessary for such a feedback. During the modelling process a quantitative expression of polarisation strength has been developed and proved to be useful for simulation comparisons. The simulation resulted in the establishment of polarisation within several minutes for most parameter settings. This may be too fast compared to biological time scales of polarisation, which is in the range of hours. However, the simulation might be scalable by adjusting the model parameters, particularly the rate of symmetric PIN membrane insertion and the basic PIN drop-off rate. This has not been undertaken on larger time scales, but variations of the PIN insertion rate ins during parameter sensitivity analysis suggest that the time frame is indeed scalable in this manner, since PIN polarisation converged more slowly with lower insertion rates. Additionally, lowering the basic drop-off rate k for PINs also counteracted the tendency towards lower polarisation strength as ins was reduced. Moreover, parameter sensitivity analysis indicated that the strength of the apoplastic auxin gradient between auxin source and sink cells is critical for a high polarisation strength (see fig. 4.8). The size of the vacuole seems not to influence auxin gradients across the plasma membrane.

The model includes several simplifications and assumptions that may not reflect the behaviour of plant cells in a way that is sufficiently realistic. Many feedback mechanisms described in Chapter 1 are not considered, such as the up-regulation of PIN expression by auxin or the role of other proteins of the PIN family or factors whose functions are necessary to establish PIN polarisation (eg. PINOID kinase or GNOM, see [67, 98, 222, 182]). However, including these factors might not change the overall results of the PIN polarisation model prototype, because they are likely to only either influence the response strength (for the case of PIN up-regulation) or provide the necessary condition for PIN cycling, both of which may not influence the qualitative behaviour of the model. Beside this, the extracellular auxin gradient in the basic model might be much steeper than in real plant tissues. Especially if the diffusion constant for Auxin is really as high as it is considered to be in some studies [73, 89], one would expect that apoplastic auxin gradients would soon blur, in which case the PIN cycling mechanism presented here would not yield clear polarisation patterns. However, exact measurements of apoplastic and cytosolic auxin concentrations are still elusive.

At this point, some very interesting questions arise which will be further investigated in the following sections. First, if PIN polarisation is driven by auxin gradients, how would PINs be able to sense these gradients? Gradients as a mechanistic explanation are not very likely, however they could, together with PIN polarisation, be the result of lower level mechanisms. What could be the nature of such mechanisms? And what is the role of apoplastic auxin gradients in this context? The discussed model gives some consistent results, but not much insight for polarisation events on a single cell scale. This might be due to an apparent lack of complexity, suggesting that more biological detail has to be added to yield a satisfactory computational model that provides us with stronger hypotheses on auxin transport and PIN polarisation on a cellular level. Because of that, in the following chapters the number of agents involved will be increased and the question of the importance of auxin/proton interaction is brought into focus.

CHAPTER 5

Auxin and protons

In the last chapter, a model prototype for auxin transport in a single plant cell has been presented. The analysis of its results showed the need to include further details in such a model in order to get more useful insights about the mechanisms driving auxin transport and the polarisation of auxin transporters at a single cell level. A very obvious aspect of auxin transport is based on steep proton gradients between compartments. Plant cells are surrounded by cell walls, which provide a rigid structure to withstand the osmotic pressure in cells [209]. The cell wall space consists of a component mixture of proteins, polysaccharides and lignins varying in composition between plant species [205], allowing small molecules to move around freely within the extracellular space. While the cytosolic compartment of cells has a pH of 7 to 7.5, the apoplast is much more acidic, with a pH usually below 6 [52]. As has been already mentioned in section 2, the chemiosmotic hypothesis of auxin transport [186] proposes that compartmental pH influences auxin, a weak acid with a pKa around 4.75, by changing its dissociation status and subsequently altering its passive transportability across the plasma membrane. This is dependent on observations that the plasma membrane has a lower permeability for anionic auxin (IAA^-) than for protonated auxin (IAAH) [74, 174].

From that, it seems that auxin and pH are related at least in part. Apoplastic and cytosolic pH play a role in determining how much auxin enters and leaves the cell passively. But not only passive auxin transport is dependent on protons. While auxin efflux is to some extent due to ABCBs (PGPs), energised by ATP alone, the activity of

two other families of auxin transporters is dependent on the proton motive force over the plasma membrane: (a) PIN auxin efflux facilitators [21, 167], especially the long PINs (PIN1, PIN2, PIN3, PIN4 and PIN7) [255], and (b) AUX/LAX importers, acting as auxin/proton symporting proteins [94, 251]. Thus, auxin transport from cell to cell is possibly dependent on compartmental pH. This has certain implications for the understanding of the dynamics of auxin transport in mathematical modelling. To estimate the strength of auxin influx and efflux, energisation by the proton motive force needs to be considered. While some available auxin transport models have included this detail [239, 103], others have merged it with auxin transport rates [4, 10, 73, 89, 207, 211]. Since the latter do not include the apoplast as a seperate compartment, this seems to be a perfectly valid method. And, assuming that compartmental pH does not change over time, it might also remain valid if the apoplast is explicitly modelled (which is the case in the root model of Grieneisen et al. [73] and in the leaf vein formation model of Alim and Frey [4]). However, there is a large body of evidence that compartmental pH is not stable during auxin transport. Auxin has been found to activate plasma membrane proton pumps, thus lowering apoplastic pH [51, 76, 91, 181, 200, 245], a finding that is often associated with the so-called acid growth hypothesis of auxin [76], which is discussed in the following section.

If auxin transport is dependent on pH and on the other hand pH itself is dependent on auxin concentration, we are confronted with an interesting feedback phenomenon, leading to questions of the specific quality and dynamic properties of such a feedback. If lower apoplastic pH causes more auxin to enter cells, more auxin in cells cause the apoplastic pH to drop, then possibly even more auxin is able to enter the cell. This could be due to (a) a stronger proton motive force over the plasma membrane, supporting AUX1/LAX action, (b) a change in auxin dissociation status in the apoplast, or (c) a mixture of both. But how valid is this idea?

The possibility of such a feedback phenomenon between auxin and pH has been presented before [73, 114], but has to our understanding not yet been tested rigorously by computational modelling. However, modelling may help to understand better the plausibility, quality and stability of such a phenomenon and can help to advance our understanding of auxin transport by simulating several possibilities of auxin/pH interactions at a cell level. In this chapter, such a model is described. First, the model construction

by splitting the modelling process into subunits is documented, and each subunit is tested against biological data. These subunits are (1) pH homeostasis in plant cells, (2) auxin dissociation and transport over cellular membranes, and (3) activation of proton pumps by auxin. After validating each submodel through experimental settings reproducing real, 'wet' experiments already undertaken, the submodels are merged into a single, non-spatial model of auxin/pH interactions. This model is again tested against biological data (mainly dose-response experiments for auxin). Finally, the parameter sensitivity of the model is evaluated and implications of the model results are discussed and compared to what we already know from plant biology.

However, before the auxin/pH model is presented, the status of relevant research is reviewed, mainly aiming to give background information on the importance of pH in plant cells, on the mechanisms that lead to pH homeostasis and on potential mechanistic explanations of the interplay between auxin and proton pumps.

In the following sections, the relationship between auxin and pH is reviewed on the basis of available literature. As well, published models of auxin transport and pH homeostasis in plants are reviewed.

5.1 Maintenance of pH in plant cells

The cytosolic pH lies between 7 and 7.5, according to most biological measurements [52, 105, 204, 254]. Cytosolic pH is regulated by four mechanisms: H^+ binding by buffering groups, H^+ transport out of the cell, H^+ transport into the vacuole, and the so-called biochemical pH-stat, controlling the number of carboxyl residues, such as malate [139]. Transmembrane proton fluxes are compensated by other ion fluxes [17]. These compensatory ion fluxes (mainly K^+ and Ca^{2+}) are not considered in the auxin/pH model. While K^+ and Ca^{2+} are contributing to the electrochemical gradient over the membrane and the inclusion of their transport mechanisms might be useful in models investigating membrane potentials, the scope of the model presented in the following sections is rather on the proton motive force over the plasma membrane which is energising auxin transporters and thus K^+ and Ca^{2+} are omitted.

Generally, the role of cytoplasmic buffering is considered to be of minor importance in overall pH homeostasis, as compared to the role of proton pumps (H^+-ATPase) [109].

Both cytosol and apoplast contain proton buffering components. The cytosol shows a mean buffer capacity of around 30 $^{mM}/_{pHunit}$ [43, 52, 76, 81], characterizing the amount of added protons to cause a drop of 1 pH unit. This buffering capacity is in the same range as in animal cells [109]. The apoplast with its typical pH between 5.25 and 6.75 shows a much bigger acidity tolerance [86] and therefore a much lower buffering capacity than the cytosol (around 3 to 4 $^{mM}/_{pHunit}$) [155]. The change of apoplastic pH depends mainly on the modulation of plasma membrane bound H^+-ATPase activity, but also on proton-coupled nutrient transporter action, on the export of acid metabolites and on CO_2 evolution [169]. These metabolic contributions to pH are not considered in the presented model. Experiments and mathematical modelling of unicellular plant organisms (*Eremosphaera viridis*) showed that, apart from cytoplasmic buffering, short-term active response of cytoplasmic pH regulation could be mainly due to the vacuolar H^+-ATPase activity [155]. Plasma membrane bound proton pumps are, according to some studies, rather exporting H^+ at a constant rate [17]. However, this might differ to the situation in multicellular plants, where apoplasts do show a low buffering capacity and thus plasma membrane bound proton pumps may not be involved in fast regulatory response to cellular acidification. As mentioned before, H^+-ATPase activity is pH-dependent: acidic conditions in the cytoplasm activate proton pumps [17], alkalinisation inhibits them [109]. Lowering the cytosolic pH, e.g. by lactic acid, induces plasma membrane H^+-ATPase (proton pump) activity [76]. Optimal pumping rates occur at cytoplasmic pH values around 6.6 and regulation of proton pump activity by pH seems to rely on a some form of direct pH sensing, however the exact mechanism behind that is not fully known [109].

5.2 Auxin/pH interactions

There is evidence that auxin and pH influence each other mutually. One side of this interaction is characterized by the pH dependence of auxin dissociation and by the dependence of auxin transport over the cell membrane by either the proton motive force (energization of auxin transporters) or the amount of dissociated auxin (permeability of the membrane for dissociated versus undissociated auxin). The other part of this interaction is auxin-dependent pH changes, especially auxin-induced apoplastic acidification (see figure 5.1). Both directions of auxin/pH interactions are briefly reviewed

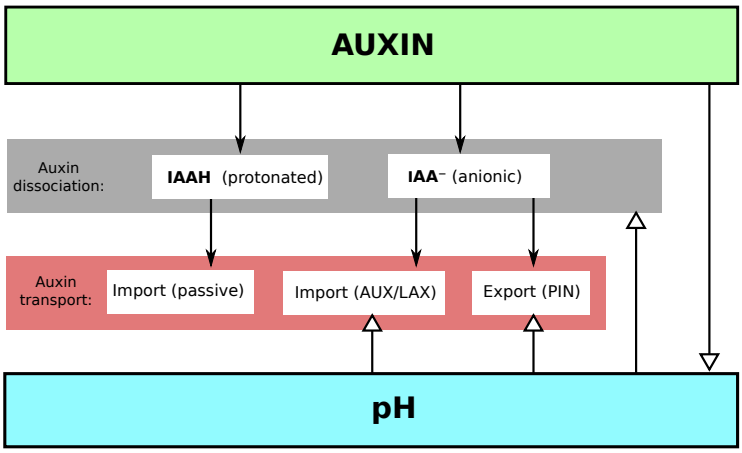

Figure 5.1: Feedbacks between auxin and pH. Auxin dissociation is dependent on pH, while (apoplastic) pH itself is altered by auxin stimulation of proton pump activity. Auxin transport is also pH-dependent, either directly by the strength of the proton motive force for transporter energization (AUX/LAX and PIN transporters) or indirectly by the abundance of protonated auxin for passive auxin uptake. Full arrow heads mean 'contributing to', while empty arrow heads mean 'influencing' or 'changing'. Empty arrow indicate the influence on processes (e.g. pH influences the rates of conversion between protonated and anionic auxin).

in this section.

5.2.1 Effect of pH on auxin

Formulating auxin dissociaton yields the kinetic equation

$$IAAH + H_2O \rightleftharpoons IAA^- + H_3O^+$$

The pKa for this reaction is 4.75 (see [220]). Therefore, the dissociation curve for auxin due to the compartmental pH can easily be calculated (see fig. 5.2). From the pH dependence of dissociation, it can be concluded that nearly all auxin is anionic inside the cell, whereas there is a higher fraction ($> 10\%$) IAAH in the apoplast, dependent on the acidity of the cell wall space: The lower the apoplastic pH, the more auxin remains undissociated.

Another influence of pH on auxin concerns auxin transport, which is pH-dependent to some extent. This relationship has been expressed as pH-dependency of auxin transport speed through plant tissues in older studies [79, 174]. Now that some of the membrane-bound transport proteins involved in this process have been identified, more detailed characterization is possible. The auxin importers of the AUX/LAX family

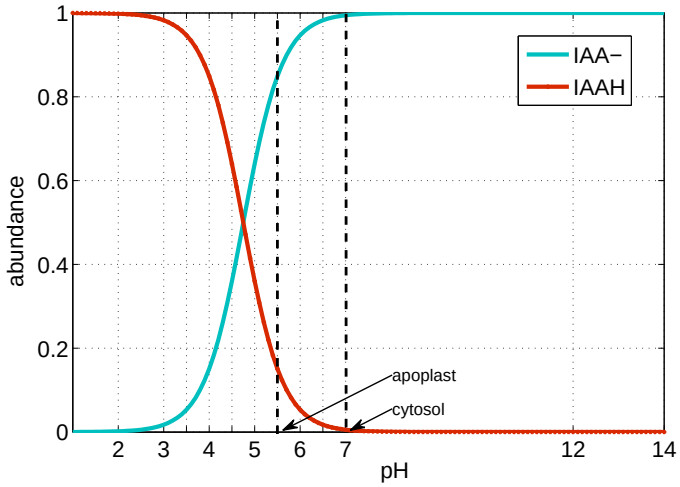

Figure 5.2: Dissociation of auxin. The dissociation curve for auxin, omitting the effect of protons bound or freed by auxin during the dissociation process. In the cytosol, nearly all auxin is anionic (IAA^-), whereas the apoplast contains a higher fraction of protonated auxin (IAAH). Auxin abundance is expressed in arbitrary units. The dissociation status in the cytosol (pH 7) and apoplast (pH 5.5) are highlighted.

act as symporters, carrying two protons for every anionic auxin molecule [94, 251]. On the other hand, efflux carriers from the PIN famliy are energised by the proton motive force across the plasma membrane [105]. And, as already stated by the chemiosmotic hypothesis of auxin transport [186], the dissociation status of auxin in the apoplast defines passive uptake of auxin in cells by defining the amount of extracellular non-polar auxin and therefore the strength of passive influx over the cell, which is limited to non-polar auxin (see figure 5.1).

5.2.2 Auxin effects on pH

Auxin acidifies the apoplast in a concentration-dependent manner within the scope of usually 1-2 pH units for maximum acidification [56, 76, 91, 200, 245]. This has in previous years often been discussed under the term *acid growth hypothesis* [76, 110, 175], which states that this acidification accounts for the loosening of the cell wall structure, which is a necessary step towards the growth of cells, since the rigidity of the cell wall does not allow for growth under normal conditions. There are also other factors involved in this process, and catalysing it, such as expansins [44, 192]. A low apoplastic pH indeed seems to be a condition for cell wall loosening, as has been shown with acidic buffer experiments and the treatment of plant tissues with the fungal toxin fu-

sicoccin, a 'super-auxin' [32], which activates plasma membrane proton pumps by the displacement of the C-terminal inhibitory domain of the H^+-ATPase [87]. However, some authors expressed doubt that auxin-induced acidification would be sufficiently strong to account for growth [110, 111, 199]. The mechanisms by which auxin induces apoplastic acidification are still unclear. However, there are three concurrent hypotheses which shall be discussed in the following: (a) the ABP_{57} hypothesis, (b) the H^+-ATPase up-regulation hypothesis, and (c) the ABP1 hypothesis.

(A) The ABP_{57} hypothesis. In one study based on data from maize seedlings, a putative candidate for a component of this mechanism, ABP_{57} , has been shown to be involved in stimulation of proton pumps in the presence of auxin in PM (plasma membrane) vesicles [95]. According to this model, ABP_{57} has two binding sites for auxin and stimulates H^+-ATPase if one, and only one, of the docking sites for auxin is occupied (see figure 5.3). This mechanism could account for the bell-shaped dose-response curves of apoplastic acidification as a response to auxin [56, 91, 200, 245]. However, there are several drawbacks to this hypothesis. First, the effect of ABP_{57} has so far only been demonstrated in vitro with isolated plasma membrane vesicles containing H^+-ATPase , but not yet in vivo, and on the other hand, ABP_{57} is not ubiquitous in plants [113], so for instance *Arabidopsis thaliana* does not have a homologue of the protein proposed to account for ABP_{57} activity in maize„ while it still shows auxin-induced apoplastic acidification [245], comparable to plants having one or more homologues.

(B) The H^+-ATPase up-regulation hypothesis. Auxin-induced apoplastic acidification could also be explained by H^+-ATPase up-regulation at a transcriptional level in the presence of auxin, according to a study of Rober-Kleber et al. [181]. Auxin at a concentration of 30 μM, according to this study, increased H^+-ATPase ex-pression levels by a factor 2 to 3. The idea behind this hypothesis is that auxin increases the amount of proton pumps. In due course, as the abundance of proton pumps in the plasma membrane rises, overall proton efflux from the cell is also elevated, thus leading to apoplastic acidification. This mechanism does not rely on further activation of proton pumps by auxin.

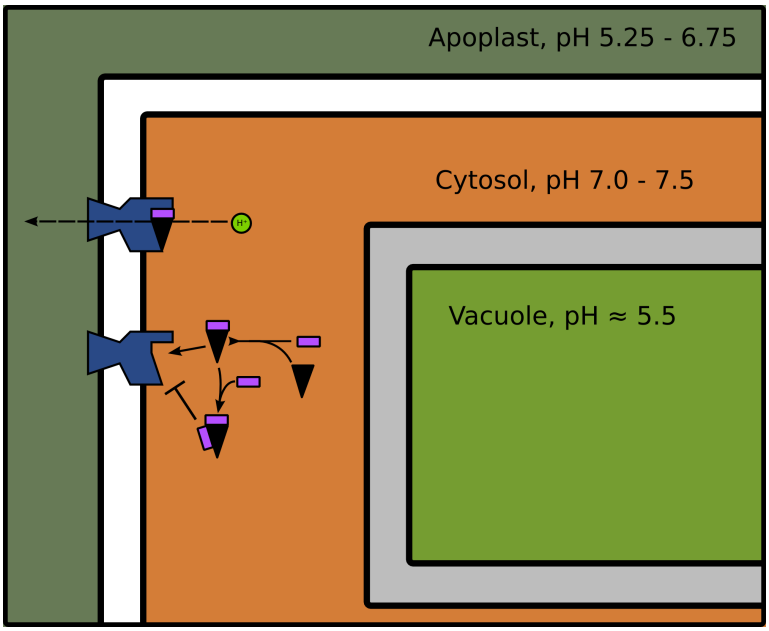

Figure 5.3: ABP_{57} -mediated proton pump activation, following the model from Kim et al., 2001 [95]: ABP_{57} (black triangles) is a protein with two binding sites for auxin (violet blocks). With one molecule auxin attached, ABP_{57} will activate proton pumps (blue structures in the plasma membrane) by interfering with the autoinhibitory domain on the proton pump, which will lead to more efflux of H^+ ions out of the cell. This is accomplished when the ABP_{57}:auxin complex at a specific site on the proton pump. However, if two auxins bind to one ABP_{57} (ABP_{57} :auxin:auxin) the activation does not occur, and the autoinhibitory domain of the H^+-ATPase remains effective.

(C) The ABP1 hypothesis. Another conflicting hypothesis of AAA (auxin-induced apoplastic acidification) mechanisms employs Auxin Binding Protein 1 (ABP1) as the mediating agent between auxin and proton pumps [230]. ABP1 is located inside the ER and at the outer side of the plasma membrane, where it acts as a hormone receptor [16, 230]. The ABP1 hypothesis for auxin-driven proton pump activation proposes a signalling cascade between ABP1 and the PM- H^+-ATPases as a result of auxin binding to ABP1. This hypothesis is interesting because it seems to oppose one assumption of the acid growth hypothesis, namely that auxin regulates proton pump activities from within the cell. In the ABP1 hypothesis, this regulation is assumed to occur in the extracellular space. However, the exact mechanism of the signalling cascade remains elusive to date.

5.3 Auxin/pH dynamics and pH homeostasis in previous computational models

Most published computational models of auxin transport do not consider compartmental pH, often due to not treating the apoplast explicitly as a compartment, but rather considering auxin transport to take place directly from cell to cell [4, 10, 134, 207, 211]. However, for those models that include pH, usually only fixed compartmental pH is defined, as a means to determine the amount of dissociated auxin and in due course the respective amount of passive auxin flux over the membrane [103, 89, 239].

It is interesting to note that pH homeostasis in higher plants has apparently not led to considerable interest in computational modelling so far, despite the impression that some of its aspects are not fully understood to date. However, there are some theoretical studies dealing with aspects of pH homeostasis, such as the regulation of pH in vacuolar vesicles by proton pump activity [92], the mechanochemical activity of vacuolar proton pumps [124], or the generation of action potentials over membranes involving H^+-ATPase activity [212]. There is one study that mathematically explored pH homeostasis dynamics of the unicellular algae *Eremosphaera viridis* [17]. In this model, pH homeostasis was based on mechanisms of passive buffering and proton pump activity and the cell reaction to weak acid application has been simulated. This approach to model pH homeostasis is similar to the approach chosen in the auxin/pH model, which is presented in the following sections.

To explore the positive feedback between auxin and protons that has been described in this section, and to investigate its effect on auxin transport, a kinetic model of auxin and proton interactions at a cell level has been formulated. Its implementation, first as a unified model, composed of separate subunits, in a non-spatial context; its subsequent minimisation; and finally its deployment in a two-dimensional spatial context will be described during the following sections.

CHAPTER 6

AP-10: A kinetic model of auxin and proton interactions

As described in the previous chapters, the relationship between auxin and pH has not yet been included in computational modelling. Therefore, based on the knowledge about feedback dynamics between auxin and pH from biology, a new model has been developed to investigate their qualitative and quantitative behaviour at a single cell level. In the following sections, the steps towards such a model are described and the rationale for its underlying assumptions is given. The model name is AP-10 (where *AP* stands for *A*uxin-*P*roton model and 10 is the number of model components in this model - see chapter 7 for further elucidations on the definitions of components and variables in this context), to distinguish it from further minimised versions of this model (AP-4 and AP-2), which are presented in chapter 7.

6.1 Model description

The overall auxin/pH feedback model consists of three subunits, which were developed and analysed separately before they were linked. These subunits are (1) pH homeostasis, (2) auxin dissociation a reversible process by which auxin as a weak acid dissociates into its anionic form IAA^-, thereby releasing a proton, and transport and (3) auxin-induced apoplastic acidification. The conceptual unified model (AP-10), resulting from merging these submodels with each other, is described in the following

sections. Three compartments are defined in the model cell: cytosol, vacuole and apoplast. Their dimensions were estimated to be typical for plant cells [11]: rectangular cells with width/height = $30\,\mu m$, length = $50\,\mu m$, containing a rectangular vacuole with half the cell width, height and length, surrounded by apoplastic space with width = $0.1\,\mu m$. The cytosol is separated from the apoplast by the plasma membrane (PM); cytosol and vacuole are separated by the vacuolar membrane or tonoplast (TP).

6.1.1 General assumptions underlying AP-10

AP-10 relies on three general assumptions. These are discussed below, before the assumptions underlying each of the submodels will be discussed in detail. First, there are no concentration gradients inside a compartment. All compartments are considered to be homogeneous, in the sense of being well mixed. In addition, the compartments are understood as containers with a defined volume and membranes therefore have a defined area. Second, the three compartments apoplast, vacuole and cytosol are, taken together, assumed to be a closed system with no input or output. This means that neither signalling nor traffic of substances from or to the outside of this closed system are considered. In addition it is assumed that substances are neither produced nor decay throughout the simulation. Finally, substance concentrations within the compartments are assumed to be high enough to model the system with a continuous approach, using ODEs that describe standard reaction kinetics.

6.1.2 Submodel 1: pH homeostasis

To investigate auxin/proton interactions in greater detail, it is a necessary first step to understand proton dynamics in a cell without any addition of auxin. If the ability of auxin to shift compartmental pH (see section 5.2.2) is to be theoretically explored, a logical first step would be to focus first on the ability of plant cells to maintain their pH (see section 5.1) and to formulate a model which is able to mimic this behaviour realistically. If auxin is later added to the model, pH shifts can then be assumed to occur within the limits of the cellular ability to withstand such changes due to the mechanisms underlying pH homeostasis. As a consequence of this, a submodel for pH homeostasis in a single plant cell has been developed. For a diagram of this submodel, see figure 6.1. In the following, the specific assumptions for the pH homeostasis submodel are listed:

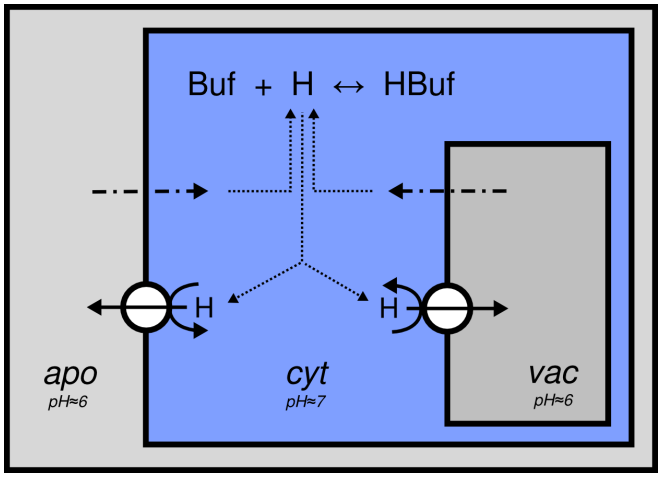

Figure 6.1: A simplified structure of submodel 1. The environment consists of 3 compartments, apoplast (apo), cytosol (cyt) and vacuole (vac). Protons are pumped over the tonoplast (cyt/vac) and plasma membrane (cyt/apo) via H^+-ATPase (full arrows). Reflux of protons over tonoplast and plasma membrane occurs due to H^+ co-transport of ions and other substances (semi-dotted line). Free H^+ concentrations in cytosol and apoplast are attenuated by buffer kinetics (HBuf dissociation and dotted lines). Only cytosolic buffering is shown, for reasons of better visibility.

Table 6.1: Kinetic reactions for the pH homeostasis model (submodel 1). The sign "=" refers to reversible reactions, A^- is the anionic form of the buffer HB.

Reaction	Rate(s)	Description
$H_2O + A^- = HB + OH^-$	$kb_{1/2}$	Buffer dissociation 1 in apo/cyt
$HB + H_2O = A^- + H_3O^+$	$ka_{1/2}$	Buffer dissociation 2 in apo/cyt
$2H_2O = OH^- + H_3O^+$	$kw_{1/2}$	Water self ionisation in apo/cyt
$H_3O_c^+ \rightarrow H_3O_a^+$	$A_p \cdot \frac{V_P \cdot (H_3O_c^+)^p}{K_P^p + (H_3O_c^+)^p}$	PM proton pump
$H_3O_c^+ \rightarrow H_3O_v^+$	$A_t \cdot \frac{V_T \cdot (H_3O_c^+)^t}{K_T^t + (H_3O_c^+)^t}$	TP proton pump
$OH_c^- \rightarrow OH_a^-$	P_{OH^-}	OH^- reflux over PM
$OH_c^- \rightarrow OH_v^-$	P_{OH^-}	OH^- reflux over TP
$H_3O_a^+ \rightarrow H_3O_c^+$	P_{H^+}	H^+ reflux over PM
$H_3O_v^+ \rightarrow H_3O_c^+$	P_{H^+}	H^+ reflux over TP

- Passive buffering and proton pump activity are sufficient to account for pH homeostasis, and the biochemical pH-stat mechanism is not considered in this submodel. The reason for not including the pH-stat mechanism is that the inclusion of metabolic pathways considerably increases complexity, without adding indispensable information.

- Passive buffering is assumed to take place both in the cytosol and in the apoplast. The buffer capacity of the cytosol is, however, around an order of magnitude higher compared with the apoplastic buffer capacity (see section 5.1).

- Passive buffering relies on single species of one mono-protic acid per compartment with a pKa value equal to the typical compartmental equilibrium pH. This assumption is a simplification, as the buffering capacity is very likely based on a mixture of several components, such as phosphate, and other n-protic acids. However, since the exact cellular buffer composition is not known and extracellular pH values during the simulations do not exceed the range between pH 4 and pH 7, which is easily buffered by cells [72], assuming a single buffer species does not seem problematic, especially since pH homeostasis does not entirely rely on chemical buffering. Proton pumps are assumed to be infinitely energized by ATP. There is no limitation of proton pump activity by a finite amount of ATP.

- There is just one type of proton pump present in both the plasma membrane and the tonoplast in the model. This is, of course, a simplification, since at least two types of proton pumps occur in plants, ATPases and PPases, which seem to show different abundances in plasma membranes and tonoplasts [65, 76, 128]. However, neither ATP nor PP are modelled explicitly and both types of proton pumps seem to transport H^+ in a pH-dependent manner [92]. Moreover, the activity of proton pumps is understood as counteracting the proton reflux over their host membrane [72]. This process is regulated directly by cytosolic pH [22, 76, 109]. Since this holds both for plasma membrane and tonoplast bound proton pumps [22, 76, 155], the assumption of single-type proton pumps, as employed here, does not contradict biological evidence for the scope of this model.

- Proton refluxes over the membrane are the sum of all proton fluxes down the electrochemical gradient. Membrane permeabilities for H^+ and co-transport of

Table 6.2: Kinetic reactions for the auxin transport/dissociation model (submodel 2)

Reaction	Rate(s)	Description
$IAAH + H_2O = IAA^- + H_3O^+$	$kaux_{1/2}$	Auxin dissociation in apo/cyt
$IAAH_a \rightarrow IAAH_c$	$\alpha \cdot (IAAH_a - IAAH_c)$	Passive auxin influx
$IAA_a^- + 2H_3O_a^+ \rightarrow IAA_c^- + 2H_3O_c^+$	β	Active auxin influx (AUX/LAX)
$IAA_c^- \rightarrow IAA_a^-$	γ	Active auxin efflux

H^+ due to several H^+- symporter activities are contributing to these ionic refluxes. However, proton influx due to AUX/LAX activity is treated separately in this submodel (see section 6.1.3).

- The vacuole is considered to act both as an infinite source and sink for protons and has a fixed pH. Vacuoles are acidic and have usually a varying pH, but since, except for proton reflux over the tonoplast, which is counteracted by vacuolar proton pump activity, no process in the model is dependent on vacuolar pH, the assumption of fixed (or infinitely strongly buffered) vacuolar pH is reasonable.

All kinetic equations, based on the above listed assumptions, are given in table 6.1.

6.1.3 Submodel 2: Auxin transport and dissociation

According to the chemiosmotic hypothesis of auxin transport, the dissociation status of auxin determines its passive transportability over the plasma membrane (see section 5.2). While protonated auxin is able to permeate membranes, anionic auxin needs the help of transporter proteins to cross the plasma membrane. The most prominent of these transporters are influx carriers of the AUX1/LAX family symporting two protons for every anionic auxin molecule [94, 251], ATP-energised ABCB (PGP) carriers [66, 226, 227], and efflux transporters of the PIN family [21, 23, 62, 105, 254], which are probably neither consuming ATP nor antiporting auxin, but are most likely efflux facilitators energised by the proton motive force across the plasma membrane [105]. In short, the assumptions for auxin transport, leading to the formulation of kinetic reactions for submodel 2 (see table 6.2), are:

Table 6.3: Kinetic reactions for the AAA submodel. ABP_a is the active form of ABP, able to activate the H^+-ATPase, while ABP_i does not result in H^+-ATPase activation.

Reaction	Rate(s)	Description
$IAA_c + ABP = ABP_a$	$k(ABP)1/-1$	ABP_x:IAA complex formation (ACF 1)
$ABP_a + IAA_c = ABP_i$	$k(ABP)2/-2$	ABP_x:IAA:IAA complex formation (ACF 2)
$H_3O_c^+ \rightarrow H_3O_a^+$	$A_p \cdot \frac{V_{ABP} \cdot ABP_a}{K_{ABP} + ABP_a}$	ABP_x:IAA activation of PM-H^+-ATPase

- Passive trans-membrane flux of IAAH relies on a single membrane permeability parameter for auxin, α.
- Active influx of IAA^- is mediated by AUX1/LAX symporters, co-transporting two H^+ with each IAA^- molecule into the cell.
- Active efflux of IAA^- relies both on ABCBs and PINs, and is treated as one single reaction. Since the model does not include spatial information, polarised auxin transport is not considered separately from symmetric auxin efflux.

6.1.4 Submodel 3: Auxin-induced apoplastic acidification (AAA)

Auxin causes apoplastic acidification by activating plasma membrane proton pumps [76]. The precise mechanism by which this stimulation of proton pumps occurs is still unclear. The model assumptions for this mechanism are based on the ABP_{57} -hypothesis (see section 5.2.2), which provides a quantitative kinetic estimation for all agents involved, and it, at least in vitro, effectively shows how AAA may work. However, since the protein which appears to have this activity in maize, ABP_{57}, does not seem to be ubiquitous in plants [113], this mechanistic assumption is modified to state simply a functional equivalent to ABP_{57} has the role of a mechanistic link between cytosolic auxin concentration and apoplastic acidification activity of PM-H^+-ATPase, which equivalent is named ABPx. The kinetic reactions of the AAA submodel are given in table 6.3. In detail, the specific assumptions for AAA are:

- ABPx has two binding sites for auxin. If only one is occupied, the resulting ABPx:auxin complex (ABPx(a) with *a* for *active*) stimulates proton pumps. If both

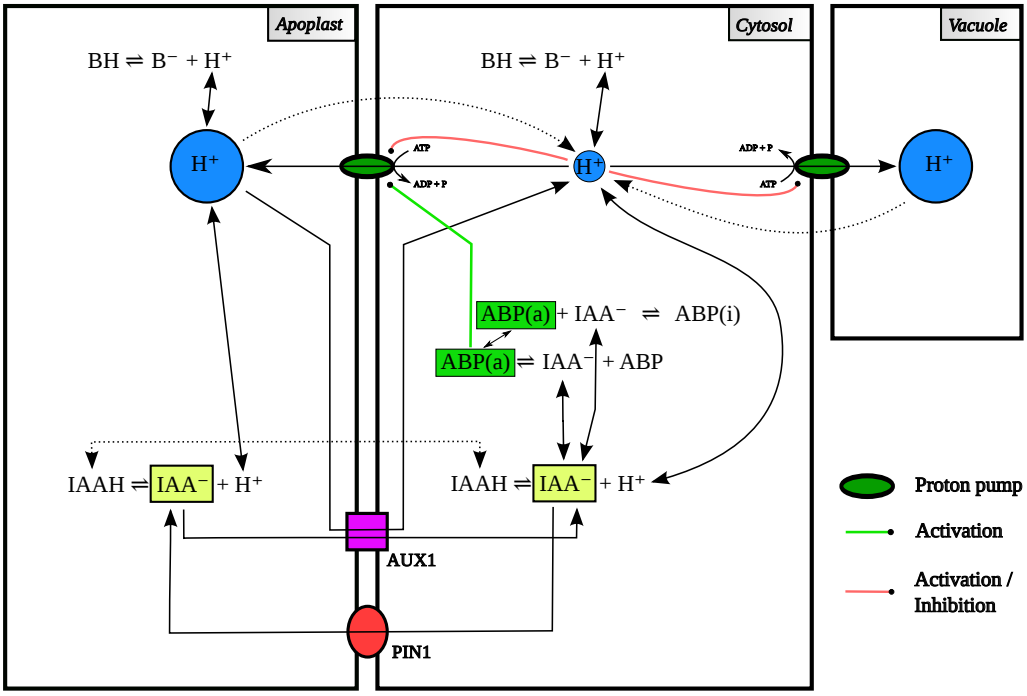

Figure 6.2: Detailed description of the AP-10 model. This model consists of 3 compartments: apoplast, cytosol and vacuole. pH homeostasis on the basis of chemical buffering and proton pump activity is linked to auxin in two ways: (1) auxin dissociation and change of auxin abundance for specific transport paths over the plasma membrane (passive uptake, active influx and active efflux), and (2) auxin-induced apoplastic acidification, mediated by an auxin binding protein, ABP. Blue circles: Proton pools inside compartments. Circle sizes correspond to proton concentrations. Buffer reactions (dissociation of BH) and auxin reactions (dissociation of IAAH) contribute to the pool of protons. Transport of protons between compartments is due to a) pumping activity via proton pumps (H^+-ATPase), b) passive reflux over membranes down the gradient (dotted arrows) or c) H+ symport connected to AUX1 mediated auxin influx. Accordingly, transport of auxin between apoplast and cytosol is due to a) passive uptake of protonated auxin, IAAH (dotted arrow), active efflux via PIN1 transporters or c) AUX1 mediated auxin influx. H^+-ATPase activity is stimulated by ABPx(a), the active form of the auxin binding protein ABPx, associated to one auxin molecule (green dot line). If another molecule binds to ABP, the inactive form ABPx(i) results, having no effect on H^+-ATPase activity. Proton pumps are also regulated directly by cytosolic pH (red dot lines).

binding sites of ABP are occupied by auxin, a complex named ABPx(i) (with *i* for *inactive*) is formed, which does not interact with proton pumps.

- Auxin induced proton pump stimulation and H^+-dependent regulation of PM proton pumps (see section 6.1.2) are additive mechanisms.

6.1.5 The unified model

After carefully checking against biological data to arrive at a realistic model of each submodel, especially for the pH homeostasis unit, the next step was to merge all three separate submodels together to a unified model (AP-10). A diagram of this model is given in figure 6.2.

6.1.6 Computer simulation

The combined model was implemented using COPASI [84]. The model consists of 16 kinetic reactions with 38 parameters. A list of all parameters and their values is given in table A.2. The complete system of ODEs of the AP-10 model can be found in the appendix A, as well as the values for initial concentration (table A.3). The set of ODEs uses a shorter notation for protons (H^+ instead of H_3O^+) for better readability, and a Hill coefficient of 1 for all Hill equations. Simulations were undertaken using the default values of the deterministic (LSODA) solver for time course analysis in COPASI: relative tolerance was set to 10^{-6}, absolute tolerance to 10^{-12}, and the maximum number of internal steps to 10000. The durations of time course tasks and parameter scan tasks were usually 2 hours, with interval sizes of 5 seconds.

6.2 Results

First, submodel 1 (pH homeostasis) was used to reproduce pH-stress tests conducted with real plants [72]. By doing so, model parameters could be fitted to available biological data on the pH homeostasis behaviour in plant cells. This fitting task was not performed by formal parameter estimation, but rather by changing parameters towards values which led to results comparable to biological experiments, especially those of Gout et al. [72]. Two underlying hypotheses for the pH homeostasis submodel were tested in the pH stress simulations: constant versus pH-dependent membrane permeabilities for H^+/OH^- (see section 6.1.2). Second, submodel 3 (auxin-induced apoplastic acidification) was implemented and its parameters fitted to the data of a model of ABP_{57}-mediated proton pump regulation, proposed by Kim et al. [95] (see section 6.1.4). Third, all three submodels were combined in one unified model (see figure 6.2) and the AAA-related parameters compared to biological data of auxin/pH dose response curves. Then, the general model behaviour as a response to AAA could be

investigated. At last, the underlying assumptions of constant versus pH-dependent membrane permeabilities for H^+/OH^- were tested in the unified model to decide the question of their respective validities.

6.2.1 pH homeostasis

The model could reproduce results of pH-stress experiments conducted on single plant cells [72], especially for acidic stress, which can be considered to be a phenomenon more likely to occur in natural environments than alkaline stress, since cells are surrounded by an acidic extracellular space and vacuolar compartments are also acidic. Extreme initial values for apoplastic pH (transient pH stresses) led to no significant changes of cytosolic pH, and recovery to apoplastic pH equilibrium occurred after about 30 minutes after stress induction. When exposed to long-term pH stress, cells could maintain their pH within the range of $\pm$ 0.25 pH units for fixed external pH values between 4.5 and 8.5 (figure 6.3).

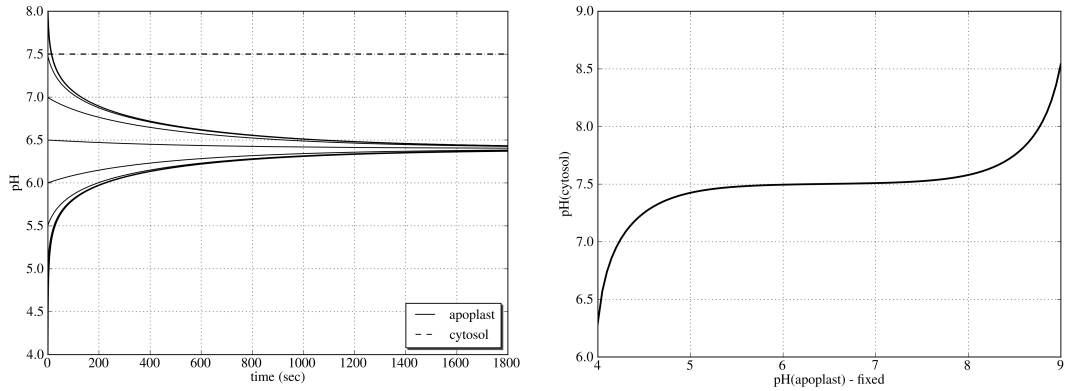

Figure 6.3: pH homeostasis behaviour of the model without auxin added (all auxin values were set to zero). *Left:* Time series for different initial apoplastic pH. Cytoplasmic pH remained closely at 7.5, while apoplastic pH converged to its equilibrium value of 6.4 within 1 hr of the simulation. *Right:* Cytosolic pH as a function of fixed apoplastic pHs at the end of pH stress experiment simulations. Data points are taken after 2 hrs simulation time.

6.2.2 Auxin/pH dose-response curves

To compare the model with available data on auxin-induced apoplastic acidification, dose-response simulations for different concentrations of exogenous auxin were carried out. Previous biological experiments had recorded acidification of the bathing medium after adding auxin to the medium in which the plant tissue was incubated [56,

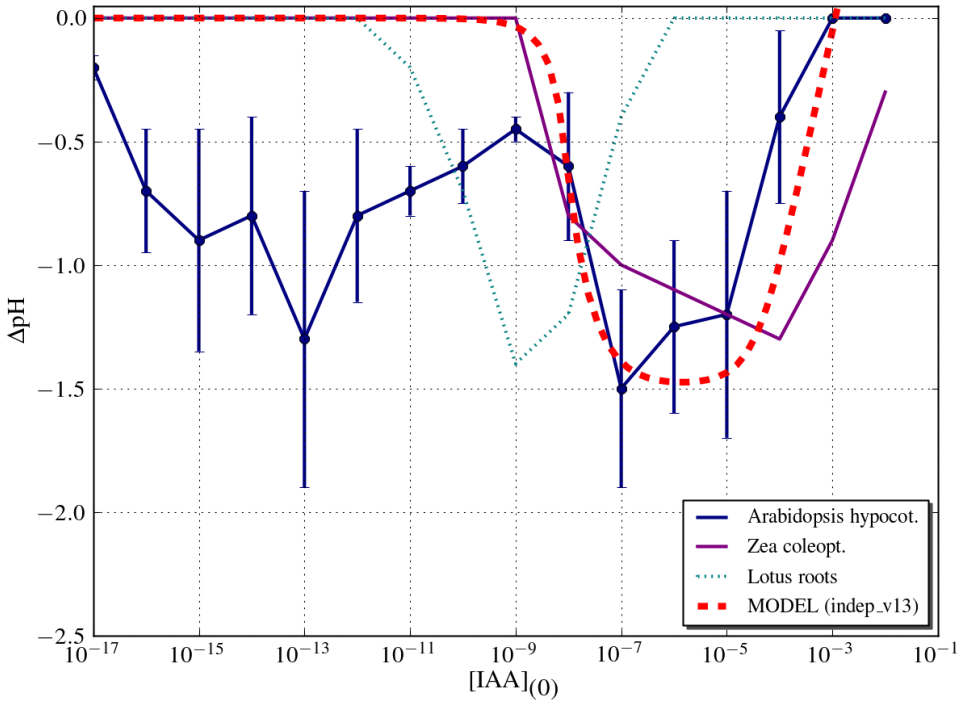

Figure 6.4: The effect of auxin on extracellular pH, as obtained from experimentally observed dose-response curves for different exogenous auxin concentrations, compared with the reproduction of dose-response experiments by the computational model. The model could reproduce the single peak of acidification around 10^{-6} M [IAA], observed in *Arabidopsis* hypocotyls [245], *Zea* coleoptiles [91], and *Lotus* roots [200] - considering that apoplastic acidification peaks in roots may be shifted to lower IAA levels [95] - but failed to reproduce the second peak around 10^{-13} M [IAA], observed in Arabidopsis alone [245]. The model output has been taken from a representative run with pH-independent membrane permeabilities for protons (see section 6.2.4).

91, 200]. This experimental setup was captured in the simulations by fixing apoplastic auxin concentration. The compartmental pH after an overall simulation time of 2 hours was recorded and compared to biological data (Figure 6.4).

Parameterisation for this data fitting task mainly concentrated on the parameters K_{ABP} and V_{ABP}, shaping the width and amplitude of the acidification peak (figure 6.5). The model produced a single peak of apoplastic acidification for applied exogenous IAA concentrations in the range between 10^{-1} to 10^{-17} M. Apoplastic acidification occurred at extracellular IAA concentrations above 10^{-10} M, with a peak at around 10^{-6} M. The intracellular IAA concentration at the AAA peak was around 10^{-8} M. This result was consistent with dose-response curves obtained from oat [56] and maize [91]. Dur-

ing the simulation, the steady-state for apoplastic pH was reached within 50 minutes for all exogenous auxin concentrations. Lower auxin concentrations generally resulted in a faster equilibration of apoplastic pH than higher concentrations. Cytoplasmic pH remained close to the assumed equilibrium value of pH 7.5, with fluctuations lower than $\pm$ 0.01 pH units throughout all simulations.

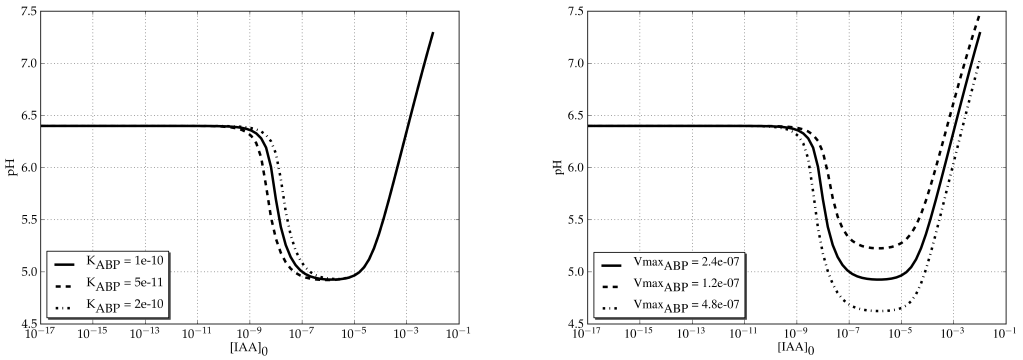

Figure 6.5: Apoplastic acidification peak changes due to alterations of parameters K_{ABP} and V_{ABP} as compared to the standard model settings (solid lines). While raising K_{ABP} shifts the acidification peak towards higher exogenous auxin levels [IAA](0), raising V_{ABP} led to symmetrically bigger peak area and stronger overall apoplastic acidification.

6.2.3 General model behaviour

Auxin-induced apoplastic acidification enhanced all auxin transport fluxes over the plasma membrane throughout a wide range of parameter settings. All auxin fluxes were increased by around one order of magnitude in the overall simulation over the range of acidification (figure 6.6, above). This flux enhancement was sensitive to changes of the auxin efflux strength parameter γ, for both low and high γ values ($\gamma < 0.01$ only showed enhancement of active auxin influx and $\gamma > 50$ resulted in no flux enhancements at all at the peak of auxin-induced apoplastic acidification). Moreover, AAA led to increased accumulation of auxin in the cytosol, as compared to the assumed apoplastic pH baseline of 6.4. Lowering the initial apoplastic pH led to the same results, suggesting that AAA was not dependent on certain initial apoplastic pH. As acidification set in, auxin was depleted from the apoplast and accumulated in the cytosol (figure 6.6, upper panel).

Throughout the simulations, the equilibrium for cytosolic and apoplastic auxin con-

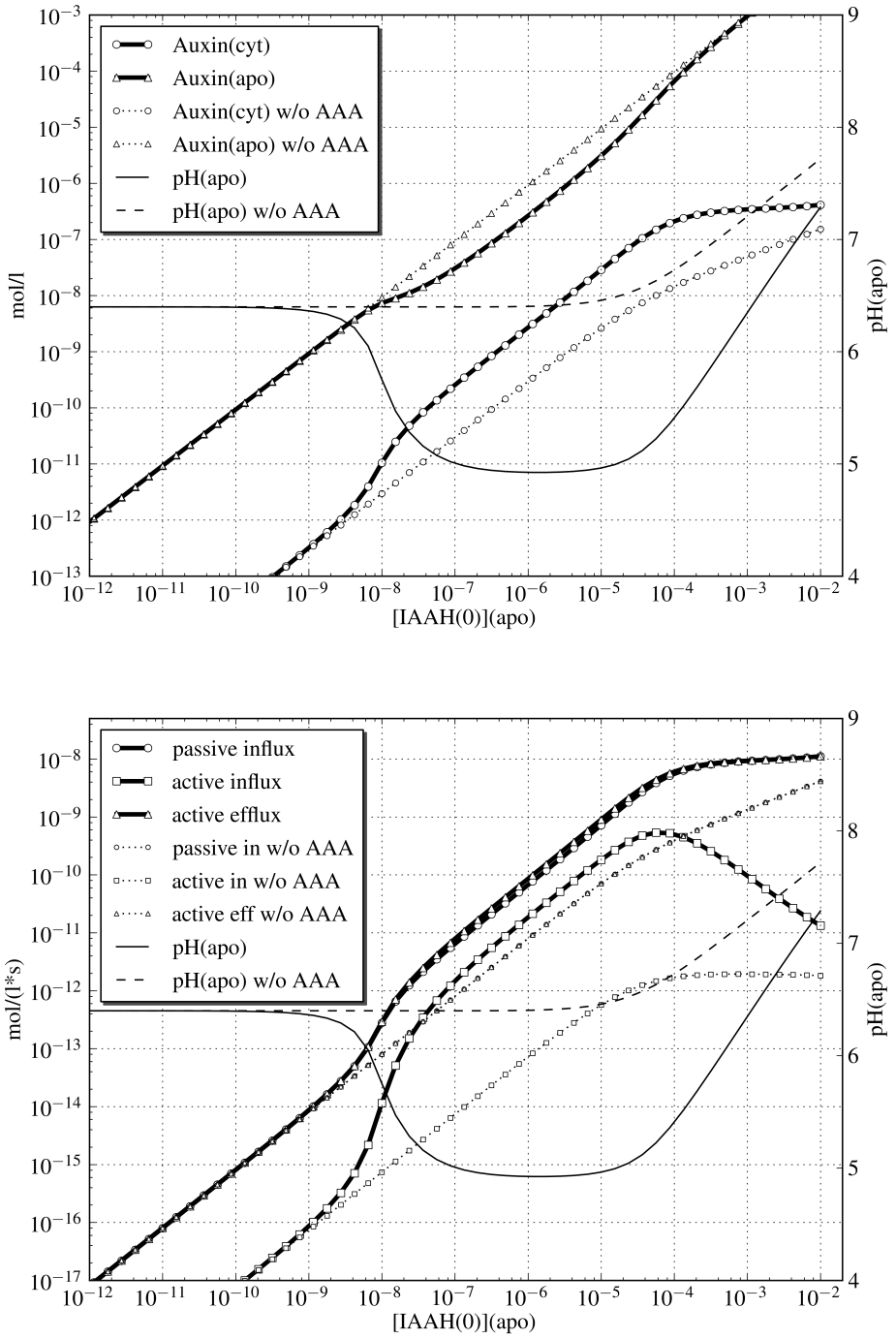

Figure 6.6: Effect of auxin-induced apoplastic acidification on auxin transport fluxes (above) and on auxin distribution (below). Output of the computational model for different exogenous auxin concentrations [IAAH](0) after 2 hours of simulation time, by which time apoplastic pH stabilized. Upper figure: All auxin transport fluxes over the plasma membrane were amplified as AAA sets in. Lower figure: Auxin accumulation in cells was greater with AAA than without AAA.

centrations after exogenous auxin applications were reached within 10 - 40 minutes, which is consistent with biological data [164]. Equilibria were reached faster at lower auxin concentrations, according to the process of auxin-induced apoplastic acidification. Not surprisingly, this result was heavily dependent on the settings of the auxin transport parameters: while low γ (efflux) and high α and β (influx) values led to a rapid accumulation of auxin in the cytosol and no flux enhancement except for active auxin influx, high γ and low α and β values resulted in no substantial auxin accumulation in the cytosol. Thus, since apoplastic acidification was dependent on cytosolic auxin concentrations, its peak was flattened and started at lower external auxin concentrations in the first case, while the latter case led only to a narrow peak at higher exogenous concentrations of auxin (see figure 6.7).

6.2.4 Influence of pH homeostasis settings on model behaviour

Influx of protons over the plasma membrane into the cell both from apoplast and vacuole down the trans-membrane proton gradient were modelled as a passive reflux rate. Two assumptions for H^+ reflux were tested in the overall model: (a) constant H^+ permeability versus (b) pH dependent H^+ permeability. For pH-dependent H^+ permeability, data from plasma membrane vesicles [138] were used to estimate permeability functions for both H^+ and OH^- ions. According to this study, at increasing pH, the permeability for H^+ was raised and the permeability for OH^- reduced. Under the assumption that the trend of pH-dependency of respective H^+/OH^- permeabilities would be constant and inferable towards lower pH, an assumption that is supported by other studies finding a constant relationship between pH and apparent proton permeability at lower pH values [154], these measurements from Miedema et al. have been fitted to curves using the least square method and extrapolated to lower pH values, since the measurements were only applied at pH above 8 (see figure 6.8). This led to the formulation of the following functions:

$$\begin{aligned} P_{(H^+)} &= x \cdot 10^{(0.52 \cdot pH - 4.53)} \\ P_{(OH^-)} &= y \cdot 10^{(-0.39 \cdot pH + 4.72)} \end{aligned} \tag{6.1}$$

with $x = 10^{-6}$ and $y = 10^{-10}$. In simulations involving theses permeability functions, the guiding pH was assumed to be the mean value between the pH of cytosol and vac-

Figure 6.7: The influence of changes of single auxin transport parameters on the shape of the AAA peak in dose-response simulations, as obtained after a simulation time of 2 hours. Reducing the value of α (upper), β (middle) or γ (lower) by an order of magnitude (dashed lines) or increasing it by an order of magnitude (dotted lines) resulted in shifts of onset and offset of the AAA peak, but did not qualitatively change the AAA peak otherwise.

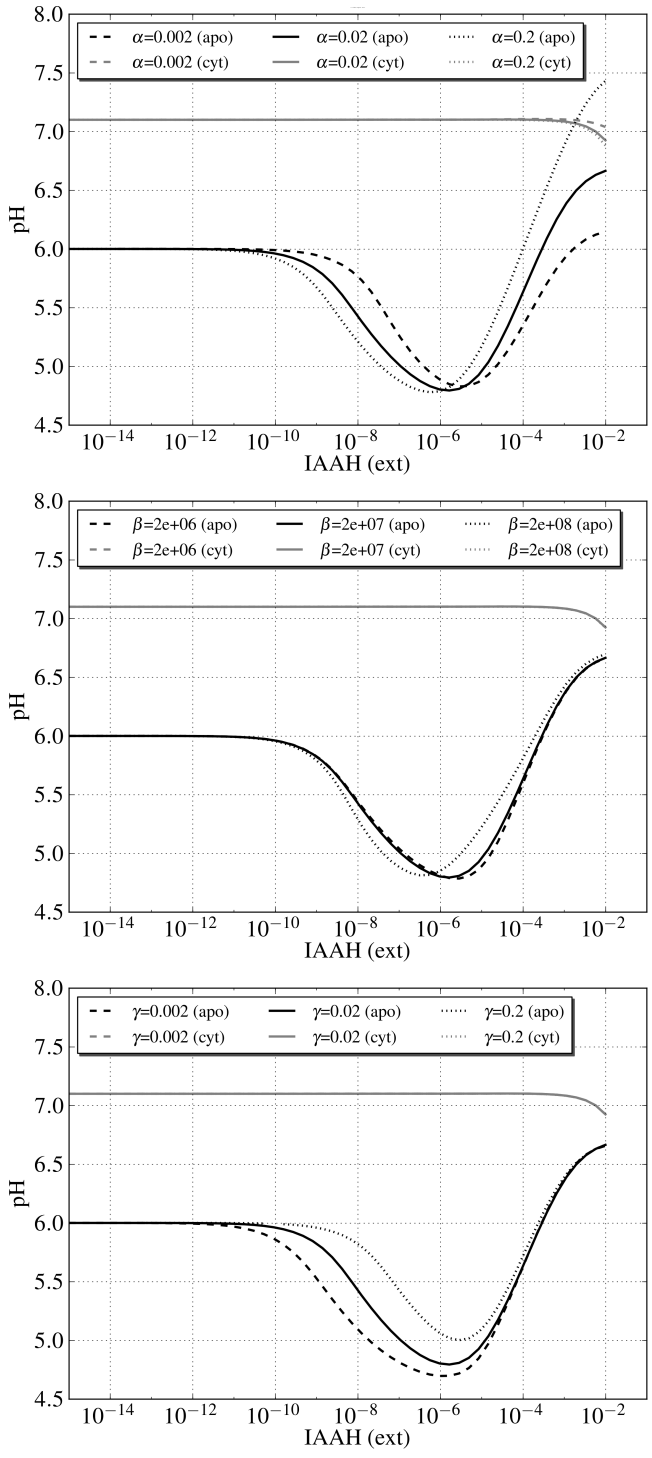

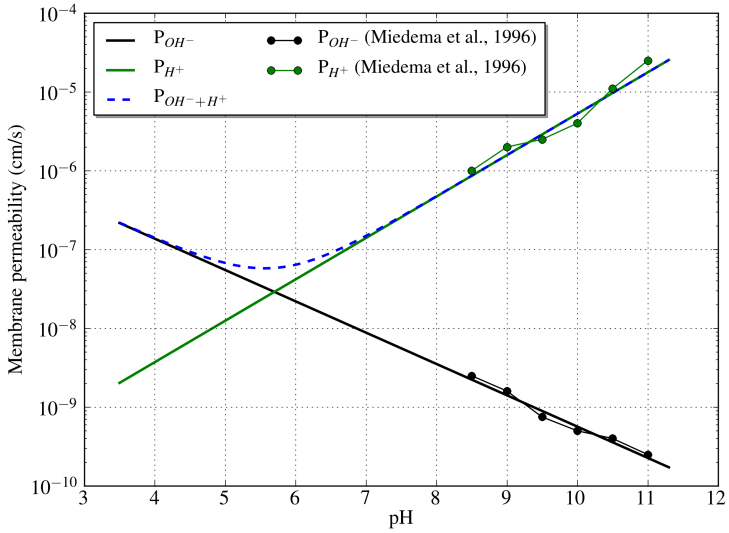

Figure 6.8: pH-dependent membrane permeabilities for H^+/OH^-. Permeability data from membrane vesicles were taken from [138] and extrapolated to lower pH values. To obtain the apparent total H^+ permeability, respective H^+ and OH^- permeabilities of the membrane are summed (dashed blue line).

uole (for tonoplast H^+/OH^- permeabilities) or between the pH of cytosol and apoplast (for plasma membrane H^+/OH^- permeabilities).

Using these fitted functions based on data of Miedema et al. for pH-dependent H^+/OH^- permeabilities in the pH stress simulations (see section 6.2.1) did not lead to a good reproduction of biological data from Gout et al. [72]. First, the pH stress reaction was much slower, compared to biological data, and the amplitude of the pH stress reaction was lower, such that it was not noticeably changing over time at all. Therefore, the respective permeabilities were approximated by simulations involving different values for x and y, to give a better representation of the pH stress experiments of Gout et al. (see fig. 6.9). A more reasonable approximation as a result of this parameter fit was obtained for $x = 0.05$ and $y = 0.002$. The huge difference of the corrected x and y to those values obtained from Miedema et al. suggests that H^+/OH^- reflux over membranes might not mainly be due to H^+/OH^- permeabilities of the membranes alone, but rather significantly due to co-transport of H^+ in substrate and ion transport across membranes [17, 72]

Based on the assumption that the overall trend of pH-dependent H^+/OH^- permeabilities, even with the corrected values for x and y, remains the same as in the study of

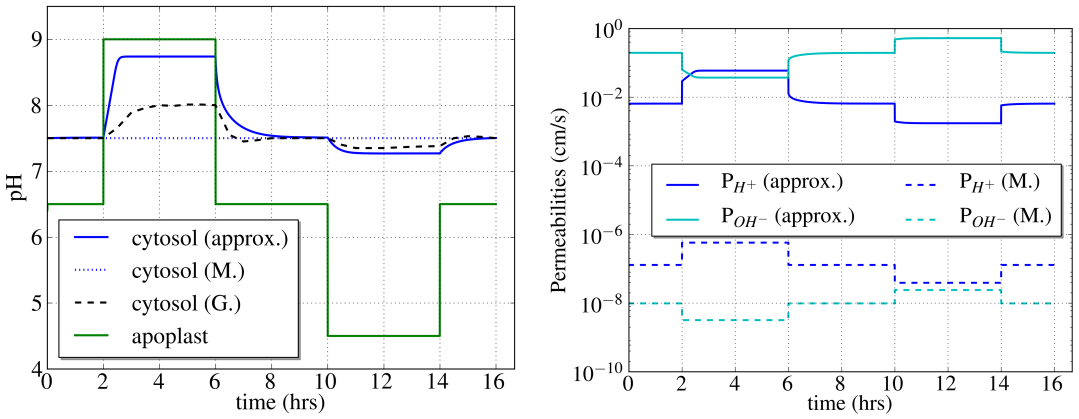

Figure 6.9: pH stress experiments with different settings for pH-dependent permeabilities. *Left:* Reproducing the pH stress experiments of Gout et al. [72], cytosolic pH changes were monitored following sudden changes in apoplastic pH (black dashed line, G.). With H^+/OH^- permeability settings inferred from Miedema et al. [138] (M.), cytosolic pH did nearly stay the same during pH stress phases, whereas with approximated (increased) H^+/OH^- permeabilities the situation in Gout et al. could be reproduced more accurately (see section 6.2.1 for more on these experiments). *Right:* Development of H^+/OH^- permeabilities over the plasma membrane during these experiments, for approximated values and values from Miedema et al. (M.)

Miedema et al., the influence of pH-dependent versus constant H^+/OH^- permeabilities has been tested in simulations including auxin transport. Dose-response experiments with pH-dependent H^+/OH^- permeabilities led to a stronger auxin-induced apoplastic acidification, compared to simulations with constant permeabilities, while the time scale of AAA was similar in both experimental settings. By adapting K_{ABP} and V_{ABP} values, AAA behaviour of the model using constant permeabilities could be approximated (see figure 6.10). With these adapted values for K_{ABP} and V_{ABP}, simulations using pH-dependent H^+/OH^- permeabilities led also to very similar results regarding auxin flux enhancement and pronounced accumulation of auxin in cells during AAA (see figure 6.11). These results justify the preference for constant proton permeability across membranes for AP-10 simulations.

To investigate the influence of proton pump parameters on the overall simulation outcome, Michaelis constants K_t for tonoplast proton pumps and K_p for plasma membrane proton pumps were tested over a range of values. K_t and K_p values varied within the interval $[10^{-7}, 10^{-5}]$, and Hill coefficients varied within the interval $[1, 3]$. The overall results of the simulations were robust to all proton pump parameter settings, and were identical both in the time scale of the solution and in the quantitative

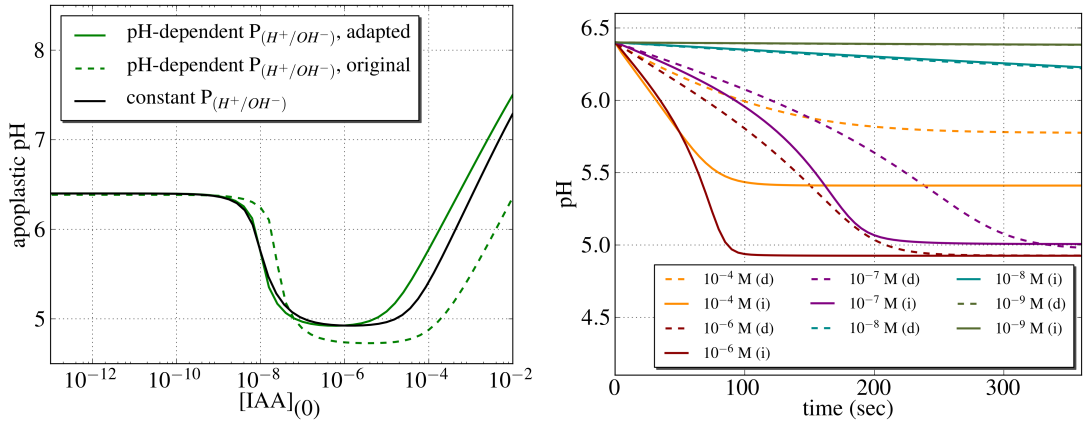

Figure 6.10: Auxin-induced apoplastic acidification under the assumptions of constant vs. pH-dependent membrane permeabilities for H^+/OH^-. *Left:* Comparison between dose-response curves for AAA with pH-dependent H^+/OH^- permeabilities (green) and with constant H^+/OH^- permeabilities after 2 hours simulation time. Using the same parameters for AAA, the pH-dependent model led to stronger AAA because of the higher OH^- permeability of the PM at lower pH (dashed green line). By adapting K_{ABP} and V_{ABP} values, AAA behaviour of the model using constant permeabilities could be approximated (full green line, see fig. 6.5). *Right:* TIme course solutions of the simulations over the first 360 seconds of simulation were comparable for constant (independent, i) and pH-dependent (dependent, d) H^+/OH^- permeabilities in simulations using different exogeneous auxin concentrations.

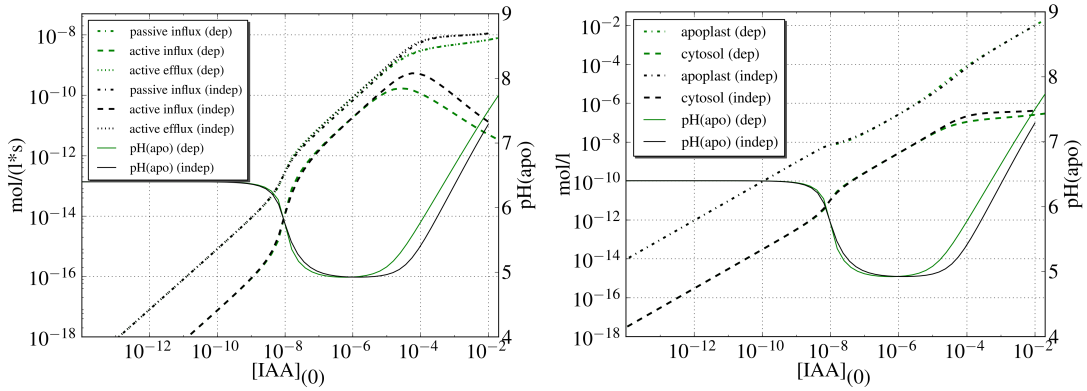

Figure 6.11: Auxin fluxes and auxin allocation under the assumptions of constant vs. pH-dependent membrane permeabilities for H^+/OH^-. *Left:* Auxin transport fluxes over the plasma membrane at the end of simulations (running time: 2 hours) with AAA in effect, for pH-dependent (green) and pH-independent H^+/OH^- permeabilities (black). *Right:* The allocation of auxin in cytosol and apoplast at the end of simulations (running time: 2 hours), for pH-dependent (green) and pH-independent H^+/OH^- permeabilities (black). Corresponding apoplastic pH values are given for identifying the range of AAA (solid lines).

and qualitative response to external pH changes. Therefore, the Hill coefficients were by default set to 1, and K_t and K_p values were by default set to 10^{-7}.

6.3 Discussion

The AP-10 model captures the dynamics of a several feedback loops between auxin and H^+, which have already been proposed [73, 114]. By interlinking the chemiosmotic hypothesis of auxin transport with auxin-induced apoplastic acidification (AAA), considering them to be two halves of a feedback loop, a framework is proposed and suggested for use in future models of auxin transport which rely on assumptions at a single cell level. The results show auxin flux enhancement and increased allocation of intra- versus intercellular auxin as the result of this feedback.

6.3.1 Modelling of pH homeostasis

The submodel employing pH homeostasis relies on many assumptions that are not readily supported by data from plant physiology. While some characteristics of plant cell pH maintenance are known and data about them are available (e.g. buffer capacity of cytosol and apoplast, cell responses to pH stress - see section 5.1 for further details and references), the submodel relies as well on assumptions that are less clear from data. pH homeostasis seems not to be critcal for the influence of AAA on auxin transport fluxes and allocation, and thus the qualitative and quantitative outcome of the AP-10 model does apparently not rely on a high accuracy of all assumptions in the pH homeostasis submodel, as can be seen in section 6.2.4. However, there are still some issues that might be interesting to discuss here, concerning differences and inconsistencies of this model with data from physiology and membrane biology.

First, in the pH homeostasis submodel as well as in the overall AP-10 model, proton fluxes across the plasma membrane and across the tonoplast are assumed to take place in similar manners. Following simulation experiments with differing proton pump activities at the plasma membrane versus at the tonoplast, and after employing different H^+/OH^- permeabilities for those two membrane species, most outcomes were qualitatively similar, as long as they were consistent with the time scale and amplitude of biological pH stress experiments [72]. While, based on that, the simplest assumption for the pH-homeostasis subunit of AP-10 was favoured, resulting in a sim-

ilar treatment of plasma membrane and tonoplast for proton fluxes, this contradicts some studies that found differences between these two membrane species, regarding proton transport properties [68]. However, some of these differences lie in variations of transport optima for protons, which are not necessarily mirroring apparent variations in H^+ transport situations near the optimum pH, which seems to be tightly controlled in the cytosol [72].

Another issue is that there is apparently no precise quantitative listing of all buffering agents available for plant cells, while the proton buffering in the cytosol is likely to be due to a mixture of different weak acids, such as phosphate and carbonate [72, 155], which contradicts the assumption of buffering being a process accomplished by a monoprotic acid. This inconsistency is relaxed towards a more general assumption during the process of further minimising the AP-10 model in chapter 7.

6.3.2 Linking auxin transport to protons

Simulation outcomes for AAA are consistent with the few biological data available on cell wall pH dose-responses to exogenous auxin [56, 91, 200, 245]. Based on the assumption that growth responses to auxin correlate with AAA [95], our results are also consistent with a greater amount of auxin growth-response data [27, 126, 150], showing bell-shaped curves with peaks around concentrations of 10^{-6} M auxin (see figure 6.4).

Previous experiments with the *Arabidopsis* proton pump AVP1 indicate the influence of proton pump availability and activity on auxin transport [119], demonstrating that reduced cell wall acidification in *avp1* mutants leads to decreased auxin transport. The exact mechanism behind this is as yet unclear, but its effect is in accordance with the hypothesis of increased auxin transport fluxes due to AAA, possibly leading to increased overall inward auxin transport, as well as with older findings demonstrating the dependence of auxin transport speed on compartmental pH [79, 164, 174]. In addition, the finding that auxin allocation in cells is promoted at lower apoplastic pH is consistent with experimental results [204].

6.3.3 Auxin influence on proton pumps

The AP-10 model relies on a functionally equivalent process to the ABP_{57} -mediated AAA, proposed by Kim et al. [95]. It has to be stated, however, that the main results of this model do not rely on the precise accuracy of the mechanism involved, and we would expect the same results with any process employed as auxin/proton pump mediation, as long as it leads to AAA in a manner that has been observed in biological experiments [56, 76, 91, 175, 200]. ABP_{57} is apparently not ubiquitous in all higher plants [113] and its effect has so far only been shown in vitro. However, among all conflicting hypotheses of AAA (see section 5.2.2) derived from biological experiments it provides the clearest kinetic assumptions to date. Our model does not depend on the exact nature of any of these proposed mechanisms driving AAA, but rather relies on the occurrence of AAA itself.

Another issue to be mentioned here is the assumption that neither auxin nor protein synthesis and degradation are considered. For the scope of the model, we rather assume all these processes to be in perfect equilibrium, based on the assumption that all turnover rates are happening at a time scale greater than our time of simulation. It is interesting to note, that for longer simulation times, including auxin turnover could lead to transient rather than stationary pH equilibria [164]. While this mechanism lies beyond the scope of the AP-10 model, it would imply that enhancement of auxin influxes and effluxes due to high auxin levels are also transient, leading to pulses of high auxin influx and efflux at high auxin concentrations.

In this chapter, a model for auxin/pH interactions has been constructed and described. Since the main results of the model: auxin flux enhancement and shift of auxin allocation towards the cytosol, following the onset of AAA, seem to be robust against a wide range of parameter changes (auxin transport rates, H^+/OH^- permeabilities of membranes, proton pump settings), and since the model includes many components that may not be of the same importance for the realisation of these results as the main components auxin and protons, this model is minimised gradually to simplify it for easier implementation in a spatial context (see chapter 8), but also to investigate the importance of each component. This minimisation process is elucidated in the following chapter.

CHAPTER 7

Minimised auxin/pH models: From AP-10 to AP-2

While the AP-10 model of auxin/pH interactions, described in the previous chapter, proved to give useful insights into dynamics between auxin and protons, minimising the AP-10 model could be desirable for the following reasons:

1. Generalising some of the processes without losing the overall model behaviour may strengthen the understanding of underlying dynamics.

2. By reducing the number of variables involved, given that the result is still equivalent to the AP-10 model, the importance and role of each variable can be clarified in simulation experiments, while at the same time satisfying the principle of parsimony.

3. When putting the kinetic model into a spatial context, as is the intention within this study (see chapter 8), model minimisation helps to reduce computational costs by removing unnecessary variables (these are variables that do not influence the model behaviour in a significant way).

In the following sections, minimisation of the AP-10 model with 19 variables (10 components) to a 4-component and further to a 2-component minimal model will be described. The 4-component model is also referred to as AP-4, while the 2-component

Table 7.1: Variables and components in the AP-10 model, the 4-component minimal model (AP-4) and the 2-component minimal model (AP-2). Subscripts of variables specify their compartmental location (apoplast (a), cytosol (c), or vacuole (v)

	AP-10		AP-4		AP-2	
	components	variables	components	variables	components	variables
Auxin	IAA^-	IAA^-_a	IAA^-	IAA^-_a	A	A_a
		IAA^-_c		IAA^-_c		
	IAAH	$IAAH_a$	IAAH	$IAAH_a$		A_c
		$IAAH_c$		$IAAH_c$		
Protons	H_3O^+	$H_3O^+_a$	H^+	H^+_a	H	H_a
		$H_3O^+_c$		H^+_c		H_c
		$H_3O^+_v$		H^+_v		H_v
Buffer	A^-	A^-_a	B	B_a		
		A^-_c				
	AH	AH_a		B_c		
		AH_c				
Other	OH^-	OH^-_a				
		OH^-_c				
		OH^-_v				
	H_2O	H_2O_a				
		H_2O_c				
	ABP_{free}	ABP_{free}				
	ABP_a	ABP_a				
	ABP_i	ABP_i				

model is named AP-2. To clarify the terminology used in this context: *Components* are specific entities, like auxin, protons or proteins, while *variables* are components in a specific compartment (apoplastic H^+, cytosolic H^+, etc.). This distinction is necessary because of the compartmental nature in the model: Kinetic rates (eg. for buffering processes or transport across membranes) are often not the same for a component in different compartments. An overview of all model variables and components is given in Table 7.1.

It has to be noted, however, that minimising the full kinetic model (AP-10) does not mean that functionalities are skipped. Rather, some reactions are still modelled as

Table 7.2: An overview of all reactions in the auxin/pH model and the way they are treated in AP-10 and minimised implementations. Some reactions are implemented as kinetic equations (K), while others are expressed as functions (F). The term AAA means here the mechanism underlying auxin-induced apoplastic acidification.

Reaction		Implementation		
		AP-10	AP-4	AP-2
Auxin dissociation		K	K	F
Proton buffering		K	K	F
Proton transport		F	F	F
Auxin transport	Auxin influx (passive)	F	F	F
	Auxin influx (active)	K	K	K
	Auxin efflux (active)	F	F	F
AAA		K	F	F

kinetic reactions, whereas others are simplified or generalized as functions. The assumptions which underlie these simplifications and the behaviour of the minimised models as compared with AP-10 will be discussed in the following sections. For a first glance at the differences between AP-10 and the minimised models, it is useful to group all reactions of the model into the following blocks: auxin dissociation, auxin transport, proton buffering, proton transport, auxin-induced apoplastic acidification. An overview of how these reactions are implemented in AP-10 and the minimised models respectively is given in table 7.2.

7.1 4-component minimal model (AP-4)

In the last section it was mentioned that during minimisation of the auxin/pH model some of the kinetic reactions are simplified or generalised. In a first step towards the 4-component minimal model, the following considerations have been taken into account, providing an argument for the validity of those generalisations:

Water self-ionisation and OH^-. When looking at the number of components in the AP-10 model, it appears that proton buffering is over-represented: 5 of 10 components are involved in proton buffering, which however seems not to be a very complicated

process. Involving the self-ionisation of water ensures that the pH never reaches unrealistic values (below 1 or above 14), however it introduces additional complexity which may be redundant for three reasons. First, H^+ and OH^- fluxes over the membrane are hard to distinguish experimentally and add up to a combined apparent H^+ flux (see [154]), which makes their separate treatment in the AP-10 model not too convincing. Second, the extreme pH values which are prevented by the self-ionisation reaction of water were not even approached in pH stress simulations, and therefore this caution seems unnecessary. And last, the kinetic buffer reactions only mimic the behaviour of a monoprotic acid, which is not a very realistic assumption, since it is very likely that cellular compartments are buffered by a mixture of mobile and stationary buffers [90]. Including a detailed kinetic model of an unsure assumption could be replaced by simpler mechanisms that meet the parsimony principle to a greater extent. Here, the simpler assumption might be more realistic.

Auxin-induced apoplastic acidification. Following from the results of the AP-10 model and the subsequent discussion of the mechanisms underlying auxin-induced apoplastic acidification (see section 6.3), a more generalised expression of the link between auxin and proton pumps seems desirable. From dose-response curves of auxin influences on medium pH as well as from growth-response curves to auxin, AAA seems to progress in a bell-shaped manner [56, 76, 91, 175, 200]. This is in accordance to the specific ABP_{57} mechanism, proposed by Kim et al. [95]. However, since it is not clear which mechanism is really driving AAA, it seems to be reasonable to extract this bell-shaped behaviour of AAA and use it as an abstraction of the precise mechanism behind it. Thus, auxin-induced proton transport (see table 6.3) was changed to X, where X is a Gaussian curve, dependent on the cytosolic auxin concentration, of the form

$$X = X_a \cdot exp\Big(-\frac{(ln(X_b) - ln([IAA]))^2}{X_c}\Big)$$

Parameters X_a (curve height), X_b (curve peak location) and X_c (curve peak width) were fitted to experimental data [56, 91, 200, 245]. A comparison of AAA strength for the fitted Gaussian is illustrated in figure 7.1. The fitted values for the Gaussian parameters can be found in parameter tables A.4 in the appendix.

Proton buffering For simplifying the proton buffering process in the 4-component model, an unspecified buffer is considered to bind free protons according to the following expression:

$$H_f \rightleftharpoons H_b \tag{7.1}$$

where H_f is the concentration of free protons and H_b are protons buffered by B. The forward and backward reaction rates of this process as well as the amounts are derived from the definition of buffer capacity,

$$\beta = \frac{d(n)}{d(pH)} \tag{7.2}$$

in which β is the buffering capacity, $d(n)$ is the amount of H^+ added and $d(pH)$ is the rate of change in pH [197, 198, 234]. From this definition it follows that the buffer capacity of a solution signifies the amount of protons that can be added to or removed from a system to change the pH for 1 unit. Since at equilibrium the forward and backward reaction of the buffering system must be the same (k_1 being the forward and k_{-1} being the backward reaction rate), it follows that at equilibrium the following condition must be fulfilled:

$$k_1 \cdot H_f = k_{-1} \cdot H_b \tag{7.3}$$

If the amount of β protons is added to the system, the pH drops 1 unit, which means a tenfold increase in proton concentration, such that

$$H_{f_{new}} = H_f + 9 \cdot H_f \tag{7.4}$$

Since all other incoming protons are buffered, the amount of H_b after adding β protons is

$$H_{b_{new}} = \beta - 9 \cdot H_f \tag{7.5}$$

Thus, as the amount of β protons is added to the system, equation (7.3) can be rewritten as

$$k_1 \cdot (10 \cdot H_f) = k_{-1} \cdot (\beta - 9 \cdot H_f) \tag{7.6}$$

and the reaction rate k_{-1} is

$$k_{-1} = 10 \cdot \frac{k_1}{\frac{\beta}{H_f} - 9} \tag{7.7}$$

given that the criterion $\beta > 9 \cdot H_f$ is met to prevent the rate getting negative. This is the case in a typical simulation since the lowest buffer capacity in the system, $\beta_{apoplast} \sim$

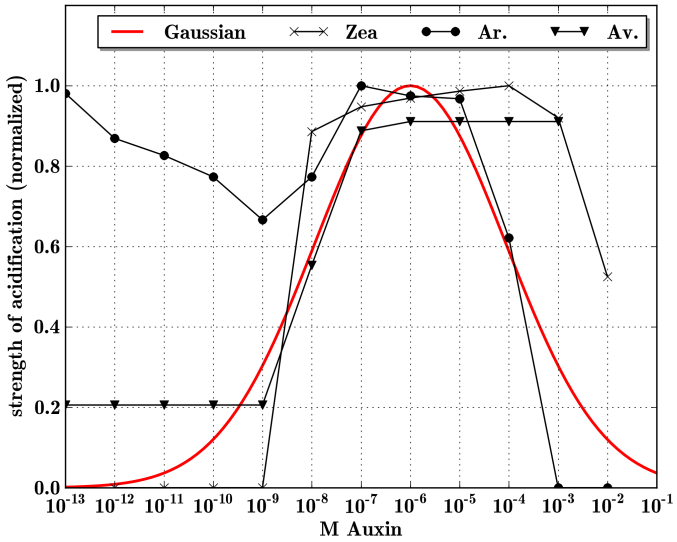

Figure 7.1: Gaussian curve fitted to AAA strengths from biological dose-response experiments, obtained from *Zea mays* [91], *Arabidopsis* hypocotyls [245] and *Avena* coleoptile [56]

0.01, and the pH in the system is not expected to fall below 3 at any point, which corresponds to a proton concentration of 0.001 M, as can be seen from the results of the full kinetic model (AP-10).

Following the considerations above, the 4-component minimal model consists of the following system of differential equations:

$$\begin{aligned}\frac{d[IAA^-]_a}{dt} &= ka_1[IAAH]_a - ka_2[IAA^-]_a[H^+]_a + \frac{1}{V_a}\Big[\gamma A_{PM}[IAA^-]_c \\ &\quad - \beta A_{PM}[IAA^-]_a[H^+]_a^2\Big]\end{aligned} \tag{7.8}$$

$$\begin{aligned}\frac{d[IAAH]_a}{dt} &= -ka_1[IAAH]_a + ka_2[IAA^-]_a[H^+]_a \\ &\quad - \frac{1}{V_a}\alpha A_{PM}\Big([IAAH]_a - [IAAH]_c\Big)\end{aligned} \tag{7.9}$$

$$\begin{aligned}\frac{d[H^+]_a}{dt} &= ka_1[IAAH]_a - ka_2[IAA^-]_a[H^+]_a + \frac{1}{V_a}\Bigg[\frac{V_X \cdot X(IAA^-)}{X(IAA^-) + K_X} \\ &\quad - r_H A_{PM}\Big([H^+]_a - [H^+]_c\Big)\Bigg] - kb_1[H^+]_a + kb_{2_a}[B]_a \\ &\quad + \frac{1}{V_a}\left[\frac{V_P \cdot [H^+]_c^p}{[H^+]_c^p + K_{PM}^p} - 2\beta A_{PM}[IAA^-]_a[H^+]_a^2\right]\end{aligned} \tag{7.10}$$

$$\frac{d[B]_a}{dt} = kb_1[H^+]_a - kb_{2_a}[B]_a \tag{7.11}$$

$$\begin{aligned}\frac{d[IAA^-]_c}{dt} &= ka_1[IAAH]_c - ka_2[IAA^-]_c[H^+]_c - \frac{1}{V_c}\Bigg[\gamma A_{PM}[IAA^-]_c \\ &\quad + \beta A_{PM}[IAA^-]_a[H^+]_a^2\Bigg]\end{aligned} \tag{7.12}$$

$$\begin{aligned}\frac{d[IAAH]_c}{dt} &= -ka_1[IAAH]_c + ka_2[IAA^-]_c[H^+]_c \\ &\quad + \frac{1}{V_c}\alpha A_{PM}\Big([IAAH]_a - [IAAH]_c\Big)\end{aligned} \tag{7.13}$$

$$\begin{aligned}\frac{d[H^+]_c}{dt} &= ka_1[IAAH]_c - ka_2[IAA^-]_c[H^+]_c - \frac{1}{V_c}\Bigg[\frac{V_X \cdot X(IAA^-)}{X(IAA^-) + K_X} \\ &\quad + r_H A_{PM}\Big([H]_a - [H^+]_c\Big) + r_H A_{TP}\Big([H^+]_v - [H^+]_c\Big)\Bigg] \\ &\quad - kb_1[H^+]_c + kb_{2_c}[B]_c - \frac{1}{V_c}\Bigg[\frac{V_P \cdot [H^+]_c^p}{[H^+]_c^p + K_P^p} \\ &\quad - \frac{A_{TP}}{A_{PM}} \cdot \frac{V_T^t \cdot [H^+]_c^t}{[H^+]_c^t + K_T^t} + 2\beta A_{PM}[IAA^-]_a[H^+]_a^2\Bigg]\end{aligned} \tag{7.14}$$

$$\frac{d[B]_c}{dt} = kb_1[H^+]_c - kb_{2_c}[B]_c \tag{7.15}$$

where the subscripts a and c refer to the compartments apoplast and cytosol, V_c and V_a are the cytosolic and apoplastic volumes, IAA^- is the anionic auxin, $IAAH$ is the protonated auxin, H^+ is the pool of free protons and B is the proton buffer. Auxin dissociation and transport involve the auxin forward dissociation rate k_{a_1} and the backward dissociation rate k_{a_2}, the passive influx rate α, the AUX/LAX dependent active influx parameter β, and the symmetric efflux rate γ, relating to auxin efflux which is not dependent on the energisation of the proton motive force (ABCBs). A_{PM} and

A_{TP} are the areas of the plasma membrane (PM) and tonoplast (TP), respectively. The parameters involved in pH homeostasis are: the proton reflux rate r_H, the forward rate for the buffer reaction, k_{b_1}, the backward rate for buffering in the cytosol, $k_{b_{2_c}}$, and in the apoplast, $k_{b_{2_a}}$, the Hill parameters V_P and V_T, referring to the maximum rate of proton pump activity at the PM and at the TP, and the Michaelis constants K_P and K_T for the proton pumps at the PM and at the TP. The Hill coefficents p and t refer to the proton pumps at the PM and TP, respectively. For auxin-induced activation of the PM-H^+-ATPase , X in equations (7.10) and (7.14) is a gaussian function representing the strength of auxin-induced apoplastic acidification,

$$X(IAA^-) = \begin{cases} X_a \cdot e^{\left(-\frac{(ln(X_b)-ln([IAA^-]_c))^2}{X_c}\right)} & \text{if } [IAA^-]_c \geq 10^{-19} \\ 0 & \text{if } [IAA^-]_c < 10^{-19} \end{cases}$$

with X_a being the parameter giving the curve maximum value, X_b is the location parameter, determining the auxin concentration at which the curve maximum occurs, and X_c is the width parameter of the curve. The parameter V_X is the maximum rate of auxin-induced PM-H^+-ATPase activation and K_X is the Michaelis constant for this reaction. All parameter values can be found in table A.4 in the appendix. For a list of initial concentrations used in the simulations, please refer to the table A.5 in the appendix.

7.2 2-component minimal model (AP-2)

There are some elements in the 4-component model (AP-4) that cause stiffness when put into a spatial context, often defined by the difficulty in obtaining a numerical solution to a system of differential equations due to non-convergence of the solution by the use of explicit step-by-step methods [210]. This occurs in problems where there are very different scales of the independent variable on which dependent variables are changing [172]. While these findings, leading to the necessity of further reducing the 4-component model to get rid of these elements in order to solve the auxin/pH model in a spatial context, will be discussed in length in chapter 8, mentioning these issues at this point emphasises the practical importance of the following considerations.

The 2-component model is a reduction of the AP-10 model to the indispensable el-

ements of the model: auxin and protons. Two kinetic reactions of the 4-component model are replaced by functions: auxin dissociation and chemical buffering (see table 7.2). In the following, the rationale for doing so is presented.

Simplifying chemical buffering. Following from the 4-component model, in which an already simplified chemical buffering mechanism was implemented, the buffer reaction itself can be assumed to be fast, compared with the time scale of the model, following the estimated reaction rates (see equation (7.7)). However, since the components of proton buffering in a cell are likely to be a mixture of mobile and fixed buffers [90, 218], the exact kinetic rates for buffering are difficult to estimate. In the AP-10 model, a monoprotic acid was assumed to be responsible for buffering, and the kinetic reaction rates were estimated from the pK_a of the pH equilibrium at which the buffer was assumed to be in dissociation equilibrium as well (see section 6). In the 4-component model, the assumption of a single buffering species was relaxed to a more general buffer with constant buffer capacities, resembling a mixture of several buffer components with differing pK_a values, therefore resulting in the same buffer capacity over the whole range of expectable pH values in a compartment, and showing a linear buffer response, whereas a mono-protic acid has a peak of its buffer capacity, where the pH of its compartment equals the pK_a value of the buffer, with a decreasing buffer capacity at compartmental pH further away from its pK_a value. Now, a further step towards generalisation is made, by not specifying the buffer components at all and not treating them as entities in the model. This has also been accomplished in other mathematical models including chemical buffering [17, 92, 100] and follows from the definition of buffer capacity in equation (7.2), whereby $(-1/\beta)$ is the attenuation of change in pH when H^+ is added or removed from the system.

Thus, if we are only interested in the rate of change of free protons in a compartment, which is attenuated by the chemical buffering, this can easily be expressed by multiplying every incoming or outgoing amount of H^+ by the factor $(ln(10) \cdot [H]_x/\beta_x)$, where $[H]_x$ is the actual H^+ concentration in the compartment x and β_x is the buffer capacity in the compartment x (see [125, 234]).

Simplifying auxin dissociation. Likewise, if we assume that auxin dissociation is very fast and could therefore approximated to be instantaneous, its kinetic expression

can be approximated using the Henderson-Hasselbalch equation [171],

$$pH = pK_a + log\frac{[A^-]}{[HA]} \tag{7.16}$$

where A^- is the anionic acid and HA is the undissociated acid. From this equation, the situation for auxin with a given total concentration of auxin, A, can therefore be formulated as

$$[IAAH] = [A] \cdot \frac{10^{(pK_a - pH)}}{1 + 10^{(pK_a - pH)}} \tag{7.17}$$

which, after tidying up on the RHS, gives

$$[IAAH] = \frac{[A]}{1 + 10^{(pH - pK_a)}} \tag{7.18}$$

and, accordingly,

$$[IAA^-] = \frac{[A]}{1 + 10^{(pK_a - pH)}} \tag{7.19}$$

This evaluation of dissociated and undissociated auxin levels due to a given compartmental pH has also been implemented in other auxin transport models [103, 106, 239]. While it takes account of the compartmental pH, the main difference to the treatment of auxin dissociation as kinetic equation, as in the AP-10 and AP-4 model, lies in the assumption that on the basis of the Henderson-Hasselbalch approximation the contribution of auxin dissociation to the proton pools in cytosolic and apoplastic compartments are omitted. This assumption is based on two considerations: (1) auxin levels in cells are very likely not in the range that they could considerably affect pH levels (for the compartment with weakest buffer capacity, the apoplast, auxin concentrations would have to be in the range of over 100 μM to change the pH in the order of 0.1 units, which might be above typical cellular auxin concentrations [165, 193, 246]. (2) If, however, the auxin concentration should be in such a range, auxin as a weak acid would also contribute to the buffer capacity and therefore have less effect on pH than the same amount of strong acid added. In the following, the ODEs of the AP-2 model are given:

$$\frac{d[A]_a}{dt} = \gamma[IAA^-]_c - \beta[IAA^-]_a[H]_a^2 - \alpha([IAAH]_a - [IAAH]_c) \tag{7.20}$$

$$\frac{d[H]_a}{dt} = \frac{[H]_a}{b_a} \cdot \frac{1}{V_a}\left[X + \frac{V_p \cdot [H]_c}{K_p + [H]_c} - r_H([H]_a - [H]_c) - 2\beta[IAA^-]_a[H]_a^2\right] \tag{7.21}$$

$$\frac{d[A]_c}{dt} = -\gamma[IAA^-]_c + \beta[IAA^-]_a[H]_a^2 + \alpha([IAAH]_a - [IAAH]_c) \tag{7.22}$$

$$\begin{aligned}\frac{d[H]_c}{dt} = \frac{[H]_c}{b_c} \cdot \frac{1}{V_c}\Bigg[& -X - \frac{V_p \cdot [H]_c}{K_p + [H]_c} - \frac{V_t \cdot [H]_c}{K_t + [H]_c} + r_H([H]_a - [H]_c) + \\ & + r_H([H]_v - [H]_c) + 2\beta[IAA^-]_a[H]_a^2\Bigg]\end{aligned} \tag{7.23}$$

where A is the auxin concentration, H is the concentration of free protons, and those parameters that the system shares with the AP-4 model are identical with those described in equations (7.8) to (7.15). Additional parameters not appearing in AP-4 are: b_a and b_c, referring to the strength of the buffer capacities in the apoplast and cytosol, V_a and V_c are apoplastic and cytosolic volumes. The accessory equations to evaluate auxin-dependent PM-H^+-ATPase activation and to evaluate the dissociation status of auxin for the the passive and active transport over the plasma membrane are

$$X(IAA^-) = X_a \cdot e^{\left(-\frac{(ln(X_b) - ln([IAA^-]_c))^2}{X_c}\right)} \tag{7.24}$$

$$[IAA^-] = \frac{[A]}{1 + 10^{(pK_a - pH)}} \tag{7.25}$$

$$[IAAH] = \frac{[A]}{1 + 10^{(pH - pK_a)}} \tag{7.26}$$

where IAA^- is the anionic auxin, $IAAH$ is the undissociated auxin, X_a, X_b and X_c are height, position and width parameters for the Gaussian function representing auxin-dependent PM-H^+-ATPase activation. Note that the auxin-induced activation of proton pumps is, in contrast to AP-10 and AP-4, no longer Michaelis-Menten. A comparison between Michaelis-Menten and non-Michaelis-Menten formulations in simulations of AP-4 and AP-2 did not hint towards a noticeable change of simulation output, provided that the height parameter of the Gaussian, X_a is adjusted for the non-Michaelis-Menten expression, such that the strength of AAA equals that of the Michaelis-Menten

expression in AP-4, given the same levels of IAA^-. Therefore the simpler formulation for $X(IAA^-)$ was preferred in AP-2. The values for all parameters can be found in table A.6 in the appendix.

7.3 A comparison of AP-10 with minimal models

To evaluate the equivalence of AP-10 with the minimised models AP-4 and AP-2, results of all models have been compared side by side with similar settings for auxin transport rates ($\alpha = 0.0006$, $\beta = 10^5$, $\gamma = 0.08$). Settings for the Gaussian function of AAA were the same in AP-4 and AP-2 (see figure 7.1). The direct comparison of the outcome of AP-10, AP-4 and AP-2 under these conditions showed that, despite some minor differences, which are discussed in the following, all models are qualitatively equivalent (figure 7.2). In particular, this means that (1) all models were able to reproduce a peak of AAA at the micromolar range of extracellular auxin, (2) AAA caused auxin influx and auxin efflux enhancement in all models during AAA, and (3) auxin allocation was shifted into cells in all models when AAA was in effect. Since these results are congruent with the main results of AP-10, as presented in chapter 6, the minimised models AP-4 and AP-2 are therefore considered to be equivalent to the unified AP-10 model.

The time scale of AAA reaction is very similar in all three models and follows the same trend: lower amplitudes of AAA due to lower auxin concentrations take longer to equilibrate than higher amplitudes of AAA due to higher auxin concentrations (see figure 7.2, upper right). As well, lower AAA amplitudes due to auxin concentrations above 10^{-6} M are reached fast in all models.

Active auxin transport due to AUX/LAX transporters are enhanced in all models due to AAA, however, in simulations with initial auxin concentrations above around 10^{-4} M, they decrease again in AP-10 and AP-4, whereas they stay nearly the same in AP-2. This might be due to the fact that in AP-10 and AP-4, auxin dissociation is modelled as kinetic equations and therefore apoplastic auxin concentrations in the range reached during these simulations might contribute to apoplastic proton buffering, causing a depletion of free H^+ which are necessary for AUX/LAX-dependent auxin influx (see also the dose-response curve of apoplastic pH in figure 7.2, upper left), a situation

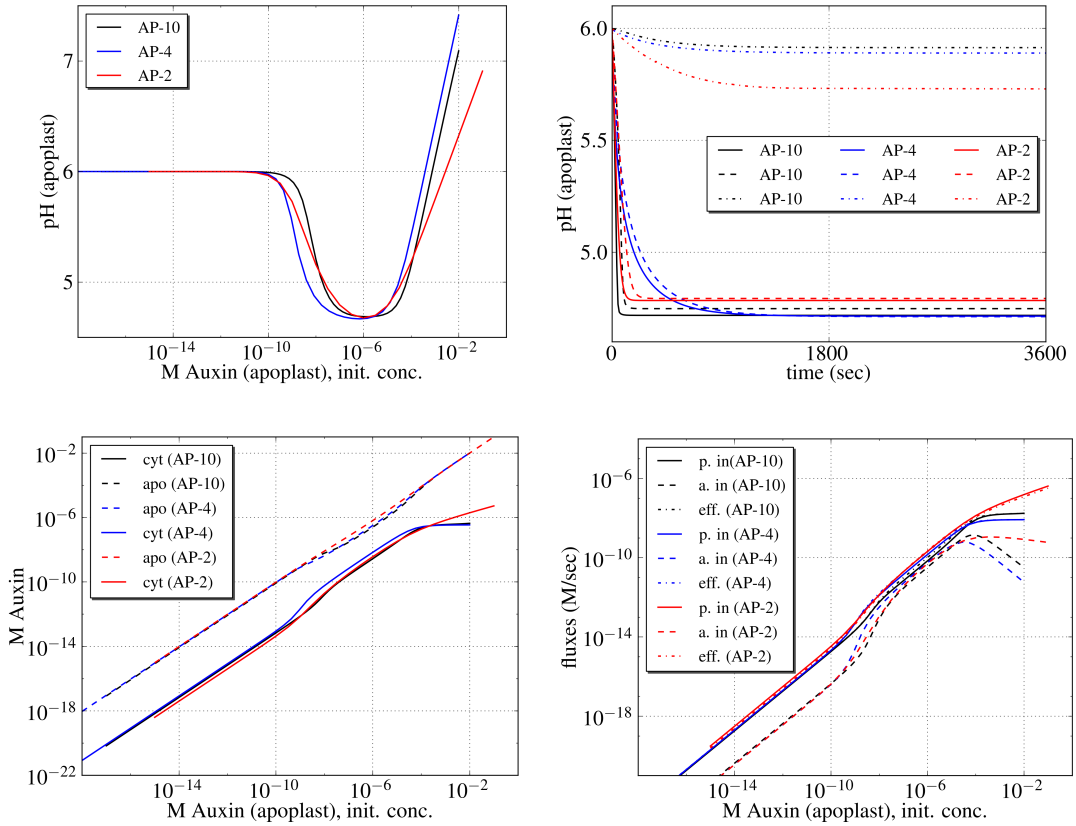

Figure 7.2: Comparison between AP-10 and minimised models with similar parameter settings for auxin transport rates ($\alpha = 0.0006$, $\beta = 10^5$, $\gamma = 0.08$). AP-4 and AP-2 had the same settings for the gaussian AAA function. *Upper left:* Auxin-induced apoplastic acidification after two hours simulation time. *Upper right:* The time scale of apoplastic acidification in simulations with extracellular auxin applied in three concentrations: 10^{-9} M (dotted line), 10^{-7} M (dashed line) and 10^{-5} M (full line). Time scales of AAA reaction were in about the same ranges for each concentration tested. *Lower left:* Auxin concentrations in cytosol (full line) and apoplast (dashed line) after two hours simulation time. *Lower right:* Auxin transport fluxes over the PM at the end of two hours of simulation time: Transport fluxes were elevated during AAA in all models.

that does not occur in AP-2, where auxin dissociation is purely pH-dependent.

During AAA, in the AP-10 model auxin is buffered in the cytosol because of binding to ABP(x), removing auxin from the overall pool. The strength of this behaviour is dependent on the concentration of free ABP(x) and is not reproduced in AP-4 and AP-2 due to their generalisation of AAA mechanism towards a Gaussian function. However, this effect of auxin buffering does not alter AAA and the mechanisms dependent on AAA to a degree that the qualitative behaviour of the models would be different as a result.

To summarise, minimised models of auxin/proton interactions with generalised equations and simplified assumptions have been shown to be qualitatively equivalent, sharing all behaviours of interest in their respective results. Thus, the simplest minimal model, AP-2, is considered to be capable of simulating auxin/proton dynamics at a single cell level in sufficient detail. Based on these considerations, the implementation of AP-2 within a spatial context is the logical next step to investigate potential spatial heterogeneities of auxin transport fluxes across the plasma membrane within extracellular auxin gradients, established by auxin sources and sinks in plant tissues, based on the dynamics of auxin and protons at a cell level. This development and implementation of a spatiotemporal model of auxin/proton interactions is the topic of the following chapter.

CHAPTER 8

SAP-2: A spatio-temporal model of auxin/proton dynamics

During chapter 6, a model of auxin/proton dynamics at a cell level, AP-10, was developed and this was reduced to a minimal set of components in chapter 7, culminating in a 2-component model, AP-2. A comparison of these models has shown that they are qualitatively equivalent, thus sharing the same behaviour: they were all able to lead to auxin-induced apoplastic acidification (AAA) with peaks at the micromolar range of exogeneous auxin applied to the system, they all exhibited enhancement of auxin influxes and effluxes over the plasma membrane when AAA was in effect, and AAA led to a pronounced allocation of auxin into cells during AAA. Neither model includes spatial information and treats the compartments involved (apoplast, cytosol and vacuole) as homogeneous containers with certain volumes. However, what would happen if this core model of auxin/pH interactions would be taken into a spatial context? Auxin distribution is not homogeneous in plants, which relies on heterogeneities of distribution of auxin synthesis sites and on variation in patterns of auxin transport (see section 2.3). In the context of the canalisation hypothesis, auxin transporting cell files in the vascular bundles could act as a sink for auxin, whereas in phyllotactic patterning auxin apparently builds up in unstable concentration maxima (see section 2.2). Therefore, concentration gradients between sites of auxin production or auxin maxima (sources) and vascular tissue draining auxin from tissues (sinks) can be expected. From chapters 2 and 3 it is apparent that the problem of how cell polarisation with respect to auxin

transport occurs is still in debate and that PIN polar targeting is still not fully understood. However, both from biological evidence and from tissue-scale models related to auxin transport it can be inferred that PIN polarisation in the direction of auxin flux (such as in canalisation) is a common phenomenon (see section 2.3.2). Therefore, there are some questions that might be interesting to put forward towards the auxin/pH models described over the last chapters: How do auxin transport fluxes over the plasma membrane change in cells within a tissue context, specifically between an auxin source and an auxin sink, if auxin/proton dynamics are considered? Is an emergence of net flux polarisation occurring with our model, if put into such a spatial context? Moreover, how does AAA affect these net fluxes - does it strengthen or weaken them, or are net fluxes not influenced by AAA? With diffusion of auxin and protons added to the system, would auxin gradients in the cell build up? And, could we detect heterogeneity in the proton motive force over the plasma membrane, potentially leading to regions of a stronger proton gradient? Since some auxin transport proteins are energised by the proton motive force (see chapter 5), such heterogeneities, if occurring in robust patterns on the plasma membrane, could suggest potential additional mechanistic explanations for auxin efflux polarisation, due to differential energisation of PINs by the proton motive force.

Such questions lead the way to including the model of auxin/proton dynamics in a spatial context. In this chapter, AP-2 will be extended towards a reaction-diffusion model. To distinguish this model from other models developed in the scope of this thesis, this new model will be referred to as SAP-2 (S stands for *s*patio-temporal, whereas AP-2 refers to the minimised auxin/proton model described in section 7.2).

8.1 Assumptions of the SAP-2 model

Since the core mechanistic model for auxin/proton interactions is transferred into the SAP-2 model unchanged, all assumption underlying this core mechanistic model (AP-2) are also underlying the SAP-2 model. For a reminder of these, please refer to sections 6.1 and 7.2. However, some additional assumptions are made, especially concerning the cell shape, distribution of proton pumps and auxin transporters on the membrane, and diffusion of substance and are discussed in this section.

Cell geometry. Cells are modelled as rectangular objects, very similar to the abstraction in the PIN polarisation model (see section 4.1), containing a rectangular vacuole and surrounded by cell wall space with constant thickness. The plasma membrane contains equally distributed proton pumps and equally distributed auxin transporters. Transporter cycling, and hence the possibility for transporter polarisation, does not occur in SAP-2. Both PINs and ABCBs contribute to a constant rate of auxin efflux. The spatial Finite Difference discretisation is identical to the one described in chapter 4 and can be found in figure 4.2.

Auxin diffusion. The diffusion constant of auxin in water is $7 \cdot 10^{-6}$ cm^2/s [31, 71]. It is interesting to note that there does not seem to exist an unambiguous experimental determination of the apparent auxin diffusion coefficient within cellular compartments. Most modellers refer to the estimation of auxin diffusion rates of Goldsmith et al. based on auxin diffusion in water [71], which is corrected by an arbitrary factor for a more viscous environment.

Thus, the model of Grieneisen et al. assumes a diffusion constant D_A of 600 μm^2/s in the cytosol, which is $6 \cdot 10^{-6}$ cm^2/s [73], about the same range that is employed in the model of Jönsson et al., where D_A is $7 \cdot 10^{-6}$ cm^2/s for the apoplast only (this model assumes no auxin diffusion in the cytosol) [89], whereas others assume lower values for D_A, especially for the apoplast, as Wabnik et al. with a D_A of 10^{-6} cm^2/s [239]. There is one modelling study defining D_A coefficients in the range of $4.4 \cdot 10^{-7}$ cm^2/s, suggesting a 5-fold lower diffusion of auxin in the apoplast than in the cytosol [103]. Because of these different suggestions, the SAP-2 model is simulated with different auxin diffusion coefficients in the range of $0.5 - 4 \cdot 10^{-6}$ cm^2/s, to test whether diffusion coefficient settings have an impact on the model outcome.

H^+ diffusion. Proton diffusion in water is in the range of 10^{-4} cm^2/s [218]. In the cytosol, due to the interactions of fixed and mobile proton buffers, the proton diffusion coefficient is slowed down to values around $1.4 \cdot 10^{-6}$ cm^2/s [3]. Thus it appears that the H^+ diffusion coefficient is in the same range as the auxin diffusion coefficient.

8.2 Extending AP-2 to a continuous reaction-diffusion system

The AP-2 model, consisting of four ODEs, which are described in equations (7.20) to (7.23), is transformed into a reaction-diffusion system in two spatial dimensions. The diffusion terms for this system can be written as follows:

$$\frac{\partial [A]_a}{\partial t} = D_A \cdot \left(\frac{\partial^2 [A]_a}{\partial x^2} + \frac{\partial^2 [A]_a}{\partial y^2} \right) \tag{8.1}$$

$$\frac{\partial [H]_a}{\partial t} = D_H \cdot \left(\frac{\partial^2 [H]_a}{\partial x^2} + \frac{\partial^2 [H]_a}{\partial y^2} \right) \tag{8.2}$$

$$\frac{\partial [A]_c}{\partial t} = D_A \cdot \left(\frac{\partial^2 [A]_c}{\partial x^2} + \frac{\partial^2 [A]_c}{\partial y^2} \right) \tag{8.3}$$

$$\frac{\partial [H]_c}{\partial t} = D_H \cdot \left(\frac{\partial^2 [H]_c}{\partial x^2} + \frac{\partial^2 [H]_c}{\partial y^2} \right) \tag{8.4}$$

with the subscripts a and c referring to apoplastic and cytosolic variables, respectively, A is the auxin concentration, H is the concentration of free protons, and D_A and D_H are the auxin and H^+ diffusion coefficients. Auxin exchange between source and sink grid points, bordering to apoplastic grid points, is provided by simple diffusion. Thus, auxin diffuses freely between grid points defining boundary regions where auxin levels are at a fixed high level (auxin sources) and the neighbouring apoplastic grid points, and the same holds for boundary grid points where auxin levels are defined to be low at a fixed concentration (auxin sinks). All initial values for these boundary conditions can be found in table A.8 in the appendix. No diffusion takes place between the apoplast and the cytosol, thus the exchange of auxin and protons between these compartments relies entirely on auxin and proton transport mechanisms. These transport mechanisms take only place at the border between apoplast and cytosol (plasma membrane) and at the border between cytosol and vacuole (tonoplast). In the discretised model environment, apoplastic grid points which have a cytosolic neighbour grid point exchange auxin with this neighbouring cytosolic grid point according to

$$\frac{d[A]_a}{dt} = \gamma [IAA^-]_c - \beta [IAA^-]_a [H]_a^2 - \alpha ([IAAH]_a - [IAAH]_c) \tag{8.5}$$

and, accordingly, cytosolic grid points exchange auxin to neighbouring apoplastic grid points in the following manner:

$$\frac{d[A]_c}{dt} = -\gamma[IAA^-]_c + \beta[IAA^-]_a[H]_a^2 + \alpha([IAAH]_a - [IAAH]_c) \tag{8.6}$$

where α is the passive influx rate for auxin, β is the active (AUX/LAX-mediated) auxin influx rate and γ is the active symmetric auxin efflux rate, which is not dependent on the proton motive force (ABCBs). The respective amounts of dissociated and undissociated auxin species are given by

$$[IAA^-] = \frac{[A]}{1 + 10^{(pK_a - pH)}} \tag{8.7}$$

and

$$[IAAH] = \frac{[A]}{1 + 10^{(pH - pK_a)}} \tag{8.8}$$

with the pH and auxin values at the actual (apoplastic or cytosolic) grid point. Proton exchange over the plasma membrane is, in a similar manner, given for apoplastic grid points neighbouring a cytosolic grid point as follows:

$$\begin{aligned}\frac{d[H]_a}{dt} &= \frac{[H]_a}{b_a} \cdot \frac{1}{V_a}\Bigg[X + \frac{V_p \cdot [H]_c}{K_p + [H]_c} - \\ &\quad - r_H([H]_a - [H]_c) - 2\beta[IAA^-]_a[H]_a^2\Bigg]\end{aligned} \tag{8.9}$$

and, similarly, for cytosolic grid points neighbouring apoplastic grid points, the proton exchange over the plasma membrane is expressed by

$$\begin{aligned}\frac{d[H]_c}{dt} &= \frac{[H]_c}{b_c} \cdot \frac{1}{V_c}\Bigg[-X - \frac{V_p \cdot [H]_c}{K_p + [H]_c} + \\ &\quad + 2\beta[IAA^-]_a[H]_a^2 + r_H([H]_a - [H]_c)\Bigg]\end{aligned} \tag{8.10}$$

whereas the proton exchange over the tonoplast (between cytosolic grid points and neighbouring vacuolar grid points) is given by

$$\frac{d[H]_c}{dt} = \frac{1}{V_c}\left[\frac{V_t \cdot [H]_c}{K_t + [H]_c} + r_H([H]_v - [H]_c)\right] \tag{8.11}$$

The pH homeostasis terms employ buffer capacity values b_a and b_c for apoplast and cytosol, the Hill equations for the proton pump activity employ the maximum pump activity parameters V_p and V_t for plasma membrane and tonoplast, respectively, and

K_p and K_t as the Michaelis constants for plasma membrane and tonoplast bound H^+-ATPases. The H^+ reflux over tonoplast and plasma membrane is dependent on the H^+ permeability parameter r_H. Volumes V_c and V_a for the cytosol and apoplast are part of the buffering expression: since buffering is, following the assumptions of AP-2, only taking place at the boundaries between cytosol and apoplast, and between cytosol and vacuole, the amount of incoming and outgoing H^+ is determined by the volume of the respective compartments (see section 7.2). The term X (Gaussian curve for auxin-dependent activation of PM-H^+-ATPase is, according to equation (7.24),

$$X(IAA^-) \;=\; X_a \cdot e^{\left(-\frac{(ln(X_b)-ln([IAA^-]_c))^2}{X_c}\right)} \tag{8.12}$$

The parameters X_a, X_b and X_c are the height, position and width parameters of the Gaussian function describing auxin-dependent activation of the PM-H^+-ATPase . All parameter values can be found in table A.8 in the appendix.

8.3 Numerical solution

As already stated earlier (see section 4.3), high values for diffusion constants call for very small time steps for straightforward explicit solutions like the FTCS scheme of numerical solution (also called Euler forward method), to meet the stability criterion for that solution. This is usually computationally expensive and therefore not recommended in models as the SAP-2 with desired simulation times in the range of hours. A solution for reaction-diffusion systems containing only linear reaction terms can therefore, without such restrictions, often be obtained successfully using implicit methods, such as the BTCS scheme or the Crank-Nicholson scheme. This was the case with the PIN polarisation model in this thesis (see chapter 4). However, the SAP-2 model is different from that, because some of its reaction terms are nonlinear. Take, for instance, equation (8.4), which contains many nonlinear terms: X, $\frac{V_t \cdot [H]_c}{K_t + [H]_c}$, $\frac{V_p \cdot [H]_c}{K_p + [H]_c}$, and $2\beta[IAA^-]_a[H]_a^2$. Using fully implicit methods, this poses the problem that in equations with a nonlinear term involving two variables, as for instance in the given example, for the term $2\beta[IAA^-]_a[H]_a^2$, $[H]_a$ and $[IAA^-]_a$ need both to be evaluated at the same time. Thus, to evaluate the value of $[H]_a$ at time $t+1$, we need to know the value of $[IAA^-]_a$ at time $t+1$, which in turn we cannot evaluate if we don't know the value of $[H]_a$ at time $t+1$.

It has to be noted, that model minimisation from AP-10 to AP-2 did not reduce the non-linearities in the system. Take, for instance, the mechanism leading to AAA. This led in AP-10, with ABP(x) employed, to the following formulation for the formation of ABP(s):IAA complex (see table 6.3)

$$\frac{d[ABP]_{act}}{dt} = k_1[IAA]_c[ABP]_{free} - k_{-1}[ABP]_{act} - k_{-2}[IAA]_c[ABP]_{act} + k_2[ABP]_{inact} \tag{8.13}$$

which contains nonlinear terms. In AP-4 and AP-2, this is reduced to the expression X, which is, as a Gaussian function involving $[IAA]_c$ as part of the exponent, still nonlinear (see equation (8.12)). Thus, even if the process is simplified by reducing the number of variables involved, non-linearity is preserved and passed on to the simplified model as well.

To summarise the problems in a numerical solution of this particular system of equations: fully explicit methods are not applicable due to stability constraints which are mainly dependent on the potentially high diffusion coefficients of auxin and proton diffusion, while fully implicit methods are not applicable due to nonlinearities in the reaction part of the equations, which generally leads to expensive computations and makes fast iterative solution techniques less efficient and more difficult to implement [188] .

To overcome this issue, several approaches are tried and tested:

1. Iterative techniques to solve nonlinear systems of equations: Fixed point iteration using the Gauss-Seidel method

2. IMEX approaches: using mixed implicit-explicit methods to solve the system of reaction-diffusion equations, especially 1-SBDF and 2-SBDF schemes (first and second order semi-implicit backward differentiation), according to [188]. These schemes solve the diffusion part of the equations implicitly, and the reaction part of the equations explicitly.

8.3.1 Solving using fixed point iteration

At each time point, for every grid point, a set of nonlinear equations was solved by a fixed point iteration, using a Gauss-Seidel relaxation scheme for iterative solving. This has been accomplished for the AP-4 model. Each PDE was discretised using the BTCS scheme, to obtain a set of full implicit nonlinear equations. After that, fixed point iteration was defined for each equation. When applied to the AP-2 model, convergence of the fixed point iterations could not be reached, therefore this method was considered unsuitable for a numerical solution of SAP-2.

8.3.2 IMEX schemes: 1-SBDF and 2-SBDF

In previous studies, 2-SBDF has been proposed to be a good method of choice among other implicit/explicit methods for reaction-diffusion systems with nonlinear reaction terms [188], with a better accuracy than 1-SBDF. Following a study of Ruuth [188], for a general reaction-diffusion equation that has been approximated by the centred finite difference method

$$\frac{dW}{dt} = F(W) + D\Delta_h W \tag{8.14}$$

where $F(W)$ arises from the reaction term and $D\Delta_h W$ is the diffusion term expressed in centred finite differences with D being the diffusion coefficient, e.g. of the form $\frac{D}{\Delta h^2}(W_{i+1} + W_{i-1} - 2W_i)$, which is a second order centred difference expression for a 1D representation, where W at grid point i and at neighbouring grid points $(i+1)$ and $(i-1)$ are considered, and Δh is the constant mesh spacing; the first order semi-implicit backwards differentiation scheme or 1-SBDF scheme is given by

$$\frac{W^{t+1} - W^t}{\Delta t} = F(W^t) + D\Delta_h W^{t+1} \tag{8.15}$$

where the diffusion term is solved implicitly for time $t+1$ and the reaction term is solved at time t. The second order semi implicit backwards differentiation scheme or 2-SBDF is given by

$$\frac{1}{2\Delta t}\left[3W^{t+1} - 4W^t + W^{t-1}\right] = 2F(W^t) - F(W^{t-1}) + D\Delta_h W^{t+1} \tag{8.16}$$

where the diffusion term is again evaluated at time $t+1$ using implicit methods, but the reaction term is solved using two time points: $t+1$ and $t-1$. To implement this method, the system state needs to be known for two consecutive time steps, and starting at

the initial values for the system is not possible, as opposed to implementations of the 1-SBDF. Therefore, an initial evaluation step needs to be done, which has been implemented by the LSODA solver [168], which uses an iterative scheme to solve for the first time step. This method is very slow, but since only the first time step was evaluated using this solver, this had no considerable consequence on the overall running time of simulations. With the initial values defined for the system, and the first time step evaluated by LSODA, the 2-SBDF scheme could be implemented, where, according to equation (8.16) above, $t-1$ corresponds to the initial values in the model, t corresponds to the first time step evaluated by LSODA and all following time steps are then obtained by iterative solving with 2-SBDF.

To evaluate the behaviour of the IMEX schemes employed with SAP-2, solutions obtained with the 1-SBDF scheme have been compared to solutions obtained with 2-SBDF, using the same set of parameters, except for different sizes of time steps. This has been done as a first test for the choice of a numerical method and to test whether the use of the more efficient 1-SBDF scheme is justified. The results of SAP are discussed in further detail in the following section, whereas here the difference in the outcome between 1-SBDF and 2-SBDF as a choice of method is discussed. The results of this test show a comparable outcome for both schemes and suggests that the use of 1-SBDF with this model is safe, thus allowing for saving extra computational costs which are connected to the use of 2-SBDF. The time step size was varied between $dt = 0.01s$ and $dt = 10s$. Except for fast changes of concentrations, typically only occurring at the start of the simulation, the results were very similar for all time steps used (see figure 8.1). Since with using bigger time steps, those fast perturbations in the results are transient and the solutions approximated following equilibrium values nearly indistinguishable from solutions obtained with smaller time steps, the choice for a 1-SBDF scheme with time steps around 1 seem to be justified.

8.4 Results

Simulations of SAP-2 with a choice for time steps $dt = 10s$ had a running time of approximately 23 minutes on a machine with a 3 GHz Core Duo E8400 processor and 4 GB RAM for 8 hours simulation time. Smaller time steps did not significantly change the simulation results (see figure 8.1). Two different settings for the SAP-2 have been

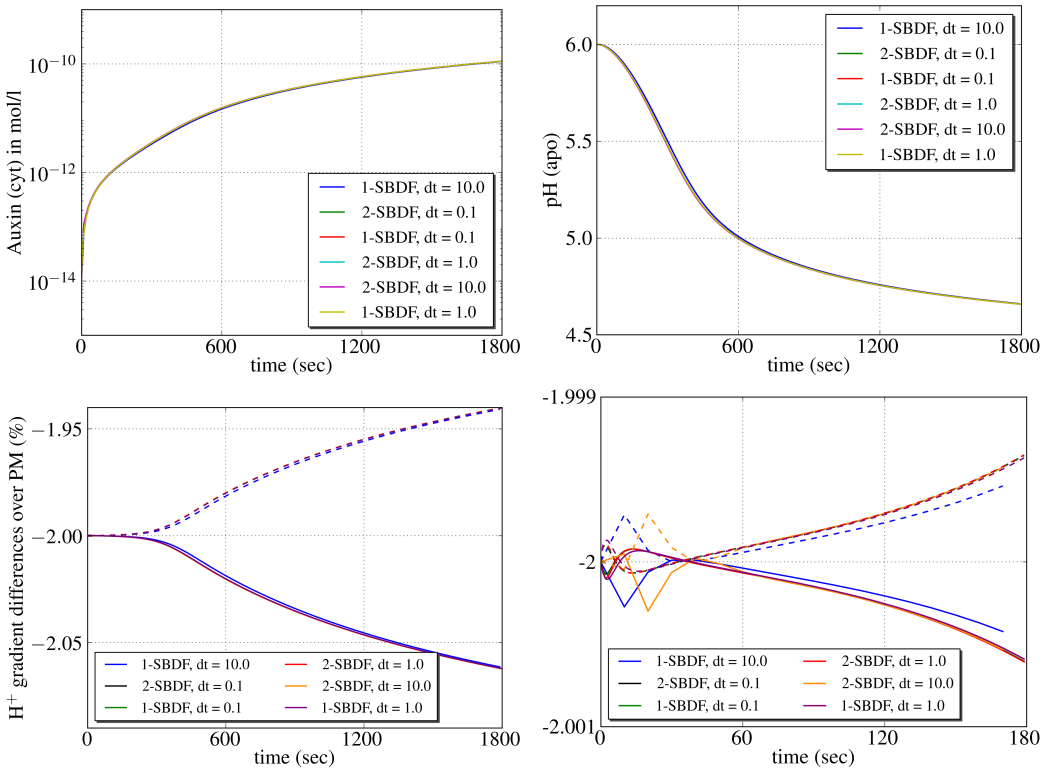

Figure 8.1: Comparison between simulations employing the 1-SBDF and 2-SBDF scheme for a numerical solution, using different time step sizes. *Upper left:* Mean auxin concentration in the cytosol, *Upper right:* Mean apoplastic pH, *Lower left:* H^+ gradients over the membrane at the membrane grid point numbers 90 (dashed line) and 198 (full line), corresponding to grid indices 1998 and 1382 in the model environment, during the first 30 minutes of the simulation. *Lower right:* The situation for membrane grid point numbers 90 (dashed line) and 198 (full line) during the first 180 seconds. Simulations with $dt = 10s$ could not capture the fast perturbations in the solutions at the start, however they later approximate the trajectories of simulations with smaller time steps. The y-axis represents H^+ gradients over the membrane (% deviation from mean gradient).

tested: (a) the situation for a single cell, surrounded by apoplastic space, bordering to one auxin source and one auxin sink field, and (b) the same situation for a file of 3 cells. The results recapitulated and confirmed the central findings of AP-10, AP-4 and AP-2, such as the general capability to reproduce pH homeostasis, the reproduction of an AAA peak in presence of auxin, auxin flux enforcement due to AAA and pronounced auxin allocation into cells with AAA in effect. Additionally, the results gave insights into the directionality of auxin flux dynamics during simulations, showing that AAA amplifies the polarity of cells with respect to auxin transport. This polarity is consistent with the canalisation hypothesis. Moreover, the relative relationship of active versus passive

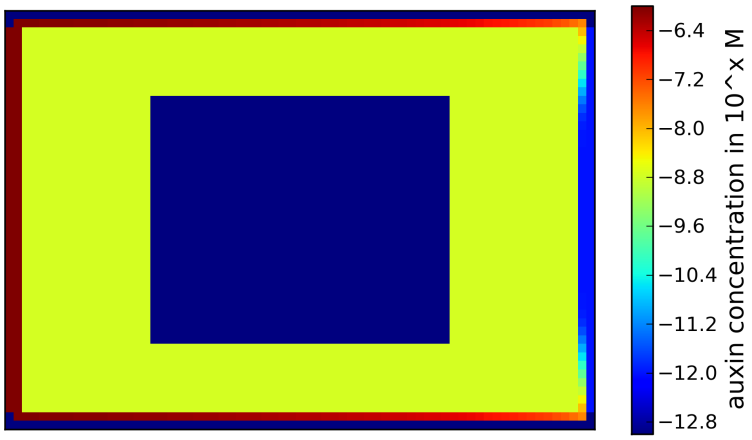

Figure 8.2: Auxin concentrations in the SAP-2 model after 8 hours of simulation time. A cell, containing a central vacuole, and surrounded by a layer of extracellular space, is transporting auxin in the context of its boundary conditions - auxin source (left) and sink (right). The colourbar represents the logarithm of auxin concentrations in the modelling environment. Concentrations are in the range of 10^{-12} to 10^{-6} M. Note that the concentration of auxin in the cell is homogeneous.

auxin transport fluxes in the course of AAA was investigated, with results showing that passive auxin influx might be important for the onset of AAA, which then turns on and increases the importance of AUX/LAX-mediated active influx, thus potentiating the main auxin/pH feedback reaction outlined in previous chapters. An interesting finding was that simulations led to considerable heterogeneities of the proton motive force as a result of auxin gradients and AAA dynamics, thereby showing clear polarisation in the proton motive force in the auxin source to sink axis, with a stronger H^+ gradient towards the auxin sink.

Thus, the model could reproduce a canalisation-type feedback of auxin on its transport, leading to polarisation patterns without any need of polarising transporters, driven mainly by symmetrically distributed AUX/LAX importers and a feedback between auxin and protons within an extracellular auxin gradient between auxin source and sink. The sensitivity of simulations to parameter choice was investigated, showing that the results of SAP-2 are generally robust against changes of most parameters. The model topology, similar to the topology of the PIN polarisation model (see section 4.1), resulting in a typical auxin distribution pattern at the end of a simulation (simulation time 8 hours) is illustrated in figure 8.2.

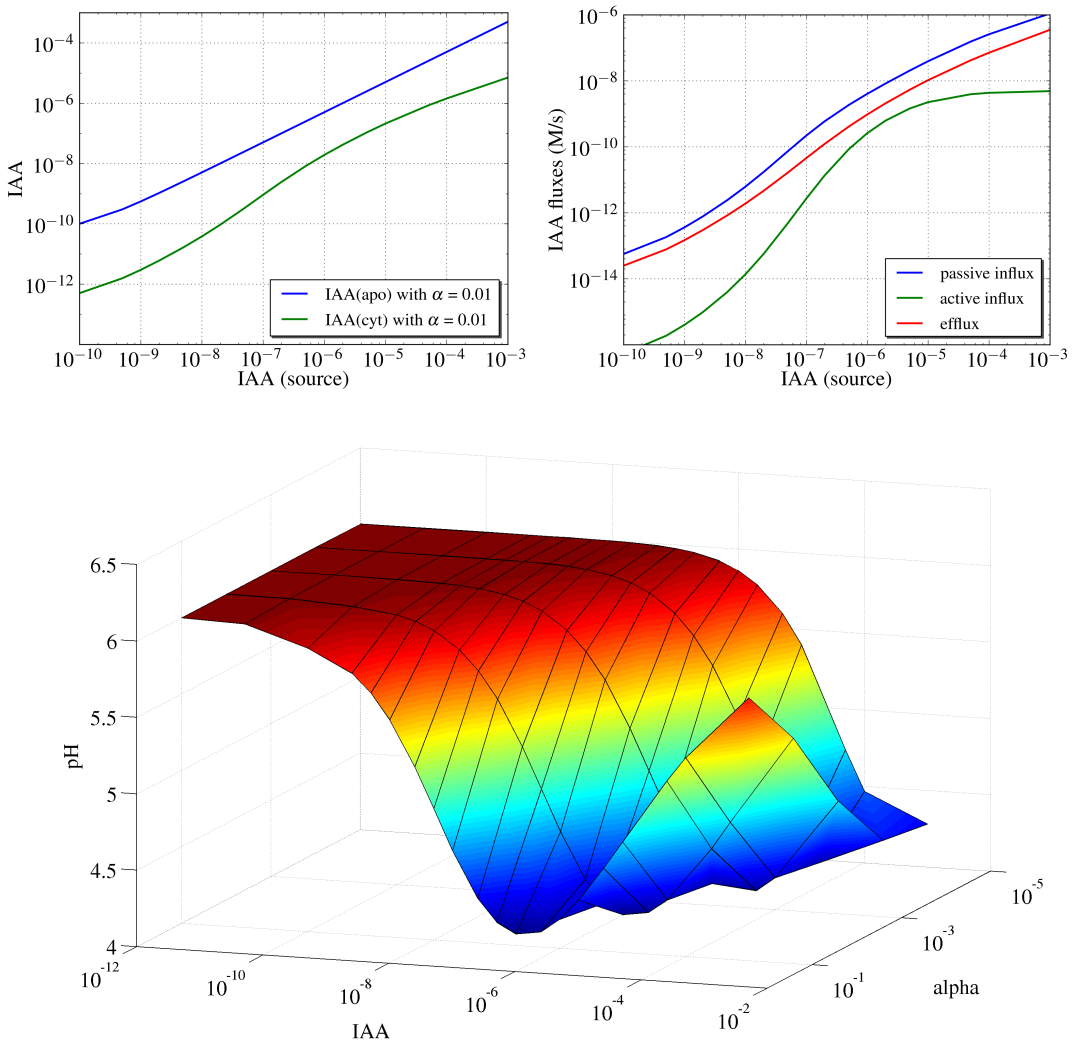

Figure 8.3: Auxin-induced apoplastic acidification and its effects on auxin transport fluxes and cytosolic auxin allocation in SAP-2. *Upper left:* Auxin allocation into cells is more pronounced when AAA is in effect. *Upper right:* Auxin transport fluxes over the membrane are elevated with AAA in effect. The corresponding AAA dose-response curve for both upper figures, showing pH values in the apoplast at external auxin concentrations, can be obtained from the lower figure with $\alpha = 0.01$. The curves represent mean values for auxin fluxes over the plasma membrane, and auxin concentrations in the respective compartments apoplast and cytosol. *Lower:* AAA as a function of boundary conditions (auxin source concentration) and the passive influx parameter, α. Lower values for α result in a shift of the AAA peak towards higher apoplastic auxin concentrations as well as in a faster onset of AAA, when compared to higher values for α. All values were taken after the end of simulations at 8 hours simulation time.

8.4.1 Reproduction of core AP model findings in SAP-2

The main findings of the AP-10, AP-4 and AP-2 model (see figure 7.2) could be reproduced in 2D: Auxin-induced apoplastic acidification (AAA) at certain auxin levels

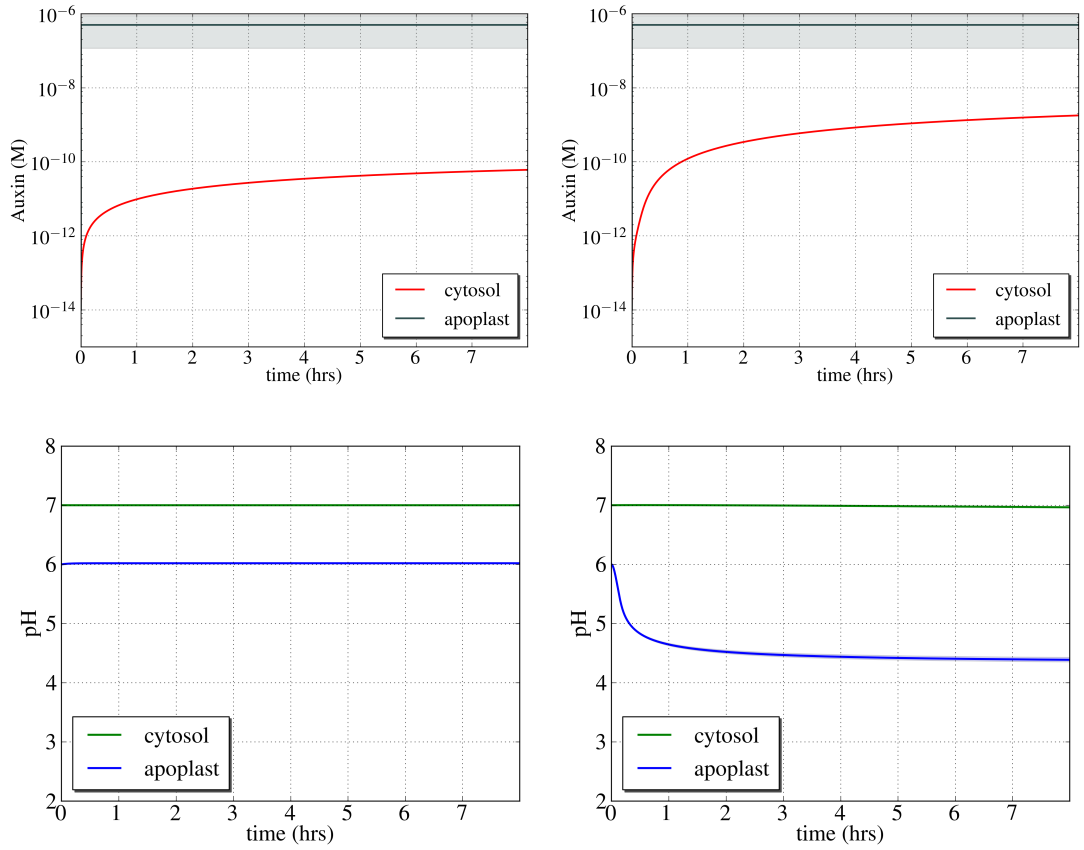

Figure 8.4: Time scale of auxin allocation and AAA in SAP-2. *Upper left:* Auxin allocation in the cell without AAA ($X_a = 0$). *Upper right:* Auxin allocation in the cell during a simulation with AAA ($X_a = 5 \cdot 10^{-10}$). Grey shaded curves signify the range of standard deviation of auxin concentration in the apoplast. *Lower left:* pH evolution without AAA and same settings as above. *Lower right:* pH evolution with AAA.

(usually in the micromolar range of extracellular auxin, depending on auxin transport parameters), pronounced auxin accumulation in cells, as AAA was in effect, and increase of auxin transport fluxes over the membrane as a result of AAA (see figure 8.3). However, due to the extracellular auxin gradient, import fluxes varied in space, being dependent on apoplastic auxin concentrations. This is in contrast to the auxin efflux, which occurs at a constant rate. Initially formed auxin gradients within cells blur out quickly (within minutes) throughout all simulations (see 8.2), which is in contrast to similar models and will be discussed in following sections. This behaviour is robust against changes of the auxin diffusion coefficient, suggesting that symmetric auxin transport rates lead to homogenisation of initial cytosolic auxin gradients.

8.4.2 Time scale of AAA in SAP-2

Equilibration of cellular auxin concentration is somewhat slower in SAP-2 than in AP-(10-2), a trend that, since AAA is dependent on cellular auxin, also holds for equilibration of apoplastic pH once AAA is in effect (figure 8.4), but occurs usually within 5-10 hours, with only slight changes in pH after the first four hours. Higher influx rates generally led to a faster equilibration and to a faster onset of AAA. Variation of values for the auxin diffusion constant D_A in the range of $D_A = 50 - 400 \mu m^2/s$ had no impact on this result, suggesting that diffusion does not have a major effect on the speed of equilibration. However, higher rates for auxin decay ($A_{decay} > 10^{-4}$) led to a slightly faster equilibration for simulations without AAA, while this also slows down the AAA mechanism. The difference in equilibration time to the AP models is presumably due to the fact that these already start with saturated apoplastic auxin concentrations, whereas in the SAP-2 model the auxin levels in the apoplast are not saturated at the start of the simulation, but are dependent on the external influx from auxin source fields and on the external efflux to auxin sink fields, which is an inclusion of auxin production and degradation terms that have not been employed in the AP models.

8.4.3 Heterogeneity in the PMF due to AAA

A clear polarisation in the proton motive force (PMF) established in simulation that involved AAA, with deviations from the PMF mean between ± 5 to 10 % for most parameter settings (see also figure 8.10). The polarisation directionality is along the axis between auxin source and auxin sink (several combinations of auxin source and sink locations around the cell have been explored in the simulation and led to the same result). During AAA, the PMF generally rises because of the falling pH in the apoplast, while the cytosol maintains to its pH close to its initial value, with heterogeneities in the PMF getting stronger, correlating to the AAA strength. These heterogeneities show a decreased strength in PMF towards the auxin source and an increased PMF towards the auxin sink. Bigger vacuole sizes generally led to a stronger PMF heterogeneity due to a stronger accumulation of auxin in the cytosol. Establishment of PMF polarisation relies on the relative strength of AUX/LAX-mediated co-transport of protons with respect to the H^+ reflux rate. Extracellular auxin gradients led to nonhomogeneous AUX/LAX influx, which led to a nonhomogeneous proton influx due to the sym-

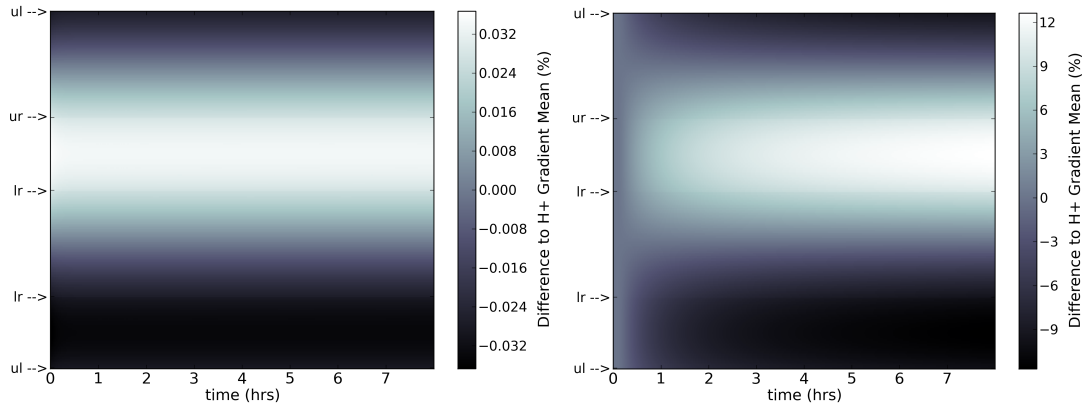

Figure 8.5: Proton gradient heterogeneities over the plasma membrane in SAP-2 over time. Proton gradients are defined as the difference in proton concentration over the plasma membrane. The vertical axis corresponds to the length of the cell membrane, as its circumference is converted into 1D. The indicators *ul, ur, lr, ll* refer to *upper left, upper right, lower right, lower left* corners of the membrane in the model environment. The horizontal axis is the time axis. The variation of proton gradients over the membrane ($H_{apoplast} - H_{cytosol}$) at each membrane grid point from the mean proton gradient over the whole membrane is displayed in percent over the whole simulation time. Overall, a clear polarisation of the proton gradient emerges after around 1 hour of simulation time with AAA in effect. *Left:* The situation without AAA: Proton gradient heterogeneity stays below ± 0.04 % throughout the simulation. *Right:* The situation with AAA: Proton gradient heterogeneity raises to ± 10 % throughout the simulation. See figure 8.6 for a polar plot representation of this H^+ gradient polarisation pattern.

porter activity of AUX/LAX transporter proteins. Towards the auxin source, with higher apoplastic auxin levels, this led to a strong active influx of auxin and a slightly diminished PMF due to co-transported H^+, while towards the auxin sink, lower apoplastic auxin levels led to relatively smaller auxin and, correspondingly, H^+ influx. An illustration proton fluxes over the plasma membrane during the simulation is given in figure 8.6.

8.4.4 Net auxin fluxes over the plasma membrane due to AAA

Consistent with the findings of the AP models described in chapters 6 and 7, AAA caused increase of auxin transport fluxes over the plasma membrane during simulations. Influxes are elevated by lower apoplastic pH, leading to pronounced accumulation of auxin in cells, which in turn increases auxin efflux. While the net auxin flux, defined as $A_{active.influx} + A_{passive.influx} - A_{efflux}$, decreases over time without AAA, it rises before equilibration with AAA (see figure 8.7, upper row). When each respective influx and efflux is considered, AAA leads to an increase of influxes, with effluxes rising in

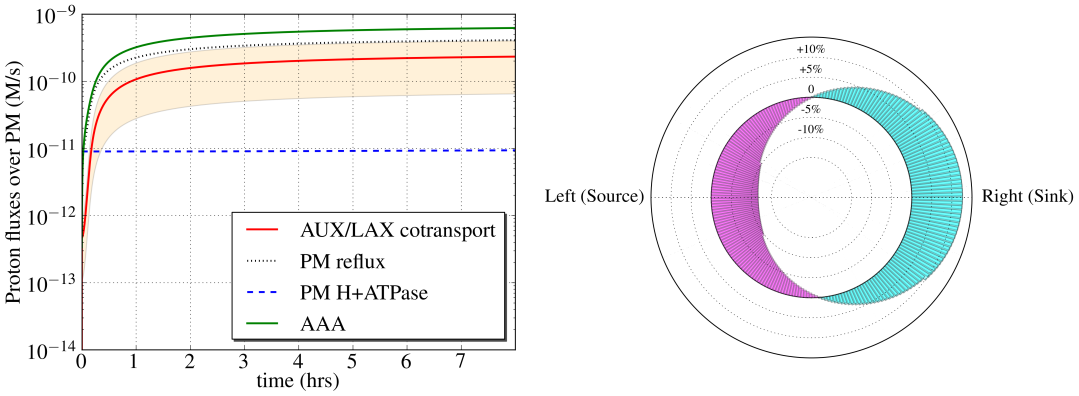

Figure 8.6: Proton fluxes and gradients in the proton motive force with AAA in effect. *Left:* Proton fluxes and their contributions during a simulation with AAA. The shaded area corresponds to $\pm$ standard deviation of H^+ influx due to AUX/LAX co-transport over all cytosolic grid points that have an apoplastic neighbour grid point (signifying the plasma membrane), which is contributing to the polarised H^+ gradient over the membrane. This shows that the AUX/LAX co-transport of protons over the membrane differs significantly in strength, depending on the auxin content of the apoplast. *Right:* Polarisation of the H^+ gradient over the membrane, illustrated as a polar plot: the proton motive force is stronger towards the auxin source and weaker towards the auxin source. The circumference corresponds to the cell membrane circumference, while radial distances correspond to deviations of the H^+ gradient in %, compared with the mean H^+ gradient over the membrane. Purple signifies negative, blue signifies positive deviation in H^+gradient.

turn (see figure 8.7, mid row). Here it appears that lower apoplastic pH triggers active auxin influxes more strongly than passive auxin influxes. Passive influx might, due to these findings, act as a spark for the onset of a stronger active influx reaction to AAA, suggesting that AUX/LAX-mediated auxin import becomes more important after AAA onset with respect to passive auxin influx.

This has been further investigated by expressing the ratio of active (A) versus passive auxin influx (P), $\phi = A/P$, and looking at the value of the ratio ϕ_n/ϕ_0 (ϕ at the start versus end of simulation) in experiments using different settings for the passive import rate (α) and different external auxin concentrations by varying the auxin concentration in auxin source fields. With this expression, the ratio ϕ_n/ϕ_0 gives a measurement of the relative development of active versus passive import fluxes during AAA. The result $\phi_n/\phi_0 = 1$ indicates that the relationship between active and passive auxin import stays the same during the simulation, while $\phi_n/\phi_0 > 1$ indicates that active auxin import gains importance, and $\phi_n/\phi_0 < 1$, accordingly, shows that active auxin

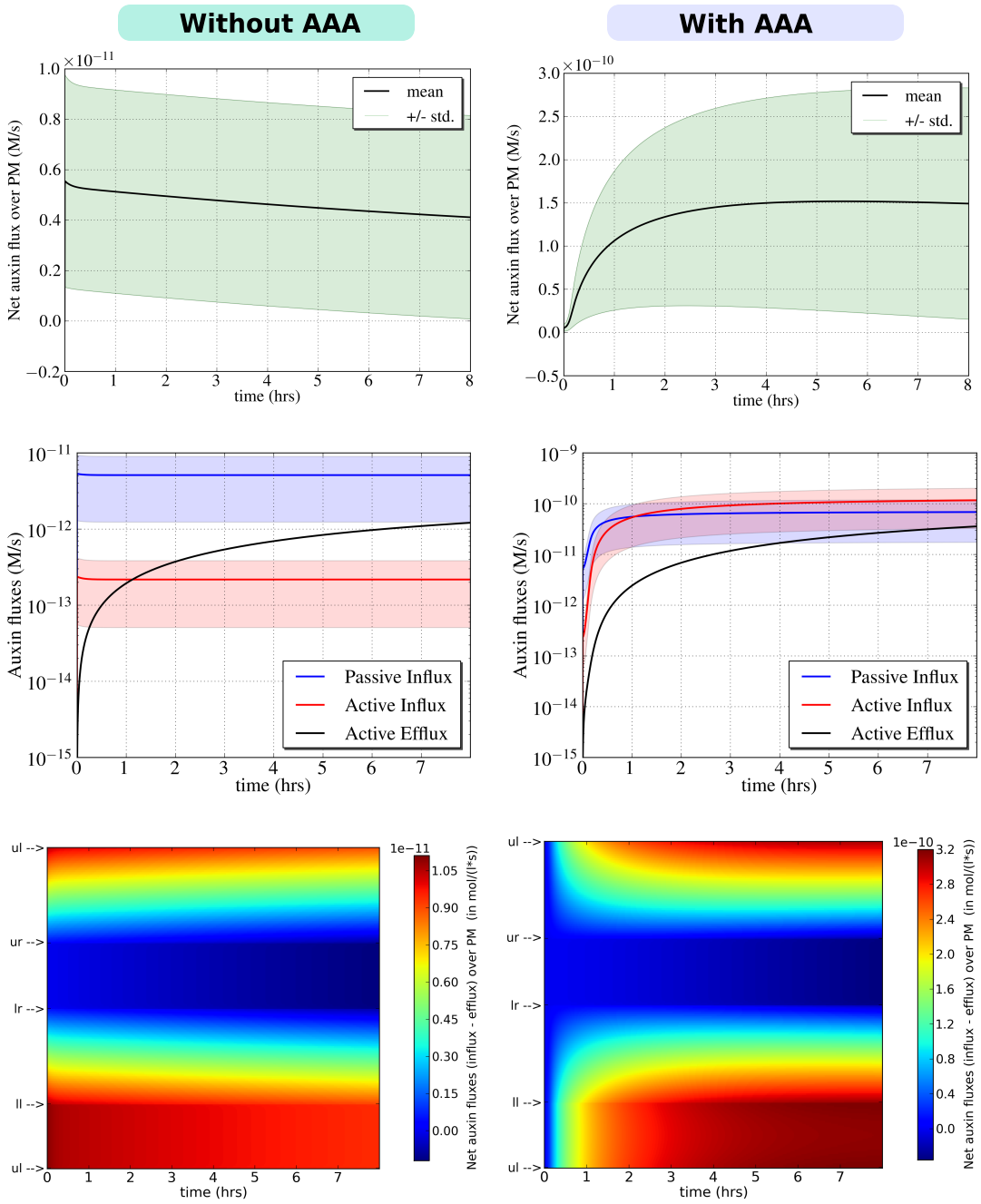

Figure 8.7: Auxin fluxes over the membrane with (*right*) and without (*left*) AAA in effect. *Upper:* Auxin net fluxes mean (solid lines) and standard deviation (shaded area) over the plasma membrane. *Middle:* Auxin influxes and efflux mean (solid lines) and standard deviation (shaded areas) over the plasma membrane. Influxes are elevated during AAA. *Lower:* Net auxin flux development over the membrane in detail in a cell with auxin source towards the left and auxin source towards the right in the modelling environment. The vertical axis corresponds to the length of the cell membrane, as its circumference is converted into 1D. The indicators *ul, ur, lr, ll* refer to *upper left, upper right, lower right, lower left* corners of the membrane in the model environment. The horizontal axis is the time axis. Net fluxes are the sum of all auxin fluxes over each grid point in the membrane, according to $A_{active.influx} + A_{passive.influx} - A_{efflux}$. Net auxin flux is generally positive towards the source and negative towards the sink, a situation that is reinforced with AAA (*lower right*). Colourbar values represent the net flux strength.

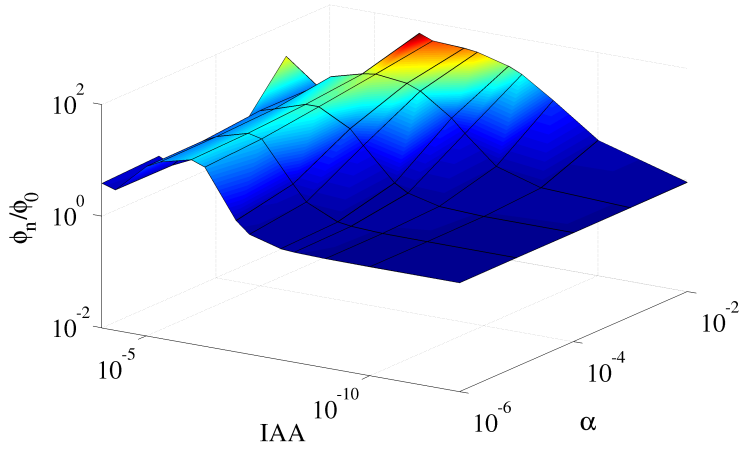

Figure 8.8: The relationship between passive and active auxin import. The ratio ϕ_n/ϕ_0 signifies the ratio of active vs. passive auxin transport at the start (ϕ_0) and at the end (ϕ_n) of the simulations. Values over 1 for the ratio ϕ_n/ϕ_0 show an increase of the relative importance of AUX/LAX-mediated active auxin influx against passive movement of auxin into the cell during the simulations, while values below 1 show an increase of passive over active auxin influx. A value around 1 means that the initial ratio ϕ_0 is maintained throughout the simulation. The ratio ϕ_n/ϕ_0 is explored for different initial values of auxin concentration in the auxin source field and for different settings of the import parameter α. Simulation times were 8 hours.

import loses importance during the simulation. The question behind this was to find out whether one could determine a switch between auxin import regimes. The outcome of this analysis does not point towards such a distinct switch, but rather towards a gradual increase of ϕ_n/ϕ_0 during AAA with a maximum around the AAA peak (figure 8.8). There is a strong correlation between AAA and the value of ϕ_n/ϕ_0, which increases as the apoplastic pH falls during AAA. However, with higher auxin concentrations, this effect is reversed (see figure 8.9).

8.4.5 Parameter sensitivity

The influence of several parameters, especially auxin transport parameters α, β and γ, as well as inclusion of auxin decay d on the overall results has been tested in simulations with and without AAA. Generally, the main simulation results (AAA, flux enhancement, auxin allocation in the apoplast and enforcement of auxin transport polarisation according to canalisation) were robust against a wide range of parameter changes. Auxin decay rate had a dampening effect on AAA by reducing the amount of free auxin accumulating in the cytosol both by reducing the concentration of auxin in

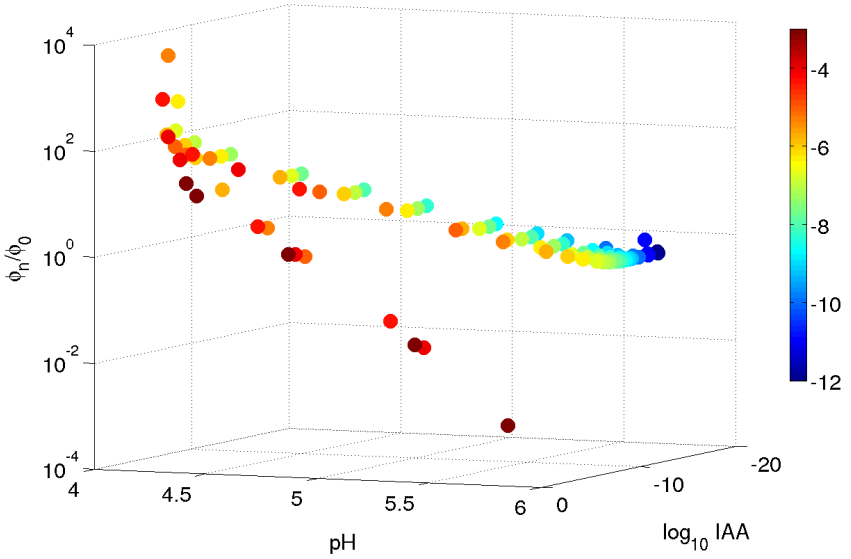

Figure 8.9: Active vs. passive transport as a function of AAA and auxin source concentration. At similar apoplastic pH values, the respective strength of active and passive auxin transport fluxes are different, dependent on apoplastic auxin concentration (the colouring refers to auxin concentration in the apoplast at the data points, colourbar shows $\log_{10}$ values of auxin concentrations. The ratio ϕ_n/ϕ_0 signifies the ratio of active vs. passive auxin transport at the start (ϕ_0) and at the end (ϕ_n) of the simulations. This value is plotted against different initial values of auxin concentrations in the auxin source field and the apoplastic pH at the end of simulations. The ratio ϕ_n/ϕ_0 increases with increasing AAA (corresponding to the 'left' side of the AAA peak in figure 8.3) and decreases again with decreasing AAA (corresponding to the 'right' side of the AAA peak). Simulation time for all parameter settings was 8 hours.

the apoplast for auxin import into the cells and by reducing the cytosolic auxin concentration itself. Changing auxin and H^+ diffusion constant over the range of $0.5 - 6 \cdot 10^{-6}$ cm^2/s both had no significant effect on either AAA, auxin allocation or auxin flux dynamics, suggesting that the effect of auxin transport is determining the system's response much more strongly than pure auxin or proton diffusion, which rather both play a supporting role in auxin and proton distribution.

The effect of auxin transport parameters on simulation outcomes has been tested in two steps: (a) import versus export parameters, focussing on α and γ in runs with fixed values for β, and (b) the two import parameters α and β against each other in runs with fixes values for γ. Auxin import versus export parameters showed very similar results for different settings of β. While not unexpectedly, import and export have antagonistic roles in the promotion of auxin allocation in cells, only higher values

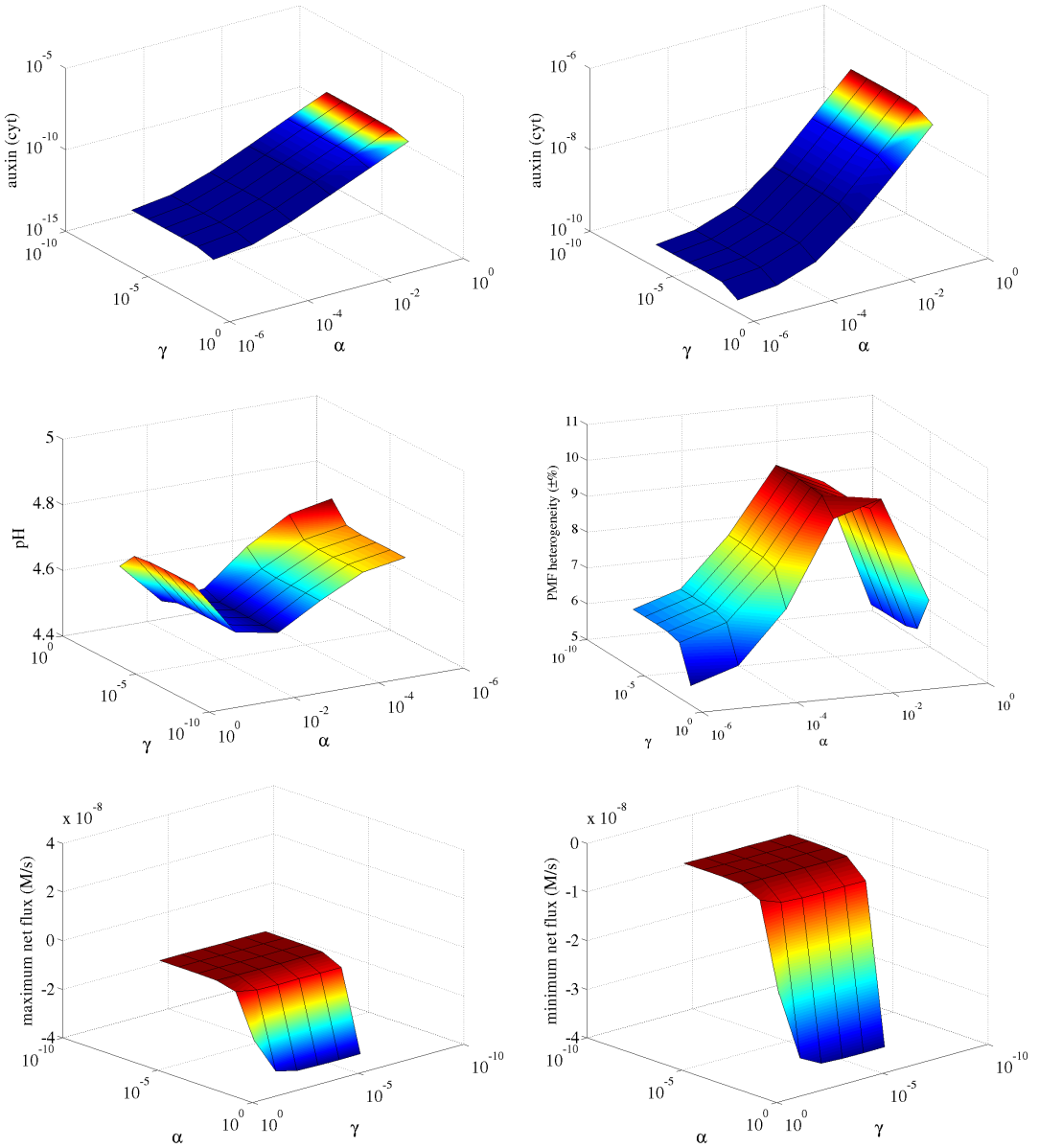

Figure 8.10: Auxin transport parameters α and γ and their influence on simulation outcomes, with active influx parameter β fixed at $\beta = 5 \cdot 10^5$. *Upper left:* Auxin accumulation in the cell at the end of simulations without AAA, as a function of α and γ. *Upper right:* Auxin accumulation in the cell at the end of simulations with AAA. *Middle left:* Apoplastic pH at the end of simulations. *Middle right:* Heterogeneity in the proton motive force over the membrane at the end of simulations (as $\pm$x % deviation from mean proton motive force). *Lower left:* The maximum net flux of auxin over the plasma membrane at the end of simulations, corresponding to the strength of flux towards the auxin sink. *Lower right:* Minimum net flux of auxin over the plasma membrane, corresponding to the strength of auxin flux into the cell near the auxin source. Simulation time for all parameter settings was 8 hours.

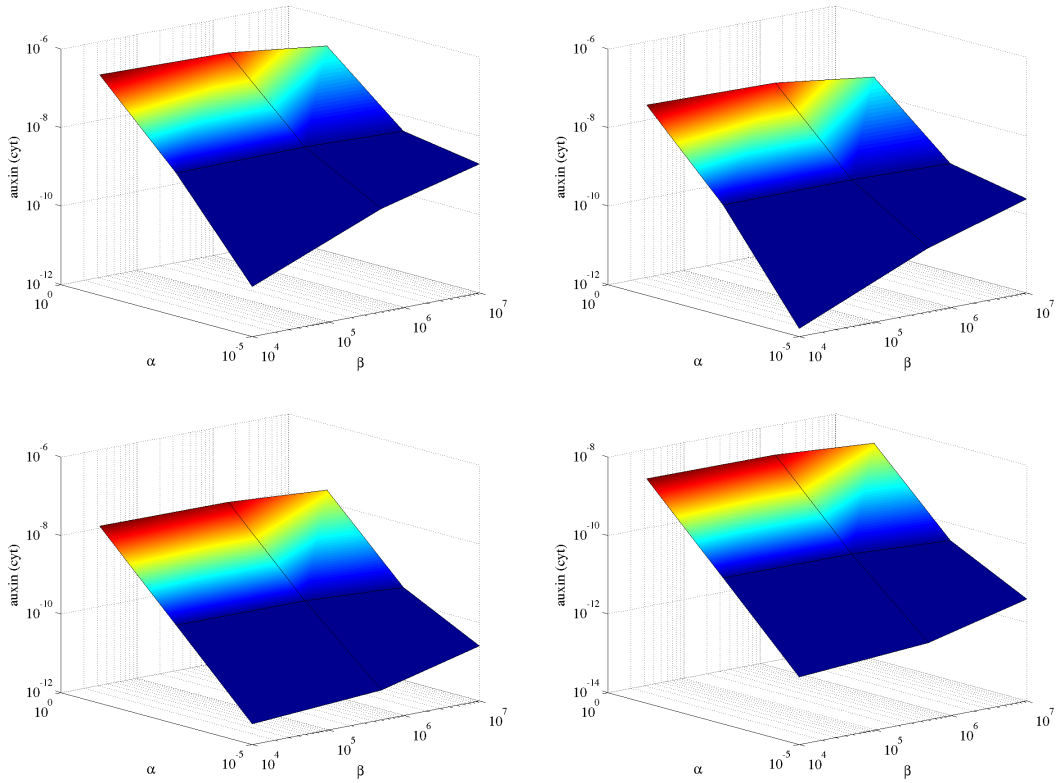

Figure 8.11: Auxin transport parameters α and β and their respective influence on auxin allocation in cells with (*upper*) and without (*lower*) AAA. Auxin efflux parameter γ settings were $\gamma = 0.01$ (*left*) and $\gamma = 0.5$ (*right*), respectively. Cellular mean auxin concentrations were evaluated at the end of simulation time (8 hours).

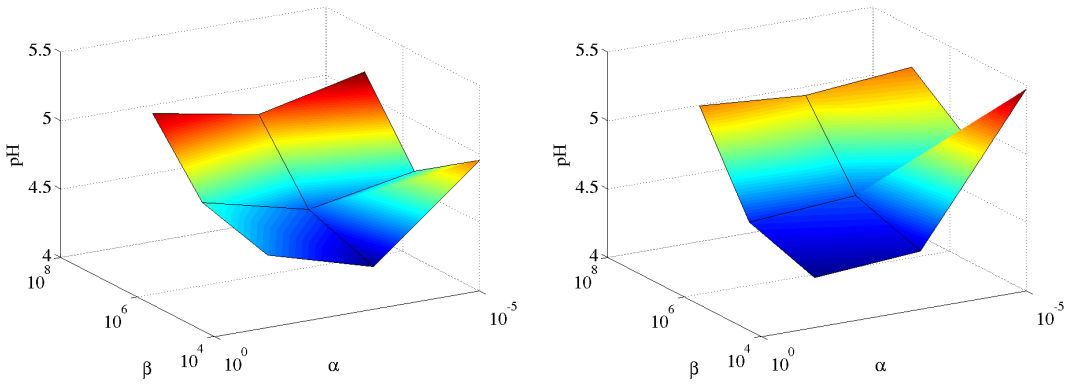

Figure 8.12: Auxin transport parameters α and β and their respective influence on the strength of AAA during simulations. Auxin efflux parameter γ settings were $\gamma = 0.01$ (*left*) and $\gamma = 0.5$ (*right*). Apoplastic pH values were evaluated at the end of simulation time (8 hours).

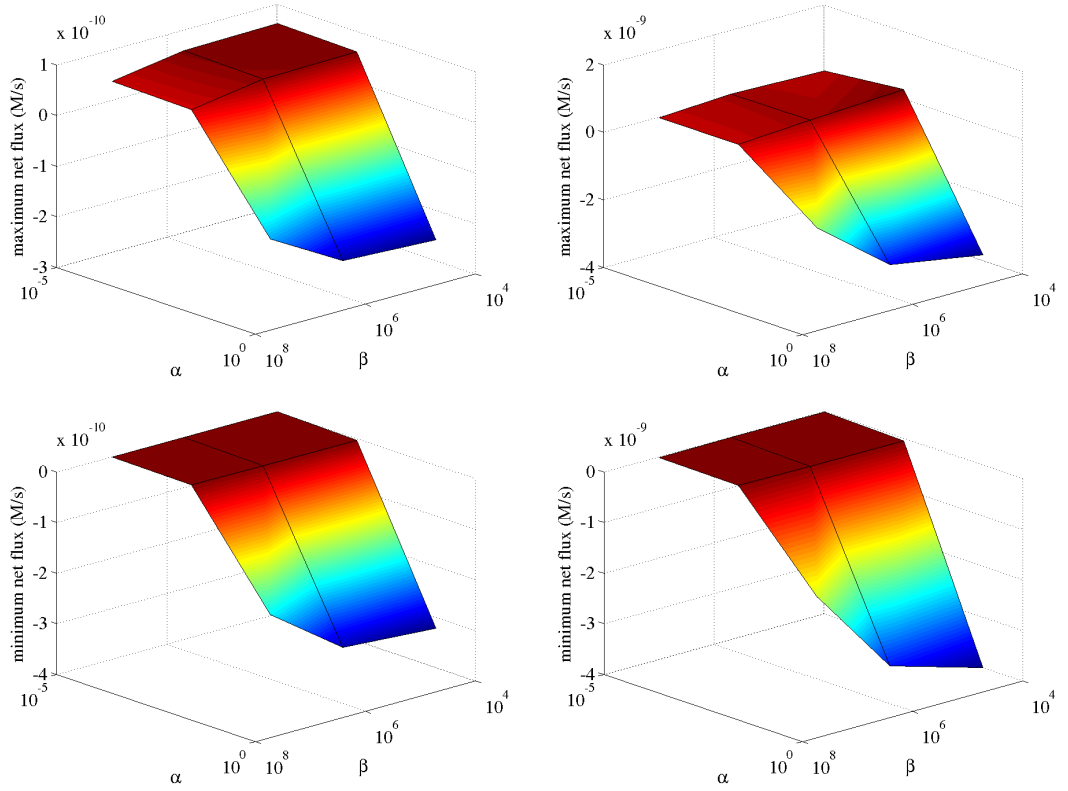

Figure 8.13: Maximum (*upper*) and minimum (*lower*) net auxin fluxes over the membrane as a function of auxin transport parameters α and β during simulations, without (*left*) and with (*right*) AAA in effect. Simulation time for all parameter settings was 8 hours.

of γ seem to have a noticeable effect as antagonists to auxin influx. (figure 8.10). This is due to the fact that higher γ helps to facilitate equilibration, but cannot otherwise change the system behaviour, which is very much dependent on the feedback between AAA and influx. Interestingly, increasing the values for γ slightly decreases the increase in net auxin efflux towards the auxin sink, presumably because it impedes the accumulation of auxin levels in the cytosol, required to activate AAA. This indicates that symmetric auxin efflux has less effect on directed flux enhancement than AAA, even on the strength of overall auxin efflux from the cell. Thereby, auxin influx (by triggering the feedbacks involved in AAA) is thought to be an important factor in the establishment of strong auxin transport polarisation.

When compared against each other, settings of the active auxin influx parameter β have a smaller impact on auxin allocation in the cell than settings of the passive auxin influx parameter α (see figure 8.11), which points towards the importance of passive

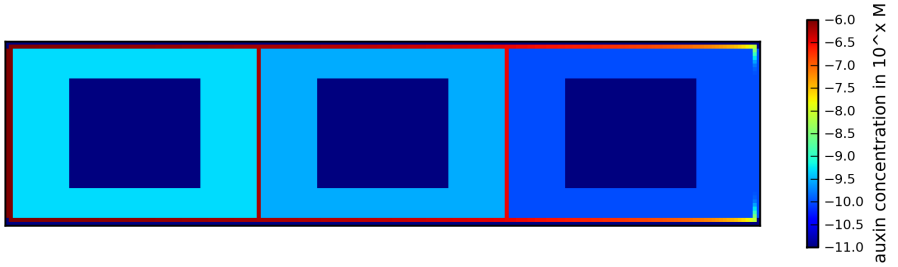

Figure 8.14: Auxin distribution in a simulation involving 3 cells in a row. An auxin source is located at the left, an auxin sink at the right side of the environment.

influx to raise auxin levels to a point where AAA sets in, which then triggers the feedback on influx. High β in combination with low α rather seems to counteract the AAA feedback, presumably because of increased H^+ reflux due to AUX/LAX co-transport. For higher values of α, in order to establish a strong AAA feedback, γ also needs to be high, presumably by raising the ϕ_0/ϕ_n ratio by counteracting passive influx. The correlation between the strength of AAA and the strength of PMF polarisation, as well as the role of γ at high α values can also be inferred from figure 8.10, where high γ increases the PMF polarisation strength slightly with high α, but decreases it with low α.

8.4.6 Auxin and proton dynamics in a file of 3 cells

To test whether the results in a single cell simulation would also hold in an assembly of cells, SAP-2 has been implemented in a file of 3 cells, with the auxin source field to the left, followed by cell 1, cell 2 and cell 3 towards the right end of the model environment. The auxin sink field was located at the right (for a topology and the auxin allocation pattern in a simulation over 8 hours see figure 8.14). Auxin allocation in cells was staggered due to the position of each cell with respect to auxin source and sink fields (fig. 8.15). Auxin flux increase followed the same overall pattern as in the single cell situation, with a more pronounced influx increase in the leftmost cell (towards auxin source) and a more pronounced efflux increase in the rightmost cell (towards auxin sink) during AAA. This finding is consistent with the canalisation hypothesis (see fig. 8.16).

The PMF polarisation pattern from the single cell simulation could be reproduced in the 3 cell simulation, with PMF heterogeneities in the same direction: stronger PMF

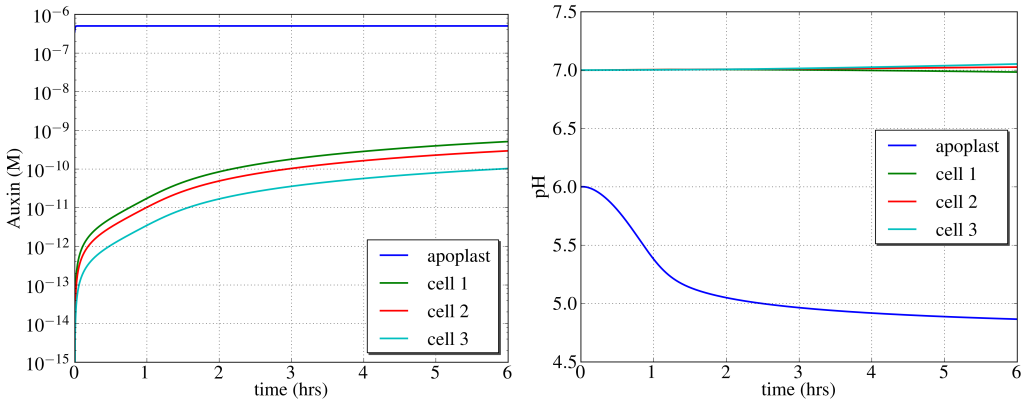

Figure 8.15: Auxin concentrations and pH evolution in a simulation involving 3 cells in a file. Cell 1 is the leftmost cell in this file, facing the auxin source field and Cell 3 is the rightmost cell in this file, facing the auxin sink field.

towards the auxin sink, weaker PMF towards the auxin source. (see fig. 8.16). Thus, the main conclusion from the of SAP-2 model seems also to be valid in situations involving more than one cell and is expected to show similar results if employed in a simulation of plant tissue.

8.5 Discussion

The SAP-2 model, implemented in a single cell and in a 3 cell file environment, led to similar results, compared with the non-spatial AP models (see sections 6 and 7): the establishment of AAA at similar auxin concentrations, pronounced allocation of auxin in the cell and elevated auxin transport fluxes across the membrane when AAA was in effect. Due to the spatial nature of SAP-2, further insights into the auxin/proton dynamics and their spatial profile could be gained. At the beginning of this current chapter, three main questions were raised: (a) How do auxin transport fluxes over the plasma membrane change in single cells or a file of cells due to the auxin/proton dynamics captured in SAP-2? (b) Do auxin gradients inside the cell build up during simulations? (c) Does AAA plus diffusion of both auxin and H^+ account for the establishment of proton gradient patterns over the membrane that are consistent with scenarios of expected PIN polarisation due to the extracellular auxin gradient between auxin source and sink?

The main findings in the SAP-2 model were that canalisation-type feedback, indepen-

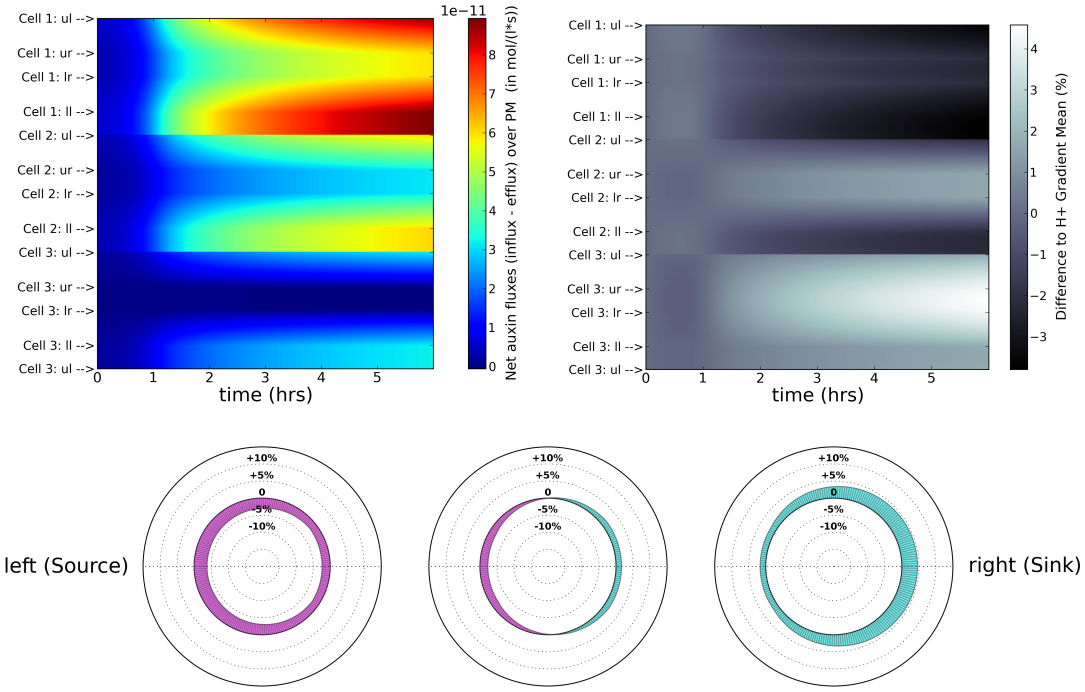

Figure 8.16: Net fluxes and PMF heterogeneities over cell membranes in a simulation involving 3 cells in a file. *Upper:*The vertical axis corresponds to the length of the cell membranes from Cell 1 (leftmost, towards auxin source) to Cell 3 (rightmost, towards auxin sink), as their circumferences are converted into 1D. The indicators *ul, ur, lr, ll* refer to *upper left, upper right, lower right, lower left* corners of the membrane in the model environment. The horizontal axis is the time axis. *Upper left:* Development of net auxin fluxes over time. Net fluxes are the sum of all auxin fluxes over each grid point in the membrane, according to the scheme $A_{active.influx} + A_{passive.influx} - A_{efflux}$. While Cell 1 shows stronger influx compared with the other cells and Cell 3 shows stronger efflux, both influxes and efflux are increased during the simulation as a result of AAA. *Upper right:* The variation of proton gradients over the membranes ($H_{apoplast} - H_{cytosol}$) at each membrane grid point from the mean proton gradient over the whole membrane is displayed in percent over the whole simulation time, for each cell. Cell 1 (towards auxin source), ahead in AAA activity, has an decreased proton gradient over its membrane in direction auxin source, compared to the other cells, and Cell 3 (towards auxin sink) has an increased proton gradient in direction auxin sink. *Lower:* The differences in proton motive force, illustrated in a polar plot. The membranes of Cell 1, 2 and 3 are drawn as circles, and the radius corresponds to the difference of proton gradients to the mean gradient of all cells. Purple bars are negative, blue bars are positive differences against the mean gradient. Cell membranes show clear polarisation patterns in the proton motive force. This plot corresponds to the situation after 7 hours simulation time.

dent of PIN localisation, between auxin and auxin transport emerges in a plant cell model, based on the feedback between auxin and protons proposed in chapter 6. Two aspects of this canalisation scenario could be identified: (1) Increasing flux strength towards the auxin sink with rising auxin levels, and (2) Emergence of polarisation in the proton motive force (PMF) over the plasma membrane such that the PMF was stronger towards the auxin sink and weaker towards the auxin source. Since PIN efflux transporter proteins are energised by the PMF, this hints towards the possibility that AAA helps to energise PINs when they are inserted in membrane parts facing the auxin sink.

Auxin transport fluxes. All auxin transport fluxes across the membrane were enforced as a reaction to AAA, in correspondence to the non-spatial AP-10 model results (see section 6). During this process, passive auxin influx into the cell seems important to increase cellular auxin concentrations towards levels that enable the AAA mechanism to lower apoplastic pH. In due course, active auxin influx get stronger and play a stronger role in the positive feedback process between auxin and pH. Given that at the start of simulations net auxin fluxes through the cell are in the direction towards the auxin sink and that increased auxin influx due to AAA enforces the auxin fluxes across the membrane, this outcome is consistent with the canalisation hypothesis, which is stating that auxin transport is polarised towards auxin sinks. However, while in some auxin transport models this polarisation is due to auxin efflux transporter insertion/retention at the membrane according to flux (PIN polarisation) [4, 10, 54, 103, 211, 239], in the SAP-2 model this polarisation is driven by the activity of symmetrically distributed AUX/LAX importers and not dependent on PIN polar targeting.

Auxin gradients. Even with small values for the auxin diffusion coefficient, auxin gradients within cells are only established at the start of the simulation and are blurred out quite rapidly after several minutes simulation time. This would raise concerns about auxin computer models employing intracellular auxin gradients [103]. However, since polarised PIN-dependent efflux is not included in this study, it could not be evaluated if the expected stronger depletion of auxin near membrane parts with more PINs inserted would nevertheless lead to intracellular auxin gradients. Thus, AAA, dependent

on the cytosolic auxin concentration, is in the SAP-2 model a symmetric process and does not directly account for the polarisation of proton gradients over the membrane. Rather, AAA leads to PMF heterogeneities despite being a symmetric process by energising the AUX/LAX importers, whose co-transport of H^+, dependent on extracelluar auxin gradients, accounts for PMF polarisation.

It is interesting to bring the ABP1 hypothesis of AAA into mind at this point (see section 5.2.2). According to this hypothesis, ABP1 in the cell wall causes AAA in the presence of auxin. Since this mechanism would depend on apoplastic rather than cytosolic auxin levels, and since between auxin source and sink fields the establishment of auxin gradients in the apoplast is evident, this mechanism could potentially lead to proton pump activation patterns matching auxin gradients in the apoplast and thus as well account for proton motive force heterogeneities. However, since directly AAA-dependent, this very likely would lead to PMF polarisation into the other direction: stronger PMF towards the source and weaker towards the sink. This hypothesis has not been further explored in SAP-2.

Polarisation of the proton motive force over the PM. One of the results in the SAP-2 model is a polarized pattern in PMF heterogeneity over the plasma membrane with an increased PMF towards the auxin sink and a decreased PMF towards the source. This could potentially drive a differential energisation of PMF-dependent auxin efflux transporters such as PIN, towards exporting more auxin towards an auxin sink as a result of the feedback between auxin and protons. To my best knowledge, there is no evidence as of yet if such PMF heterogeneities occur in plant cells which are involved in auxin transport. However, spatial variations in the membrane potential after the application of stimuli such as physical touch or by electrical fields in excitable cells have been reported [80, 45], which may be accounting for the plausibility of such a mechanism. In plant systems, the growing pollen tube cell has been shown to exhibit internal H^+ gradients that could be linked to growth phenomena [135]. An experimental investigation on PMF heterogeneities in plant cells could help to evaluate the usefulness of the predictions of the SAP-2 model.

The PMF polarisation pattern is due to the H^+ influx of AUX/LAX-mediated auxin symport. The contribution of auxin from passive influx is not included here, as the underly-

ing AP-2 core model approximates auxin dissociation by the Henderson-Hasselbalch equation (see section 7.2). However, since protonated auxin, passively entering the near neutral cell, readily dissociates, this passive influx also releases protons in an extracellular auxin gradient dependent manner, which could contribute to establish the PMF polarisation.

To validate the predictions of the SAP-2 model, additional biological experiments would be necessary, assessing the probability of PMF polarisation patterns as well as the role of AUX/LAX importers in AAA. Some results of the model are, however, corroborated by biological data. First, the feedback of auxin on its transport by AAA, as presented in this model, leads to cells with higher auxin concentration, which are simultaneously exhibiting higher auxin flux towards the sink, which is in accordance with biological findings suggesting high concentration, high flux canals of auxin transport in auxin transport canalisation [194]. As well, in experiments on *AVP1* over-expression and *avp1-1* null mutants in *Arabidopsis*, a gene coding for a H^+-PPase, it has been shown that proton pump activity and polar auxin transport as well as auxin-dependent organogenesis are linked together [119], suggesting that proton-pump dependent system properties could regulate auxin transport to some extent.

CHAPTER 9

Conclusion and Outlook

In this thesis, I focused on the nature and implications of feedback in the self-organisation of auxin transport within the single plant cell. After the development of a single cell model of PIN polarisation (see chapter 4), which failed to give new interesting mechanistic insights, a novel model based on a feedback mechanism between auxin and protons that is well grounded in biological evidence was developed and evaluated. This feedback was formulated in a core model (AP-10) and was subsequently reduced towards a minimum number of assumptions (AP-4 to AP-2). The main finding of the core model were that this feedback accounts for promoted allocation of auxin into cells and enhancement of both auxin influx and auxin efflux over the cell membrane. In a spatial context (SAP-2), this core model was able to reproduce polarisation that is in accordance with the canalisation hypothesis. The feedback between auxin and protons leads to increased fluxes through cells in the direction of the external sink by increased influx, due to apoplastic acidification. Secondly, the activity of active auxin importers (AUX/LAX) accounts for heterogeneities in the proton motive force over the plasma membrane. The emerging PMF polarisation pattern shows stronger PMF towards auxin sinks and weaker PMF towards auxin sources. This could potentially influence the activity of PIN-dependent transport, since PINs are energised by the PMF.

Both mechanisms, stronger flux through a cell and PMF patterning, are PIN-independent feedback mechanisms by which auxin influences its own efflux from cells in the context of canalisation. These mechanisms do not need any flux sensor and rely to-

tally on the self-organising principles of auxin/pH interactions. The mechanisms could provide functional redundancy of auxin transport polarisation in cells. This means that the mechanisms have the same or very similar functions in establishing auxin transport polarisation, which also includes PIN polarisation. However, it is unlikely that this redundancy represents a full back-up of polarisation without PINs, since (a) pin mutants show strongly altered auxin transport behaviour [21], and (b) AUX/LAX mutants do not seem to have strongly altered phenotypic appearance [127, 255]. However, this feedback could be important for two reasons:

1. It could help the onset of PIN polarisation (and thus be a self-organising 'starter' or 'guide' of the PIN polarisation machinery)
2. It could help to maintain PIN polarisation by providing a certain background directionality

The contribution of this present study in the field of auxin transport biology lies in its focus on PIN-independent feedback mechanisms between auxin and its transport at a cell level. The vast majority of auxin transport models employ PIN polarisation in cell membranes as a driving factor in directionality, with less attention on other auxin transporters. One exception is a canalisation model proposed by Wabnik et al. which uses intracellular PIN polarisation ('short' PINs inserting into the endoplasmatic reticulum and by storing auxin in the ER likewise regulating the amount of available auxin for polar transport) as a hypothetical prototype for auxin transport in earlier evolutionary stages [240] and another is an auxin transport model by Kramer et al. [101], suggesting that AUX/LAX proteins may play a role in accumulating auxin in cells.

By integrating biological results on auxin-induced apoplastic acidification into cell scale models of auxin transport, it was possible to focus on principles in auxin transport feedbacks that have, at least to my knowledge, not been used in auxin transport models before. Other models have included rates of auxin transport dependent on the membrane potential [190, 239], however the membrane potential relies on the proton motive force and a change in apoplastic pH due to auxin, as has been found to occur in biological experiments also changes the membrane potential, thus altering auxin fluxes between cells. The dynamics of such events have been investigated in this thesis and

point towards multiple nonlinear feedbacks in auxin transport at a cell level that are consistent with auxin transport canalisation.

Outlook and further questions

It is often said that answering a question only produces more questions. This is, of course, also true for the present thesis. Many questions arose during this work that unfortunately could not be followed due to time constraints. Some of them, however, shall be mentioned at this point since I find them particular interesting:

Further exploration of the multicellular simulation of SAP-2. SAP-2 has in this study only been tested for a maximum of three cells. Auxin source and auxin sink were explicitly defined, thus enforcing an auxin gradient in the system. It would be interesting to test the system behaviour without such settings. This could be done with a simulation involving more cells with periodic boundary conditions, where each cell produces (and degrades) auxin, but with different initial auxin concentrations. With this, it could be tested whether the SAP-2 model always results in canalisation-type auxin transport polarisation or if there are other possible transport phenomena emerging from this model.

Specific roles of auxin efflux carriers: ABCBs vs PINs. In AP-10 as well as in the spatiotemporal auxin/pH model, auxin efflux is a constant rate, γ. However, we know that there are different auxin efflux transporters, namely ABCBs and PINs. It could be that ABCBs provide a symmetric auxin efflux that is necessary for auxin transport polarisation. This could be tested by the implementation of two different auxin efflux mechanisms, one that is PMF-dependent (PINs) and one that is not (ABCBs).

The role of ATP as a resource for ATP-dependent processes. Inclusion of ATP as a limiting resource for energisation of H^+-ATPase and ABCBs could lead to interesting competition phenomena between auxin and proton transport. Since ATP production is linked to metabolic processes, which to include would increase the model complexity considerably, a simplifying assumption that may work could be to add an ATP pool with constant production and decay rate for ATP, which could provide such a resource limiting mechanism.

Auxin and membrane potentials Especially interesting could be the inclusion of membrane potential shifts in auxin transport. While this thesis included only gradual shifts in proton gradients over membranes, there is also evidence of more dramatic responses of the membrane potential to auxin. Following auxin perfusion of Vigna hypocotyl segments membrane hyperpolarisation could be detected [76]. The membrane potential subsequently changed from -150mV to -165mV. Older works of Felle have shown that this hyperpolarisation is repeatedly up- and downregulated, leading to oscillations with periods of about 20-30 min [51]. According to these results, auxin causes first a slight depolarisation, then hyperpolarisation. Hyperpolarisation may result from auxin-dependent H^+-ATPase regulation, while depolarisation could be due to anion channel activation, leading to anion efflux (see [257] and references therein). Linked to that, oscillations of calcium also occurred in some experiments (for a review of different causes and effects of calcium oscillations, see [49]).

By including other ions relevant for the regulation of membrane potential (K^+, Cl^- and Ca^{2+}) in a cellular auxin transport model, as well as including experiments on real plants to investigate further membrane potential alterations in auxin transport contexts, implications on auxin fluxes and polarisation events could be investigated. A quite speculative question in this context would be if such changes in membrane potential, if occurring at all in generic auxin transport situations, could be transmittable from cell to cell and if therefore auxin could be involved in what are sometimes called system potentials, which are long-range apoplastic signals [256].

Model validation by biological experiments

Since the study presented in this thesis does not include 'wet' experiments, model validation had its focus on the accordance of simulation results with previously obtained and published biological data, such as dose-response curves of auxin-induced apoplastic acidification, pH stress experiments or the unfortunately still very few data of how auxin transport links to pH, for instance the finding that mutants with impaired expression of a proton pump gene show reduced auxin transport strength [119].

Some of the hypotheses in this thesis may be hard to evaluate biologically at the moment due to the difficulties in measuring auxin concentrations in cells at the present

time (one of those hypotheses would be the results of SAP-2 indicating high concentration and high flux of auxin in cells during canalisation, which, however, is corroborated by some biological results implying such a phenomenon, by showing that regions undergoing vascular differentiation also have a high expression of the DR5 auxin reporter gene [194]). However, the measurement of pH in tissues that are involved in auxin transport, for instance a situation in stem segments with an auxin source and auxin sink, by confocal imaging and a pH-sensitive fluorescent reporter such as pHluorin or other pH-sensitive dyes [7, 135, 253] could be helpful to test the model predictions such as pH gradients emerging at specific sites during auxin transport. Including mutants with impaired proton pump activity (such as in [119]) in further experiments that focus on canalisation-type auxin transport polarisation within plant tissues may also help to evaluate the importance of auxin/proton feedback for auxin transport canalisation. One hypothesis of the SAP-2 model is that H^+ co-transport by AUX/LAX importers, based on extracellular auxin gradients between auxin sources and sinks, establish PMF polarisation patterns. Experiments with AUX/LAX mutants or with plant tissue showing uneven AUX/LAX distribution at plasma membranes, together with the use of pH-sensitive dyes, could shed a light on the plausibility of this hypothesis. And last, the SAP-2 model predicts homogeneity of auxin concentration within plant cells in the absence of polarised PIN accumulation at the cell membrane. If in the future direct measurement of auxin in living tissue is made possible, this hypothesis could be tested directly and help to re-evaluate auxin transport rates, which were only estimated in this thesis.

As a general conclusion it can be said that there is need for more data from biological experiments to evaluate the validity of some assumptions in the presented theoretical models and of their predictions. Apart from those suggested in the last paragraph, there is a lack of good data from AAA dose-response experiments in higher plants, and the precise mechanism by which auxin acidifies the apoplast is still elusive. However, the computational models of auxin and proton interactions that are presented in this thesis are well corroborated by available data and provide useful insights on feedback mechanisms in cells in the context of auxin transport polarisation. The presented hypotheses and predictions are clearly targeted towards future biological experiments.

APPENDIX A

Model Parameters
Initial Conditions
Equations

Table A.1: List of parameters in the PIN polarisation model, described in chapter 4

Param.	Description	Value	units	Reference
D	Diffusion constant	600	$\mu m^2/s$	[73]
μ	Membrane permeability for IAAH	0.2	-	this study
p	fraction IAAH/IAA^- in apoplast	0.2	-	[104]
K_{AUX}	Saturation param. f. AUX-mediated influx	0.3	-	this study
m	Hill coeff. f. AUX-mediated influx	3	-	this study
K_{PIN}	Saturation param. f. PIN-mediated efflux	0.3	-	this study
n	Hill coeff. f. PIN-mediated efflux	3	-	this study
η	PIN insertion rate	1 to 10	1/s	this study
k	Basic PIN drop-off rate	0.01 to 0.2	PIN/s	this study

Table A.2: List of all parameters used in the unified auxin/pH model, AP-10 (see chapter 6).

Parameter	Description	Value	Unit	Source / Comments
α	Auxin passive influx rate	$6 \cdot 10^{-2}$	cm/s	estimated
β	Auxin active influx rate	$5 \cdot 10^{6}$	$nl/(nmol * s)$	estimated
γ	Auxin active efflux rate	$8 \cdot 10^{-2}$	cm/s	estimated
A_p	Area of plasma membrane (PM)	$7.8 \cdot 10^{-5}$	cm^2	estimated., see sec. 6.1 for detailed derivation
A_t	Area of tonoplast (TP)	$1.95 \cdot 10^{-5}$	cm^2	estimated, see sec. 6.1 for detailed derivation
V_c	Volume of cytosol	$3.9 \cdot 10^{-2}$	nl	estimated, see sec. 6.1 for detailed derivation
V_a	Volume of apoplast	$3.9 \cdot 10^{-4}$	nl	estimated, see sec. 6.1 for detailed derivation
HA_a	Apoplastic buffer concentration	$3 \cdot 10^{-3}$	$nmol/nl$	[155, 52]
HA_c	Cytosolic buffer concentration	$3 \cdot 10^{-2}$	$nmol/nl$	[155, 52]
$k(aux)_1$	fw rate auxin dissociation	1	s^{-1}	auxin pK_a
$k(aux)_{-1}$	bw rate auxin dissociation	$5.6 \cdot 10^{5}$	$nl/(nmol * s)$	auxin pK_a
kaa_1	fw rate buffer dissociation 2 (apo)	1	s^{-1}	buffer pK_a
kaa_2	bw rate buffer dissociation 2 (apo)	$2.5 \cdot 10^{6}$	$nl/(nmol * s)$	buffer pK_a
kac_1	fw rate buffer dissociation 2 (cyt)	1	s^{-1}	buffer pK_a
kac_2	bw rate buffer dissociation 2 (cyt)	$3.2 \cdot 10^{7}$	$nl/(nmol * s)$	buffer pK_a
kba_1	fw rate buffer dissociation 1 (apo)	1	s^{-1}	buffer pK_a
kba_2	bw rate buffer dissociation 1 (apo)	$3.9 \cdot 10^{7}$	$nl/(nmol * s)$	buffer pK_a
kbc_1	fw rate buffer dissociation 1 (cyt)	1	s^{-1}	buffer pK_a
kbc_2	bw rate buffer dissociation 1 (cyt)	$3.2 \cdot 10^{6}$	$nl/(nmol * s)$	buffer pK_a
$k(ABP)_1$	fw rate ACF 1	$5 \cdot 10^{5}$	s^{-1}	estimated using [95]
$k(ABP)_{-1}$	bw rate ACF 1	$2 \cdot 10^{-2}$	$nl/(nmol * s)$	estimated using [95]
$k(ABP)_2$	fw rate ACF 2	80	s^{-1}	estimated using [95]
$k(ABP)_{-2}$	bw rate ACF 2	$7 \cdot 10^{-5}$	$nl/(nmol * s)$	estimated using [95]
K_P	Michaelis const. PM-H^+-ATPase	10^{-7}	$nmol/nl$	estimated using [250]
K_T	Michaelis const. TP-H^+-ATPase	10^{-7}	$nmol/nl$	estimated using [250]
kW_1	fw rate water self-ionization	10^{-13}	$nl/(nmol * s)$	H_2O ionic product: 10^{-14}
kW_{-1}	bw rate water self-ionization	10	$nl/(nmol * s)$	H_2O ionic product: 10^{-14}
$pK_{a(apo)}$	pK_a value apoplastic buffer	6.4	-	estimated using [52, 155, 19], pK_a = pH(apo) equil.
$pK_{a(cyt)}$	pK_a value cytosolic buffer	7.5	-	estimated using [52, 155, 204, 72], pK_a = pH(cyt) equil.
$pK_{a(IAA)}$	pK_a value for auxin	4.75	-	[220]
P_{OH-}	membrane permeability for OH^-	10^{-4}	cm/s	estimated using [77, 138]
P_{H^+}	membrane permeability for H^+	10^{-3}	cm/s	estimated. using [138]
V_{ABP}	max. rate of AAA	$2.4 \cdot 10^{-7}$	nmol/s	estimated
V_P	max. pumping rate of PM-H^+-ATPase	$2.7 \cdot 10^{-7}$	nmol/s	estimated
V_T	max. pumping rate of TP-H^+-ATPase	$3.3 \cdot 10^{-7}$	nmol/s	estimated
K_{ABP}	Michaelis const. of AAA	$1.09 \cdot 10^{-10}$	nmol/s	estimated
p	Hill coeff. PM-H^+-ATPase	1	nmol/s	estimated
t	Hill coeff. TP-H^+-ATPase	1	nmol/s	estimated

Table A.3: Initial conditions in the AP-10 model.

Variable	Value	Unit
$[A^-]_a$	0.0015	nmol/nl
$[ABP]_a$	0	nmol/nl
$[ABP]$	$1.91 \cdot 10^{-7}$	nmol/nl
$[ABP]_i$	0	nmol/nl
$[A^-]_c$	0.015	nmol/nl
$[H_2O]_c$	1	nmol/nl
$[H_2O]_a$	1	nmol/nl
$[H_3O^+]_c$	$3.16 \cdot 10^{-8}$	nmol/nl
$[H_3O^+]_a$	$3.98 \cdot 10^{-7}$	nmol/nl
$[H_3O^+]_v$	10^{-6}	nmol/nl
$[HA]_a$	0.0015	nmol/nl
$[HA]_c$	0.0149	nmol/nl
$[IAA^-]_a$	0	nmol/nl
$[IAA^-]_c$	0	nmol/nl
$[IAAH]_a$	0 - 1	nmol/nl
$[IAAH]_c$	0	nmol/nl
$[OH^-]_a$	$2.15 \cdot 10^{-8}$	nmol/nl
$[OH^-]_c$	$3.16 \cdot 10^{-7}$	nmol/nl
$[OH^-]_v$	10^{-8}	nmol/nl

Table A.4: List of all parameters used in the 4-component minimal model of auxin/proton interactions, AP-4 (see chapter 7).

Parameter	Description	Value	Unit	Source / Comments
A_p	Area of plasma membrane (PM)	$7.8 \cdot 10^{-5}$	cm^2	estimated., see sec. 6.1
A_p	Area of tonoplast (TP)	$1.95 \cdot 10^{-5}$	cm^2	estimated, see sec. 6.1
V_c	Volume of cytosol	$3.9 \cdot 10^{-2}$	nl	estimated, see sec. 6.1
V_a	Volume of apoplast	$3.9 \cdot 10^{-4}$	nl	estimated, see sec. 6.1
α	Auxin passive influx rate	$1 \cdot 10^{-3}$	-	estimated
β	Auxin active influx rate	$5 \cdot 10^{6}$	-	estimated
γ	Auxin active efflux rate	$5 \cdot 10^{-2}$	-	estimated
ka_1	fw rate auxin dissociation	1	s^{-1}	auxin pK_a
ka_2	bw rate auxin dissociation	$5.6 \cdot 10^{5}$	nl/(nmol*s)	auxin pK_a
kb_1	fw rate buffer reaction	$2.296 \cdot 10^{7}$	s^{-1}	see sec. 7.1
$kb_2(apo)$	bw rate buffer reaction - apo	$2.3 \cdot 10^{6}$	nl/(nmol*s)	see sec. 7.1
$kb_2(cyt)$	bw rate buffer reaction - cyt	$4.8 \cdot 10^{2}$	nl/(nmol*s)	see sec. 7.1
pH_a	apoplastic pH	6	-	[52, 86]
pH_c	cytosolic pH	7	-	[52, 105, 204]
pH_v	vacuolar pH	$5-6$	-	[129, 130, 219]
K_P	Michaelis const. PM-H^+-ATPase	10^{-7}	nmol/nl	estimated using [250]
K_T	Michaelis const. TP-H^+-ATPase	10^{-7}	nmol/nl	estimated using [250]
pK_a	pK_a value for auxin	4.75	-	[220]
r_H	reflux rate for H^+	$0.01 - 1 \cdot 10^{-3}$	cm/s	estimated using [77, 138]
X_a	height par. of Gaussian AAA-curve	$0.1 - 5 \cdot 10^{-5}$	nmol/s	estimated
X_b	location par. of Gaussian AAA-curve	$0.1 - 1 \cdot 10^{-7}$	-	estimated
X_c	width par. of Gaussian AAA-curve	25	-	estimated
p	Hill coeff. PM-H^+-ATPase	1	nmol/s	estimated
t	Hill coeff. TP-H^+-ATPase	1	nmol/s	estimated

Table A.5: Initial conditions in the AP-4 model (see chapter 7).

Variable	Value	Unit
$[B]_a$	$9.91 \cdot 10^{-5}$	nmol/nl
$[B]_c$	$2.99 \cdot 10^{-3}$	nmol/nl
$[H]_a$	10^{-6}	nmol/nl
$[H]_c$	$6.3 \cdot 10^{-8}$	nmol/nl
$[H]_v$	$10^{-6} - 10^{-5}$	nmol/nl
$[IAA]_a$	0	nmol/nl
$[IAA]_c$	0	nmol/nl
$[IAAH]_a$	0 - 1	nmol/nl
$[IAAH]_c$	0	nmol/nl

Table A.6: List of all parameters used in the 2-component minimal model of auxin/proton interactions, AP-2 (see chapter 7).

Parameter	Description	Value	Unit	Source / Comments
A_p	Area of plasma membrane (PM)	$7.8 \cdot 10^{-5}$	cm^2	estimated., see sec. 6.1 for detailed derivation
A_p	Area of tonoplast (TP)	$1.95 \cdot 10^{-5}$	cm^2	estimated, see sec. 6.1 for detailed derivation
V_c	Volume of cytosol	$3.9 \cdot 10^{-2}$	nl	estimated, see sec. 6.1 for detailed derivation
V_a	Volume of apoplast	$3.9 \cdot 10^{-4}$	nl	estimated, see sec. 6.1 for detailed derivation
α	Auxin passive influx rate	$1 \cdot 10^{-3}$	-	estimated
β	Auxin active influx rate	$5 \cdot 10^{6}$	-	estimated
γ	Auxin active efflux rate	$5 \cdot 10^{-2}$	-	estimated
$k1_a$	fw rate auxin dissociation	1	s^{-1}	auxin pK_a
$k2_a$	bw rate auxin dissociation	$5.6 \cdot 10^{5}$	nl/(nmol*s)	auxin pK_a
pH_a	apoplastic pH	6	-	[52, 86]
pH_c	cytosolic pH	7	-	[52, 105, 204]
pH_v	vacuolar pH	$5-6$	-	[129, 130, 219]
K_P	Michaelis const. PM-H^+-ATPase	10^{-7}	nmol/nl	estimated using [250]
K_T	Michaelis const. TP-H^+-ATPase	10^{-7}	nmol/nl	estimated using [250]
pK_a	pK_a value for auxin	4.75	-	[220]
r_H	reflux rate for H^+	$0.01 - 1 \cdot 10^{-3}$	cm/s	estimated using [77, 138]
X_a	height par. of Gaussian AAA-curve	$0.1 - 5 \cdot 10^{-5}$	nmol/s	estimated
X_b	location par. of Gaussian AAA-curve	$0.1 - 1 \cdot 10^{-7}$	-	estimated
X_c	width par. of Gaussian AAA-curve	25	-	estimated
p	Hill coeff. PM-H^+-ATPase	1	nmol/s	estimated
t	Hill coeff. TP-H^+-ATPase	1	nmol/s	estimated

Table A.7: Initial conditions in the AP-2 model (see chapter 7).

Variable	Value	Unit
$[A]_a$	0 - 1	nmol/nl
$[A]_c$	0	nmol/nl
$[H]_a$	10^{-6}	nmol/nl
$[H]_c$	10^{-7}	nmol/nl
$[H]_v$	10^{-6}	nmol/nl

Table A.8: List of all parameters used in simulations of the spatiotemporal auxin/pH model, SAP-2 (see chapter 8).

Parameter	Description	Value	Unit	Source / Comments
$CellL$	Length of cell	65	μm	estimated using [11]
$CellW$	Width of cell	45	μm	estimated using [11]
$VacL$	Length of vacuole	36	μm	estimated using [11]
$VacW$	Width of vacuole	29	μm	estimated using [11]
apo	Apoplast thickness	1	μm	estimated using [11]
dx	grid point width/length	1	μm	estimated
V_c	Volume of cytosol	$1.013 \cdot 10^{-7}$	ml	see cell dimensions
V_a	Volume of apoplast	$1.637 \cdot 10^{-8}$	ml	see cell dimensions
D_A	Auxin diffusion coefficient	$50 - 400$	$\mu m^2/s$	[73, 89, 71]
D_H	H^+diffusion coefficient	$50 - 400$	μm^2	[3]
A_{decay}	Auxin decay rate	$0 - 1 \cdot 10^{-4}$	s^{-1}	estimated
α	Auxin passive influx rate	$1 \cdot 10^{-3}$	-	estimated
β	Auxin active influx rate	$5 \cdot 10^{6}$	-	estimated
γ	Auxin active efflux rate	$5 \cdot 10^{-2}$	-	estimated
$k1_a$	fw rate auxin dissociation	1	s^{-1}	auxin pK_a
$k2_a$	bw rate auxin dissociation	$5.6 \cdot 10^{5}$	nl/(nmol*s)	auxin pK_a
pH_a	apoplastic pH	6	-	[52, 86]
pH_c	cytosolic pH	7	-	[52, 105, 204]
pH_v	vacuolar pH	$5 - 6$	-	[129, 130, 219]
K_P	Michaelis const. PM-H^+-ATPase	10^{-7}	nmol/nl	estimated using [250]
K_T	Michaelis const. TP-H^+-ATPase	10^{-7}	nmol/nl	estimated using [250]
pK_a	pK_a value for auxin	4.75	-	[220]
r_H	reflux rate for H^+	$0.01 - 1 \cdot 10^{-3}$	cm/s	estimated using [77, 138]
X_a	height par. of Gaussian AAA-curve	$0.1 - 5 \cdot 10^{-5}$	nmol/s	estimated
X_b	location par. of Gaussian AAA-curve	$0.1 - 1 \cdot 10^{-7}$	-	estimated
X_c	width par. of Gaussian AAA-curve	25	-	estimated
p	Hill coeff. PM-H^+-ATPase	1	nmol/s	estimated
t	Hill coeff. TP-H^+-ATPase	1	nmol/s	estimated
A_{source}	Auxin source concentration	$10^{-10} - 10^{-5}$	nmol/nl	estimated
A_{sink}	Auxin sink concentration	10^{-11}	nmol/nl	estimated
dt	time step size	$0.1 - 10$	s	estimated

The system of ODEs in AP-10 (see chapter 6)

$$\begin{aligned}\frac{d[H^+]_c}{dt} &= kw_1 \cdot [H_2O]_c^2 - kw_2 \cdot [H^+]_c[OH^-]_c + \frac{1}{V_c} \cdot A_p \cdot 2 \cdot \beta \cdot [IAA^-]_a[H^+]_a^2 \\ &+ kaux_1[IAAH]_c[H_2O]_c - kaux_2[IAA^-]_c[H^+]_c \\ &- \frac{1}{V_c}\left[A_p \cdot \frac{V_{ABP} \cdot ABP_a}{K_{ABP} + ABP_a} - A_p \cdot P_H\Big([H^+]_a - [H^+]_c\Big) - A_t \cdot P_H\Big([H^+]_v - [H^+]_c\Big)\right. \\ &\left. + A_p\frac{V_p \cdot [H^+]_c}{K_p + [H^+]_c} + A_t\frac{V_t \cdot [H^+]_c}{K_t + [H^+]_c}\right] + kac_1[HA]_c[H_2O]_c - kac_2[A^-]_c[H^+]_c\end{aligned} \tag{A.1}$$

$$\begin{aligned}\frac{d[OH^-]_c}{dt} &= kw_1 \cdot [H_2O]_c^2 - kw_2 \cdot [H^+]_c[OH^-]_c \\ &+ kbc_1[H_2O]_c[A^-]_c - kbc_2[HA]_c[OH^-]_c \\ &- \frac{1}{V_c} \cdot P_{OH}\left[A_p\Big([OH^-]_c - [OH^-]_a\Big) + A_t\Big([OH^-]_c - [OH^-]_v\Big)\right]\end{aligned} \tag{A.2}$$

$$\frac{d[A^-]_c}{dt} = kac_1[HA]_c[H_2O]_c - kac_2[A^-]_c[H^+]_c - kbc_1[H_2O]_c[A^-]_c + kbc_2[HA]_c[OH^-]_c \tag{A.3}$$

$$\begin{aligned}\frac{d[HA]_c}{dt} &= -kac_1[HA]_c[H_2O]_c + kac_2[A^-]_c[H^+]_c \\ &+ kbc_1[H_2O]_c[A^-]_c - kbc_2[HA]_c[OH^-]_c\end{aligned} \tag{A.4}$$

$$\begin{aligned}\frac{d[IAA^-]_c}{dt} &= kaux_1[IAAH]_c[H_2O]_c - kaux_2[IAA^-]_c[H^+]_c \\ &+ \frac{1}{V_c} \cdot A_p\Big[\beta[IAA^-]_a[H^+]_a^2 - \gamma[IAA^-]_c\Big] \\ &+ k(ABP)_{-2}[ABP]_i + k(ABP)_{-1}[ABP]_a \\ &- k(ABP)_1[ABP][IAA^-]_c - k(ABP)_2[ABP]_a[IAA^-]_c\end{aligned} \tag{A.5}$$

$$\begin{aligned}\frac{d[IAAH]_c}{dt} &= -kaux_1[IAAH]_c[H_2O]_c + kaux_2[IAA^-]_c[H^+]_c \\ &\quad + \frac{1}{V_c}\cdot A_p\cdot\alpha\big([IAAH]_a - [IAAH]_c\big)\end{aligned} \tag{A.6}$$

$$\begin{aligned}\frac{d[H^+]_a}{dt} &= kw_1\cdot[H_2O]_a^2 - kw_2\cdot[H^+]_a[OH^-]_a - \frac{1}{V_a}\cdot A_p\cdot 2\cdot\beta\cdot[IAA^-]_a[H^+]_a^2 \\ &\quad + kaux_1[IAAH]_a[H_2O]_a - kaux_2[IAA^-]_a[H^+]_a \\ &\quad + \frac{1}{V_a}\left[A_p\cdot\frac{V_{ABP}\cdot ABP_a}{K_{ABP}+ABP_a} - A_p\cdot P_H\Big([H^+]_a - [H^+]_c\Big) + A_p\frac{V_p\cdot[H^+]_c}{K_p+[H^+]_c}\right] \\ &\quad + kaa_1[HA]_a[H_2O]_a - kaa_2[A^-]_a[H^+]_a\end{aligned} \tag{A.7}$$

$$\begin{aligned}\frac{d[OH^-]_a}{dt} &= kw_1\cdot[H_2O]_a^2 - kw_2\cdot[H^+]_a[OH^-]_a + kba_1[H_2O]_a[A^-]_a \\ &\quad - kba_2[HA]_a[OH^-]_a + \frac{1}{V_a}\cdot P_{OH}\cdot A_p\Big([OH^-]_c - [OH^-]_a\Big)\end{aligned} \tag{A.8}$$

$$\frac{d[A^-]_a}{dt} = kaa_1[HA]_a[H_2O]_a - kaa_2[A^-]_a[H^+]_a - kba_1[H_2O]_a[A^-]_a + kba_2[HA]_a[OH^-]_a \tag{A.9}$$

$$\begin{aligned}\frac{d[HA]_a}{dt} &= -kaa_1[HA]_a[H_2O]_a + kaa_2[A^-]_a[H^+]_a + kba_1[H_2O]_a[A^-]_a \\ &\quad - kba_2[HA]_a[OH^-]_a\end{aligned} \tag{A.10}$$

$$\begin{aligned}\frac{d[IAA^-]_a}{dt} &= kaux_1[IAAH]_a[H_2O]_a - kaux_2[IAA^-]_a[H^+]_a \\ &\quad + \frac{1}{V_a}\cdot A_p\left[\gamma[IAA^-]_c - \beta[IAA^-]_a[H^+]_a^2\right]\end{aligned} \tag{A.11}$$

$$\begin{aligned}\frac{d[IAAH]_a}{dt} &= -kaux_1[IAAH]_a[H_2O]_a + kaux_2[IAA^-]_a[H^+]_a \\ &\quad - \frac{1}{V_a}\cdot A_p\cdot\alpha\big([IAAH]_a - [IAAH]_c\big)\end{aligned} \tag{A.12}$$

$$\frac{d[ABP]}{dt} = k(ABP)_{-1}[ABP]_a - k(ABP)_1[ABP][IAA^-]_c \tag{A.13}$$

$$\begin{aligned}\frac{d[ABP]_a}{dt} &= k(ABP)_1[ABP][IAA^-]_c + k(ABP)_{-2}[ABP]_i \\ &- k(ABP)_{-1}[ABP]_a - k(ABP)_2[ABP]_a[IAA^-]_c\end{aligned} \tag{A.14}$$

$$\frac{d[ABP]_i}{dt} = -k(ABP)_{-2}[ABP]_i + k(ABP)_2[ABP]_a[IAA^-]_c \tag{A.15}$$

Bibliography

[1] Adler, I., Barabe, D., and Jean, R. V. A history of the study of phyllotaxis. *Annals of Botany 80* (1997), 231–244.

[2] Aida, M., Beis, D., Heidstra, R., Willemsen, V., Blilou, I., Galinha, C., Nussaume, L., Noh, Y.-S., Amasino, R., and Scheres, B. The PLETHORA genes mediate patterning of the *Arabidopsis* root stem cell niche. *Cell 119*, 1 (2004), 109–120.

[3] al Baldawi, N. F., and Abercrombie, R. F. Cytoplasmic hydrogen ion diffusion coefficient. *Biophysical Journal 61*, 6 (1992), 1470–1479.

[4] Alim, K., and Frey, E. Quantitative predictions on auxin-induced polar distribution of PIN proteins during vein formation in leaves. *The European Physical Journal E: Soft Matter and Biological Physics 33*, 2 (2010), 165–173.

[5] Aloni, R., Schwalm, K., Langhans, M., and Ullrich, C. I. Gradual shifts in sites of free-auxin production during leaf-primordium development and their role in vascular differentiation and leaf morphogenesis in *Arabidopsis*. *Planta 216*, 5 (2003), 841–853.

[6] Alpi, A., Amrhein, N., Bertl, A., Blatt, M. R., Blumwald, E., Cervone, F., Dainty, J., Michelis, M. I. D., Epstein, E., Galston, A. W., Goldsmith, M. H. M., Hawes, C., Hell, R., Hetherington, A., Hofte, H., Juergens, G., Leaver, C. J., Moroni, A., Murphy, A., Oparka, K., Perata, P., Quader, H., Rausch, T., Ritzenthaler, C., Rivetta, A., Robinson, D. G., Sanders, D., Scheres, B., Schumacher, K., Sentenac, H., Slayman, C. L., Soave, C., Somerville, C., Taiz, L., Thiel, G., and Wagner, R. Plant neurobiology: no brain, no gain? *Trends in Plant Science 12*, 4 (2007), 135–136.

[7] Ashby, M. C., Ibaraki, K., and Henley, J. M. It's green outside: tracking cell surface proteins with pH-sensitive GFP. *Trends in Neuroscience 27*, 5 (2004), 257–261.

[8] Bainbridge, K., Guyomarc'h, S., Bayer, E., Swarup, R., Bennett, M., Mandel, T., and Kuhlemeier, C. Auxin influx carriers stabilize phyllotactic patterning. *Genes and Development 22* (2008), 810–823.

[9] Baluska, F., Samaj, J., and Menzel, D. Polar transport of auxin: carrier-mediated flux across the plasma membrane or neurotransmitter-like secretion? *Trends in cell biology 13*, 6 (2003), 282–285.

[10] Bayer, E., Smith, R., Mandel, T., Nakayama, N., Sauer, M., Prusinkiewicz, P., and Kuhlemeier, C. Integration of transport-based models for phyllotaxis and midvein formation. *Genes and Development 23* (2009), 373–384.

[11] Beck, C. B. *An Introduction to Plant Structure and Development. Plant Anatomy for the Twenty-First Century*. Cambridge University Press, 2010.

[12] Benjamins, R., Malenica, N., and Luschnig, C. Regulating the regulator: the control of auxin transport. *Bioessays 27*, 12 (2005), 1246–1255.

[13] Benjamins, R., and Scheres, B. Auxin: The looping star in plant development. *Annual Review of Plant Biology 59* (2008), 443–465.

[14] Benková, E., and Hejátko, J. Hormone interactions at the root apical meristem. *Plant Molecular Biology 69* (2009), 383–396.

[15] Bennett, M. J., Marchant, A., Green, H. G., May, S. T., Ward, S. P., Millner, P. A., Walker, A. R., Schulz, B., and Feldmann, K. A. Arabidopsis AUX1 gene: a permease-like regulator of root gravitropism. *Science 273*, 5277 (1996), 948–950.

[16] Bertoša, B., Kojić-Prodić, B., Wade, R. C., and Tomić, S. Mechanism of auxin interaction with Auxin Binding Protein (ABP1): a molecular dynamics simulation study. *Biophysical Journal 94*, 1 (2008), 27–37.

[17] Bethmann, B., and Schönknecht, G. pH regulation in an acidophilic green alga - a quantitative analysis. *New Phytologist 183*, 2 (2009), 327–339.

[18] Bianco, M. D., and Kepinski, S. Context, specificity, and self-organization in auxin response. *Cold Spring Harbour Perspectives in Biology 3*, 1 (2011), a001578.

[19] Bibikova, T. N., Jacob, T., Dahse, I., and Gilroy, S. Localized changes in apoplastic and cytoplasmic pH are associated with root hair development in *Arabidopsis thaliana*. *Development 125*, 15 (1998), 2925–2934.

[20] Blakeslee, J. J., Bandyopadhyay, A., Lee, O. R., Mravec, J., Titapiwatanakun, B., Sauer, M., Makam, S. N., Cheng, Y., Bouchard, R., Adamec, J., Geisler, M., Nagashima, A., Sakai, T., Martinoia, E., Friml, J., Peer, W. A., and Murphy, A. S. Interactions among PIN-FORMED and P-glycoprotein auxin transporters in *Arabidopsis*. *The Plant Cell 19*, 1 (2007), 131–147.

[21] Blilou, I., Xu, J., Wildwater, M., Willemsen, V., Paponov, I., Friml, J., Heidstra, R., Aida, M., Palme, K., and Scheres, B. The PIN auxin efflux facilitator network controls growth and patterning in *Arabidopsis* roots. *Nature 433*, 7021 (2005), 39–44.

[22] Bobik, K., Boutry, M., and Duby, G. Activation of the plasma membrane H^+-ATPase by acid stress. *Plant Signalling and Behaviour 5*, 6 (2010), 681–683.

[23] Boutté, Y., Crosnier, M.-T., Carraro, N., Traas, J., and Satiat-Jeunemaitre, B. The plasma membrane recycling pathway and cell polarity in plants: studies on PIN proteins. *Journal of Cell Science. 119*, Pt 7 (2006), 1255–1265.

[24] Brenner, E. D., Stahlberg, R., Mancuso, S., Baluska, F., and Volkenburgh, E. V. Response to alpi et al.: plant neurobiology: the gain is more than the name. *Trends in Plant Science 12*, 7 (2007), 285–286.

[25] Bryden, J., and Noble, J. Computational modelling, explicit mathematical treatments, and scientific explanation. In *Artificial Life X: Proceedings of the Tenth International Conference on Artificial Life* (2006), MIT Press, pp. 520–526.

[26] Callis, J. Auxin action. *Nature 435* (2005), 436–437.

[27] Campanoni, P., and Blatt, M. R. Membrane trafficking and polar growth in root hairs and pollen tubes. *Journal of Experimental Botany 58*, 1 (2007), 65–74.

[28] Carrier, D. J., Bakar, N. T. A., Swarup, R., Callaghan, R., Napier, R. M., Bennett, M. J., and Kerr, I. D. The binding of auxin to the *Arabidopsis* auxin influx transporter AUX1. *Plant Physiology 148* (2008), 529–535.

[29] Casimiro, I., Marchant, A., Bhalerao, R. P., Beeckman, T., Dhooge, S., Swarup, R., Graham, N., Inzé, D., Sandberg, G., Casero, P. J., and Bennett, M. Auxin transport promotes *Arabidopsis* lateral root initiation. *The Plant Cell 13*, 4 (2001), 843–852.

[30] Chandler, J. W. Local auxin production: a small contribution to a big field. *BioEssays 31* (2009), 60–70.

[31] Chavarría-Krauser, A., and Ptashnyk, M. Homogenization of long-range auxin transport in plant tissues. *Nonlinear Analysis Real World Applications* (2009), article in press.

[32] Cleland, R. E. Fusicoccin-induced growth and hydrogen ion excretion of *Avena* coleoptiles: Relation to auxin responses. *Planta 128*, 3 (1976), 201–206.

[33] Colasanti, R. L., and Hunt, R. Resource dynamics and plant growth: a self-assembling model for individuals, populations and communities. *Functional Ecology 11* (1997), 133–145.

[34] Cosgrove, D. J. Growth of the plant cell wall. *Nature Reviews Molecular Cell Biology 6*, 11 (2005), 850–861.

[35] Crawford, S., Shinohara, N., Sieberer, T., Williamson, L., George, G., Hepworth, J., Müller, D., Domagalska, M. A., and Leyser, O. Strigolactones enhance competition between shoot branches by dampening auxin transport. *Development 137*, 17 (2010), 2905–2913.

[36] Darwin, C., and Darwin, F. *The power of movement in plants*. London: John Murray, 1880.

[37] de Reuille, P. B., Bohn-Courseau, I., Ljung, K., Morin, H., Carraro, N., Godin, C., and Traas, J. Computer simulations reveal properties of the cell-cell signaling network at the shoot apex in *Arabidopsis*. *Proceedings of the National Academy of Sciences of the United States of America 103*, 5 (2006), 1627–1632.

[38] Delattre, M., and Félix, M.-A. The evolutionary context of robust and redundant cell biological mechanisms. *Bioessays 31*, 5 (2009), 537–545.

[39] Dettmer, J., Elo, A., and Helariutta, Y. Hormone interactions during vascular development. *Plant Molecular Biology 69* (2009), 347–360.

[40] Dhonukshe, P., Tanaka, H., Goh, T., Ebine, K., Mähönen, A. P., Prasad, K., Blilou, I., Geldner, N., Xu, J., Uemura, T., Chory, J., Ueda, T., Nakano, A., Scheres, B., and Friml, J. Generation of cell polarity in plants links endocytosis, auxin distribution and cell fate decisions. *Nature 456* (2008), 962–966.

[41] Ding, Z., and Friml, J. Auxin regulates distal stem cell differentiation in *Arabidopsis* roots. *Proceedings of the National Academy of Sciences of the United States of America 107*, 26 (2010), 12046–12051.

[42] Doerner, P. Plant roots: recycled auxin energizes patterning and growth. *Current Biology 18*, 2 (2008), R72–R74.

[43] Dreyer, I., Müller-Röber, B., and Köhler, B. Voltage-gated ion channels. *Annual Plant Reviews 15* (2004), 150–192.

[44] Durachko, D. M., and Cosgrove, D. J. Measuring plant cell wall extension (creep) induced by acidic pH and by alpha-expansin. *Journal of Visualized Experiments*, 25 (2009), 1–4.

[45] Eisenberg, R. S., and Engel, E. The spatial variation of membrane potential near a small source of current in a spherical cell. *Journal of General Physiology 55*, 6 (1970), 736–757.

[46] ELLINGER, A. Ueber die Constitution der Indolgruppe im Eiweiss (Synthese der sogen. Skatolcarbonsäure) und die Quelle der Kynurensäure. *Berichte der deutschen chemischen Gesellschaft 37*, 2 (1904), 1801–1808.

[47] ESTELLE. Polar auxin transport. new support for an old model. *The Plant Cell 10*, 11 (1998), 1775–1778.

[48] EVANS, G., BLACKLEDGE, J., AND YARDLEY, P. *Numerical Methods for Partial Differential Equations*. Springer Undergraduate Mathematics Series. Springer Verlag Berlin Heidelberg New York, 2000.

[49] EVANS, N. H., MCAINSH, M. R., AND HETHERINGTON, A. M. Calcium oscillations in higher plants. *Current Opinion in Plant Biology 4*, 5 (2001), 415–420.

[50] FELDWISCH, J., ZETTL, R., HESSE, F., SCHELL, J., AND PALME, K. An auxin-binding protein is localized to the plasma membrane of maize coleoptile cells: identification by photoaffinity labeling and purification of a 23-kda polypeptide. *Proceedings of the National Academy of Sciences of the United States of America 89*, 2 (1992), 475–479.

[51] FELLE, H. Auxin causes oscillations of cytosolic free calcium and pH in *Zea mays* coleoptiles. *Planta 174* (1988), 495–499.

[52] FELLE, H. pH: Signal and messenger in plant cells. *Plant Biology 3* (2001), 577–591.

[53] FERARU, E., AND FRIML, J. PIN polar targeting. *Plant Physiology 147* (2008), 1553–1559.

[54] FEUGIER, F. G., MOCHIZUKI, A., AND IWASA, Y. Self-organization of the vascular system in plant leaves: inter-dependent dynamics of auxin flux and carrier proteins. *Journal of Theoretical Biology 236* (2005), 366–375.

[55] FISHER, J., AND HENZINGER, T. A. Executable cell biology. *Nature Biotechnology 25*, 11 (2007), 1239–1249.

[56] FITZSIMONS, P. J. The determination of sensitivity parameters for auxin-induced H^+-efflux from *Avena* coleoptile segments. *Plant, Cell and Environment 12* (1989), 737–746.

[57] FRIML, J. Subcellular trafficking of PIN auxin efflux carriers in auxin transport. *European Journal of Cell Biology 89*, 2-3 (2010), 231–235.

[58] FRIML, J., AND PALME, K. Polar auxin transport–old questions and new concepts? *Plant Molecular Biology 49*, 3-4 (2002), 273–284.

[59] FRIML, J., VIETEN, A., SAUER, M., WEIJERS, D., SCHWARZ, H., HAMANN, T., OFFRINGA, R., AND JÜRGENS, G. Efflux-dependent auxin gradients establish the apical-basal axis of *Arabidopsis*. *Nature 426*, 6963 (2003), 147–153.

[60] GALINHA, C., HOFHUIS, H., LUIJTEN, M., WILLEMSEN, V., BLILOU, I., HEIDSTRA, R., AND SCHERES, B. PLETHORA proteins as dose-dependent master regulators of *Arabidopsis* root development. *Nature 449*, 7165 (2007), 1053–1057.

[61] GÄLWEILER, L., GUAN, C., MÜLLER, A., WISMAN, E., MENDGEN, K., YEPHREMOV, A., AND PALME, K. Regulation of polar auxin transport by AtPIN1 in *Arabidopsis* vascular tissue. *Science 282*, 5397 (1998), 2226–2230.

[62] GAO, X., NAGAWA, S., WANG, G., AND YANG, Z. Cell polarity signaling: focus on polar auxin transport. *Molecular Plant 1*, 6 (2008), 899–909.

[63] GARNETT, P., STEINACHER, A., STEPNEY, S., CLAYTON, R., AND LEYSER, O. Computer simulation: the imaginary friend of auxin transport biology. *Bioessays 32*, 9 (2010), 828–835.

[64] Garnett, P., Stepney, S., Day, F., and Leyser, O. Using the CoSMoS process to enhance an executable model of auxin transport canalisation. In *CoSMoS workshop, Odense, Denmark, August 2010* (2010), Lunvier Press, pp. 9–32.

[65] Gaxiola, R. A., Palmgren, M. G., and Schumacher, K. Plant proton pumps. *FEBS Letters 581* (2007), 2204–2214.

[66] Geisler, M., and Murphy, A. S. The ABC of auxin transport: the role of p-glycoproteins in plant development. *FEBS Letters 580*, 4 (2006), 1094–1102.

[67] Geldner, N., Anders, N., Wolters, H., Keicher, J., Kornberger, W., Muller, P., Delbarre, A., Ueda, T., Nakano, A., and Jürgens, G. The *Arabidopsis* GNOM ARF-GEF mediates endosomal recycling, auxin transport, and auxin-dependent plant growth. *Cell 112*, 2 (2003), 219–230.

[68] Giannini, J. L., and Briskin, D. P. Proton transport in plasma membrane and tonoplast vesicles from red beet (*Beta vulgaris L.*) storage tissue : A comparative study of ion effects on δ pH and $\delta\psi$. *Plant Physiology 84*, 3 (1987), 613–618.

[69] Gilpin, M. E., and Ayala, F. J. Global models of growth and competition. *Proceedings of the National Academy of Sciences of the United States of America 70*, 12 (1973), 3590–3593.

[70] Goldsmith, M. H. The polar transport of auxin. *Annual Review of Plant Physiology 28* (1977), 439–478.

[71] Goldsmith, M. H., Goldsmith, T. H., and Martin, M. H. Mathematical analysis of the chemosmotic polar diffusion of auxin through plant tissues. *Proceedings of the National Academy of Sciences of the United States of America 78*, 2 (1981), 976–980.

[72] Gout, E., Bligny, R., and Douce, R. Regulation of intracellular pH values in higher plant cells. *Journal of Biological Chemistry 267*, 20 (1992), 13903–13909.

[73] Grieneisen, V. A., Xu, J., Marée, A. F. M., Hogeweg, P., and Scheres, B. Auxin transport is sufficient to generate a maximum and gradient guiding root growth. *Nature 449* (2007), 1008–1013.

[74] Gutknecht, J., and Walter, A. Transport of auxin (indoleacetic acid) through lipid bilayer membranes. *Journal of Membrane Biology 56*, 1 (1980), 65–72.

[75] Haga, and Iino. Auxin-growth relationships in maize coleoptiles and pea internodes and control by auxin of the tissue sensitivity to auxin. *Plant Physiology 117*, 4 (1998), 1473–1486.

[76] Hager, A. Role of the plasma membrane H^+-ATPase in auxin-induced elongation growth: historical and new aspects. *Journal of Plant Research 116*, 6 (2003), 483–505.

[77] Haines, T. H. Do sterols reduce proton and sodium leaks through lipid bilayers? *Progress in Lipid Research 40*, 4 (2001), 299–324.

[78] Hamant, O., Heisler, M. G., Jönsson, H., Krupinski, P., Uyttewaal, M., Bokov, P., Corson, F., Sahlin, P., Boudaoud, A., Meyerowitz, E. M., Couder, Y., and Traas, J. Developmental patterning by mechanical signals in *Arabidopsis*. *Science 322*, 5908 (2008), 1650–1655.

[79] Hasenstein, K. H., and Rayle, D. Cell wall pH and auxin transport velocity. *Plant Physiology 76*, 1 (1984), 65–67.

[80] HASSAN, N., CHATTEJEE, I., PUBLICOVER, N. G., AND CRAVIS, G. L. A combined experimental and computational analysis of membrane potential variations in excitable cells in response to DC electric fields. In *2002 Annual Report Conference on Electrical Insulation and Dielectric Phenomena* (2002), pp. 91–94.

[81] HAUSER, M., EICHELMANN, H., HEBER, U., AND LAISK, A. Chloroplast pH values and buffer capacities in darkened leaves as revealed by CO_2 solubilization in vivo. *Planta 196* (1995), 199–204.

[82] HODKIN, A. L., AND HUXLEY, A. F. A quantitative description of membrane current and its application to conduction and excitation in nerve. *Journal of Physiology 117*, 4 (1952), 500–544.

[83] HOFMEISTER, W. *Allgemeine Morphologie der Gewächse*. Handbuch der physiologischen Botanik. Engelmann, Leipzig, 1868.

[84] HOOPS, S., SAHLE, S., GAUGES, R., LEE, C., PAHLE, J., SIMUS, N., SINGHAL, M., XU, L., MENDES, P., AND KUMMER, U. COPASI–a COmplex PAthway SImulator. *Bioinformatics 22*, 24 (2006), 3067–3074.

[85] IVANCHENKO, M. G., MUDAY, G. K., AND DUBROVSKY, J. G. Ethylene-auxin interactions regulate lateral root initiation and emergence in *Arabidopsis thaliana*. *The Plant Journal 55*, 2 (2008), 335–347.

[86] JIA, W., AND DAVIES, W. J. Modification of leaf apoplastic pH in relation to stomatal sensitivity to root-sourced abscisic acid signals. *Plant Physiology 143*, 1 (2007), 68–77.

[87] JOHANSSON, F., SOMMARIN, M., AND LARSSON, C. Fusicoccin activates the plasma membrane H^+-ATPase by a mechanism involving the C-terminal inhibitory domain. *Plant Cell 5*, 3 (1993), 321–327.

[88] JONES, B., GUNNERÅS, S. A., PETERSSON, S. V., TARKOWSKI, P., GRAHAM, N., MAY, S., DOLEZAL, K., SANDBERG, G., AND LJUNG, K. Cytokinin regulation of auxin synthesis in *Arabidopsis* involves a homeostatic feedback loop regulated via auxin and cytokinin signal transduction. *The Plant Cell 22*, 9 (2010), 2956–2969.

[89] JÖNSSON, H., HEISLE, M. G., SHAPIRO, B. E., MEYEROWITZ, E. M., AND MJOLSNESS, E. An auxin-driven polarized transport model for phyllotaxis. *Proceedings of the National Academy of Sciences of the United States of America 103* (2006), 1633–1638.

[90] JUNGE, W., AND MCLAUGHLIN, S. The role of fixed and mobile buffers in the kinetics of proton movement. *Biochimica et Biophysica Acta 890*, 1 (1987), 1–5.

[91] KARCZ, W., STOLAREK, J., PIETRUSZKA, M., AND MALKOWSKI, E. The dose-response curves for IAA induced elongation growth and acidification of the incubation medium of *Zea mays* coleoptile segments. *Physiologica Plantarum 80* (1990), 257–261.

[92] KAWAMURA, Y. Improved mathematical model for estimating H^+ influx and H^+ efflux in plant vacuolar vesicles acidified by ATPase or pyrophosphatase. *Analytical Biochemistry 369*, 2 (2007), 137–148.

[93] KELLER, C. P. Leaf expansion in *Phaseolus*: transient auxin-induced growth increase. *Physiologia Plantarum 130* (2007), 580–589.

[94] KERR, I. D., AND BENNETT, M. J. New insight into the biochemical mechanisms regulating auxin transport in plants. *Biochemical Journal 401*, 3 (2007), 613–622.

[95] KIM, Y. S., MIN, J. K., KIM, D., AND JUNG, J. A soluble auxin-binding protein, ABP57. Purification with anti-bovine serum albumin antibody and characterization of its mechanistic role in the auxin effect on plant plasma membrane H^+-ATPase. *Journal of Biological Chemistry 276*, 14 (2001), 10730–10736.

[96] Kitano, H. Systems biology: a brief overview. *Science 295*, 5560 (2002), 1662–1664.

[97] Kleine-Vehn, J., and Friml, J. Polar targeting and endocytic recycling in auxin-dependent plant development. *Annual Review of Cell and Developmental Biology 24* (2008), 447–473.

[98] Kleine-Vehn, J., Huang, F., Naramoto, S., Zhang, J., Michniewicz, M., Offringa, R., and Friml, J. PIN auxin efflux carrier polarity is regulated by PINOID kinase-mediated recruitment into GNOM-independent trafficking in *Arabidopsis*. *The Plant Cell 21*, 12 (2009), 3839–3849.

[99] Kögl, F. Über ein Phytohormon der Zellstreckung. Zur Chemie des kristallisierten Auxins. *Zeitschrift für Physiologische Chemie 216* (1933), 31.

[100] Korzeniewski, B., and Zoladz, J. A. Influence of rapid changes in cytosolic pH on oxidative phosphorylation in skeletal muscle: theoretical studies. *Biochemical Journal 365* (2002), 249–258.

[101] Kramer, E. M. PIN and AUX/LAX proteins: their role in auxin accumulation. *Trends in Plant Science 9*, 12 (2004), 578 – 582.

[102] Kramer, E. M. Computer models of auxin transport: a review and commentary. *Journal of Experimental Botany 59*, 1 (2008), 45–53.

[103] Kramer, E. M. Auxin-regulated cell polarity: an inside job? *Trends in Plant Science 14*, 5 (2009), 242–247.

[104] Kramer, E. M., and Bennett, M. J. Auxin transport: a field in flux. *Trends in Plant Science 11*, 8 (2006), 382–386.

[105] Křeček, P., Skupa, P., Libus, J., Naramoto, S., Tejos, R., Friml, J., and Zažímalová, E. The PIN-FORMED (PIN) protein family of auxin transporters. *Genome Biology 10*, 12 (2009), 249.

[106] Krupinski, P., and Jönsson, H. Modeling auxin-regulated development. *Cold Spring Harbour Perspectives in Biology 2*, 2 (2010), a001560.

[107] Kuhlemeier, C. Phyllotaxis. *Trends in Plant Science 12*, 4 (2007), 143–150.

[108] Kuhlemeier, C., and Reinhardt, D. Auxin and phyllotaxis. *Trends in Plant Science 6*, 5 (2001), 187–189.

[109] Kurkdjian, A., and Guern, J. Intracellular pH: Measurement and importance in cell activity. *Annual Review of Plant Physiology and Plant Molecular Biology 40* (1989), 271–303.

[110] Kutschera, U. The current status of the acid-growth hypothesis. *New Phytologist 4* (1994), 549–569.

[111] Kutschera, U. Acid growth and plant development. *Science 311*, 5763 (2006), 952–954.

[112] Laskowski, M., Grieneisen, V. A., Hofhuis, H., Hove, C. A. T., Hogeweg, P., Marée, A. F. M., and Scheres, B. Root system architecture from coupling cell shape to auxin transport. *PLoS Biology 6* (2008), e307.

[113] Lee, K., Kim, M.-I., Kwon, Y.-J., Kim, M., Kim, Y.-S., and Kim, D. Cloning and characterization of a gene encoding ABP57, a soluble auxin-binding protein. *Plant Biotechnology Reports 3* (2009), 293–299.

[114] Leyser, O. Auxin distribution and plant pattern formation: how many angels can dance on the point of PIN? *Cell 121*, 6 (2005), 819–822.

[115] Leyser, O. Dynamic integration of auxin transport and signalling. *Current Biology 16* (2006), R424–R433.

[116] LEYSER, O. The control of shoot branching: an example of plant information processing. *Plant, Cell and Environment 32*, 6 (2009), 694–703.

[117] LEYSER, O. The power of auxin in plants. *Plant Physiology 154*, 2 (2010), 501–505.

[118] LEYSER, O. Auxin, self-organisation, and the colonial nature of plants. *Current Biology 21*, 9 (2011), R331–R337.

[119] LI, J., YANG, H., PEER, W. A., RICHTER, G., BLAKESLEE, J., BANDYOPADHYAY, A., TITAPIWANTAKUN, B., UNDURRAGA, S., KHODAKOVSKAYA, M., RICHARDS, E. L., KRIZEK, B., MURPHY, A. S., GILROY, S., AND GAXIOLA, R. *Arabidopsis* H^+-PPase AVP1 regulates auxin-mediated organ development. *Science 310*, 5745 (2005), 121–125.

[120] LIM, P. O., LEE, I. C., KIM, J., KIM, H. J., RYU, J. S., WOO, H. R., AND NAM, H. G. Auxin response factor 2 (ARF2) plays a major role in regulating auxin-mediated leaf longevity. *Journal of Experimental Botany 61*, 5 (2010), 1419–1430.

[121] LIU, J., GRIESON, C. S., WEBB, A. A., AND HUSSEY, P. J. Modelling dynamic plant cells. *Current Opinion in Plant Biology 13* (2010), 1–6.

[122] LJUNG, K., BHALERAO, R. P., AND SANDBERG, G. Sites and homeostatic control of auxin biosynthesis in *Arabidopsis* during vegetative growth. *The Plant Journal 28*, 4 (2001), 465–474.

[123] LJUNG, K., HULL, A. K., KOWALCZYK, M., MARCHANT, A., CELENZA, J., COHEN, J. D., AND SANDBERG, G. Biosynthesis, conjugation, catabolism and homeostasis of indole-3-acetic acid in *Arabidopsis thaliana*. *Plant Molecular Biology 49* (2002), 249–272.

[124] LUO, C., CLARK, J. W., HEMING, T. A., AND BIDANI, A. A simplified model for V-ATPase H^+ extrusion. *IEEE Transactions of Nanobioscience 3*, 4 (2004), 257–264.

[125] LUO, C., CLARK, J. W., HEMING, T. A., AND BIDANI, A. A macrophage cell model for pH and volume regulation. *Jounral of Theoretical Biology 238*, 2 (2006), 449–463.

[126] MACDOWALL, F. D., AND SIROIS, J. C. Importance of time after excision and of pH on the kinetics of response of wheat coleoptile segments to added indoleacetic acid. *Plant Physiology 59*, 3 (1977), 405–410.

[127] MARCHANT, A., KARGUL, J., MAY, S. T., MULLER, P., DELBARRE, A., PERROT-RECHENMANN, C., AND BENNETT, M. J. AUX1 regulates root gravitropism in *Arabidopsis* by facilitating auxin uptake within root apical tissues. *The EMBO Journal 18*, 8 (1999), 2066–2073.

[128] MARTINOIA, E., MAESHIMA, M., AND NEUHAUS, H. E. Vacuolar transporters and their essential role in plant metabolism. *Journal of Experimental Botany 58*, 1 (2007), 83–102.

[129] MARTY, F. Plant vacuoles. *The Plant Cell 11* (1999), 587–599.

[130] MATHIEU, Y., GUERN, J., KURKDJIAN, A., MANIGAULT, P., MANIGAULT, J., ZIELINSKA, T., GILLET, B., BELOEIL, J.-C., AND LALLEMAND, J.-Y. Regulation of vacuolar pH of plant cells: I. isolation and properties of vacuoles suitable for P NMR studies. *Plant Physiology 89*, 1 (1989), 19–26.

[131] MATTSSON, J., SUNG, Z. R., AND BERLETH, T. Responses of plant vascular systems to auxin transport inhibition. *Development 126*, 13 (1999), 2979–2991.

[132] Maxfield, F. R., and McGraw, T. E. Endocytic recycling. *Nature Reviews Molecular Cell Biology 5*, 2 (2004), 121–132.

[133] McSteen, P., and Leyser, O. Shoot branching. *Annual Reviews of Plant Biology 56* (2005), 353–374.

[134] Merks, R. M. H., Van de Peer, Y., Inzé, D., and Beemster, G. T. S. Canalization without flux sensors: a traveling-wave hypothesis. *Trends in Plant Science 12*, 9 (2007), 384–390.

[135] Michard, E., Alves, F., and Feijó, J. A. The role of ion fluxes in polarized cell growth and morphogenesis: the pollen tube as an experimental paradigm. *International Journal of Developmental Biology 53*, 8-10 (2009), 1609–1622.

[136] Michniewicz, M., Zago, M. K., Abas, L., Weijers, D., Schweighofer, A., Meskiene, I., Heisler, M. G., Ohno, C., Zhang, J., Huang, F., Schwab, R., Weigel, D., Meyerowitz, E. M., Luschnig, C., Offringa, R., and Friml, J. Antagonistic regulation of PIN phosphorylation by PP2A and PINOID directs auxin flux. *Cell 130*, 6 (2007), 1044–1056.

[137] Middleton, A. M., King, J. R., Bennett, M. J., and Owen, M. R. Mathematical modelling of the Aux/IAA negative feedback loop. *Bulletin of Mathematical Biology 72*, 6 (2010), 1383–1407.

[138] Miedema, H., Staal, M., and Prins, H. B. pH-induced proton permeability changes of plasma membrane vesicles. *Journal of Membrane Biology 152*, 2 (1996), 159–167.

[139] Mimura, T., Shindo, C., Kato, M., Yokota, E., Sakano, K., Ashihara, H., and Shimmen, T. Regulation of cytoplasmic pH under extreme acid conditions in suspension cultured cells of *Catharanthus roseus*: a possible role of inorganic phosphate. *Plant Cell Physiology 41*, 4 (2000), 424–431.

[140] Mitchison, G. J. The dynamics of auxin transport. *Proceedings of the Royal Society B 209* (1980), 489–511.

[141] Mitchison, G. J. A model for vein formation in higher plants. *Proceedings of the Royal Society B 207* (1980), 79–109.

[142] Mitchison, G. J. The polar transport of auxin and vein patterns in plants. *Philosophical Transactions of the Royal Society B 295*, 1978 (1981), 461–471.

[143] Mjolsness, E. The growth and development of some recent plant models: A viewpoint. *Journal of Plant Growth Regulation 25*, 4 (2006), 270–277.

[144] Mockaitis, K., and Estelle, M. Auxin receptors and plant development: A new signaling paradigm. *Annual Review of Cell and Developmental Biology 24* (2008), 55–80.

[145] Moubayidin, L., Mambro, R. D., and Sabatini, S. Cytokinin-auxin crosstalk. *Trends in Plant Science 14*, 10 (2009), 557–562.

[146] Mravec, J., Kubeš, M., Bielach, A., Gaykova, V., Petrášek, J., Skůpa, P., Chand, S., Benková, E., Zažímalová, E., and Friml, J. Interaction of PIN and PGP transport mechanisms in auxin distribution-dependent development. *Development 135* (2008), 3345–3354.

[147] Mravec, J., Skůpa, P., Bailly, A., Hoyerová, K., Krecek, P., Bielach, A., Petrášek, J., Zhang, J., Gaykova, V., Stierhof, Y.-D., Dobrev, P. I., Schwarzerová, K., RolcÃŋk, J., Seifertová, D., Luschnig, C., Benková, E., Zažímalová, E., Geisler, M., and Friml, J. Subcellular homeostasis of phytohormone auxin is mediated by the ER-localized PIN5 transporter. *Nature 459*, 7250 (2009), 1136–1140.

[148] Muday, G. K. Auxins and tropisms. *Journal of Plant Growth Regulation 20* (2001), 226–243.

[149] Muday, G. K., and DeLong, A. Polar auxin transport: controlling where and how much. *Trends in Plant Science 6*, 11 (2001), 535 – 542.

[150] Mulkey, T. J., Kuzmanoff, K. M., and Evans, M. L. Promotion of growth and hydrogen ion efflux by auxin in roots of maize pretreated with ethylene biosynthesis inhibitors. *Plant Physiology 70*, 1 (1982), 186–188.

[151] Nakamura, A., Higuchi, K., Goda, H., Fujiwara, M. T., Sawa, S., Koshiba, T., Shimada, Y., and Yoshida, S. Brassinolide induces IAA5, IAA19, and DR5, a synthetic auxin response element in *Arabidopsis*, implying a cross talk point of brassinosteroid and auxin signaling. *Plant Physiology 133*, 4 (2003), 1843–1853.

[152] Newell, A. C., Shipman, P. D., and Sun, Z. Phyllotaxis: Cooperation and competition between mechanical and biochemical processes. *Journal of Theoretical Biology 251* (2008), 421–439.

[153] Norman, J. M. V., Breakfield, N. W., and Benfey, P. N. Intercellular communication during plant development. *The Plant Cell 23*, 3 (2011), 855–864.

[154] Norris, F. A., and Powell, G. L. The apparent permeability coefficient for proton flux through phosphatidylcholine vesicles is dependent on the direction of flux. *Biochimica et Biophysica Acta 1030*, 1 (1990), 165–171.

[155] Oja, V., Savchenko, G., Burkhard, J., and Heber, U. pH and buffer capacities of apoplastic and cytoplasmic cell compartments in leaves. *Planta 209*, 2 (Aug 1999), 239–249.

[156] Osborne, D. J. Control of leaf senescence by auxins. *Nature 183*, 4673 (1959), 1459–1460.

[157] Østergaard, L. Don't 'leaf' now. the making of a fruit. *Current Opinion in Plant Biology 12* (2008), 36–41.

[158] Overbeek, J. "laziness" in maize due to abnormal distribution of growth hormone. *The Journal of Heredity 29* (1938), 339–431.

[159] Paciorek, T., Zažímalová, E., Ruthardt, N., Petrášek, J., Stierhof, Y.-D., Kleine-Vehn, J., Morris, D. A., Emans, N., Jürgens, G., Geldner, N., and Friml, J. Auxin inhibits endocytosis and promotes its own efflux from cells. *Nature 435* (2005), 1251–1256.

[160] Pan, J., Fujioka, S., Peng, J., Chen, J., Li, G., and Chen, R. The E3 ubiquitin ligase SCFTIR1/AFB and membrane sterols play key roles in auxin regulation of endocytosis, recycling, and plasma membrane accumulation of the auxin efflux transporter PIN2 in *Arabidopsis thaliana*. *The Plant Cell 21*, 2 (2009), 568–580.

[161] Peer, W. A., Blakeslee, J. J., Yang, H., and Murphy, A. S. Seven things we think we know about auxin transport. *Molecular Plant 4*, 3 (2011), 487–504.

[162] Pérez-Gómez, J., and Moore, I. Plant endocytosis: It is clathrin after all. *Current Biology 17*, 6 (2007), R217–R219.

[163] Perrot-Rechenmann, C. Cellular responses to auxin: division versus expansion. *Cold Spring Harbor Perspectives in Biology 2*, 5 (2010), a001446.

[164] Peters, W. S., Lommel, C., and Felle, H. IAA breakdown and its effect on auxin-induced cell wall acidification in maize coleoptile segments. *Physiologia Plantarum 100* (1997), 415–422.

[165] Petersson, S. V., Johansson, A. I., Kowalczyk, M., Makoveychuk, A., Wang, J. Y., Moritz, T., Grebe, M., Benfey, P. N., Sandberg, G., and Ljung, K. An auxin gradient and maximum in the *Arabidopsis* root apex shown by high-resolution cell-specific analysis of IAA distribution and synthesis. *The Plant Cell 21*, 6 (2009), 1659–1668.

[166] Petrášsek, J., and Friml, J. Auxin transport routes in plant development. *Development 136*, 16 (Aug 2009), 2675–2688.

[167] Petrášsek, J., Mravec, J., Bouchard, R., Blakeslee, J. J., Abas, M., Seifertová, D., Wiśniewska, J., Tadele, Z., Kubeš, M., Čovanová, M., Dhonukshe, P., Skůpa, P., Benková, E., Perry, L., Křeček, P., Lee, O. R., Fink, G. R., Geisler, M., Murphy, A. S., Luschnig, C., Zažímalová, E., and Friml, J. PIN proteins perform a rate-limiting function in cellular auxin efflux. *Science 312* (2006), 914–918.

[168] Petzold, L. Automatic selection of methods for solving stiff and nonstiff systems of ordinary differential equations. *SIAM Journal on Scientific Computing 4* (1983), 136–148.

[169] Pitann, B., Kranz, T., and Mühling, K. H. The apoplastic pH and its significance in adaptation to salinity in maize (*Zea mays L.*): Comparison of fluorescence microscopy and pH-sensitive microelectrodes. *Plant Science 176* (2009), 497–504.

[170] Platt, J. R. Strong inference: Certain systematic methods of scientific thinking may produce much more rapid progress than others. *Science 146*, 3642 (1964), 347–353.

[171] Po, H. N., and Senozan, N. M. The Henderson-Hasselbalch equation: Its history and limitations. *Journal of Chemical Education 78* (2001), 1499–1503.

[172] Press, W. H., Teukolsky, S. A., Vetterling, W. T., and Flannery, B. P. *Numerical Recipes in C: The Art of Scientific Computing. Second Edition*. Cambridge University Press, 1992.

[173] Prusinkiewicz, P., Crawford, S., Smith, R. S., Ljung, K., Bennett, T., Ongaro, V., and Leyser, O. Control of bud activation by an auxin transport switch. *Proceedings of the National Academy of Sciences 106*, 41 (2009), 17431–17436.

[174] Raven, J. A. Transport of indoleacetic acid in plant cells in relation to pH and electrical potential gradients, and its significance for polar IAA transport. *New Phytologist 74*, 2 (1975), 163–172.

[175] Rayle, D. L., and Cleland, R. E. The acid growth theory of auxin-induced cell elongation is alive and well. *Plant Physiology 99*, 4 (1992), 1271–1274.

[176] Rayle, D. L., Evans, M. L., and Hertel, R. Action of auxin on cell elongation. *Proceedings of the National Academy of Sciences of the United States of America 65*, 1 (1970), 184–191.

[177] Reed, J. W. Roles and activities of Aux/IAA proteins in arabidopsis. *Trends in Plant Science 6*, 9 (2001), 420–425.

[178] Reinhardt, D. Regulation of phyllotaxis. *International Journal of Developmental Biology 49* (2005), 539–546.

[179] Reinhardt, D., Mandel, T., and Kuhlemeier, C. Auxin regulates the initiation and radial position of plant lateral organs. *Plant Cell 12*, 4 (2000), 507–518.

[180] Reinhardt, D., Pesce, E.-R., Stieger, P., Mandel, T., Baltensperger, K., Bennett, M., Traas, J., Friml, J., and Kuhlemeier, C. Regulation of phyllotaxis by polar auxin transport. *Nature 426* (2003), 255–260.

[181] Rober-Kleber, N., Albrechtová, J. T. P., Fleig, S., Huck, N., Michalke, W., Wagner, E., Speth, V., Neuhaus, G., and Fischer-Iglesias, C. Plasma membrane H^+-ATPase is involved in auxin-mediated cell elongation during wheat embryo development. *Plant Physiology 131*, 3 (2003), 1302–1312.

[182] Robert, H. S., and Offringa, R. Regulation of auxin transport polarity by AGC kinases. *Current Opinion in Plant Biology 11* (2008), 495–502.

[183] Roeder, A. H. K., Tarr, P. T., Tobin, C., Zhang, X., Chickarmane, V., Cunha, A., and Meyerowitz, E. M. Computational morphodynamics of plants: integrating development over space and time. *Nature Reviews Molecular Cell Biology 12*, 4 (2011), 265–273.

[184] Rolland-Lagan, A.-G. Vein patterning in growing leaves: axes and polarities. *Current Opinion in Genetics & Development 18*, 4 (2008), 348–353.

[185] Rolland-Lagan, A.-G., and Prusinkiewicz, P. Reviewing models of auxin canalization in the context of leaf vein pattern formation in *Arabidopsis*. *The Plant Journal 44*, 5 (2005), 854–865.

[186] Rubery, P. H., and Sheldrake, A. R. Carrier-mediated auxin transport. *Planta 118*, 2 (1974), 101–121.

[187] Rutschow, H. L., Baskin, T. I., and Kramer, E. M. Regulation of solute flux through plasmodesmata in the root meristem. *Plant Physiology 155*, 4 (2011), 1817–1826.

[188] Ruuth, S. J. Implicit-explicit methods for reaction-diffusion problems in pattern formation. *Journal of Mathematical Biology 34* (1995), 148–176.

[189] Sachs, T. The control of the patterned differentiation of vascular tissues. *Advances in Botanical Research 9* (1981), 151–262.

[190] Sahlin, P., Söderberg, B., and Jönsson, H. Regulated transport as a mechanism for pattern generation: Capabilities for phyllotaxis and beyond. *Journal of Theoretical Biology 258*, 1 (2009), 60–70.

[191] Salkowski, E. Über das Verhalten der Skatolcharbonsäure im Organismus. *Zeitschrift für Physiologische Chemie 9* (1885), 23–33.

[192] Sampedro, J., and Cosgrove, D. J. The expansin superfamily. *Genome Biology 6*, 12 (2005), 242.

[193] Sankar, M., Osmont, K. S., Rolcik, J., Gujas, B., Tarkowska, D., Strnad, M., Xenarios, I., and Hardtke, C. S. A qualitative continuous model of cellular auxin and brassinosteroid signaling and their crosstalk. *Bioinformatics 27* (2011), 1404–1412.

[194] Scarpella, E., Marcos, D., Friml, J., and Berleth, T. Control of leaf vascular patterning by polar auxin transport. *Genes and Development 20*, 8 (2006), 1015–1027.

[195] Scherer, G. F. E. AUXIN-BINDING-PROTEIN1, the second auxin receptor: what is the significance of a two-receptor concept in plant signal transduction? *Journal of Experimental Botany 62*, 10 (2011), 3339–3357.

[196] Scheres, B., and Xu, J. Polar auxin transport and patterning: grow with the flow. *Genes and Development 20* (2006), 922–926.

[197] Schmitt, B. M. The quantitation of buffering action i. A formal & general approach. *Theoretical Biology and Medical Modelling 2* (2005), 8.

[198] Schmitt, B. M. The quantitation of buffering action ii. Applications of the formal & general approach. *Theoretical Biology and Medical Modelling 2* (2005), 9.

[199] Schopfer, P. Determination of auxin-dependent pH changes in coleoptile cell walls by a null-point method. *Plant Physiology 103*, 2 (1993), 351–357.

[200] Shen, W. H., Petit, A., Guern, J., and Tempé, J. Hairy roots are more sensitive to auxin than normal roots. *Proceedings of the National Academy of Sciences of the United States of America 85*, 10 (1988), 3417–3421.

[201] Shimizu-Sato, S., Tanaka, M., and Mori, H. Auxin-cytokinin interactions in the control of shoot branching. *Plant Molecular Biology 69* (2009), 429–435.

[202] Shin, H., Shin, H.-S., Guo, Z., Blancaflor, E. B., Masson, P. H., and Chen, R. Complex regulation of arabidopsis AGR1/PIN2-mediated root gravitropic response and basipetal auxin transport by cantharidin-sensitive protein phosphatases. *The Plant Journal 42*, 2 (2005), 188–200.

[203] Shinkle, J. R., and Briggs, W. R. Auxin concentration/growth relationship for *Avena* coleoptile sections from seedlings grown in complete darkness. *Plant Physiology 74* (1984), 335–339.

[204] Shinohara, N., Sugiyama, M., and Fukuda, H. Higher extracellular pH suppresses tracheary element differentiation by affecting auxin uptake. *Planta 224* (2006), 394–404.

[205] Showalter, A. M. Structure and function of plant cell wall proteins. *The Plant Cell 5* (1993), 9–23.

[206] Skoog, F., and Thimann, K. V. Further experiments on the inhibition of the development of lateral buds by growth hormone. *Proceedings of the National Academy of Sciences of the United States of America 20* (1934), 480–485.

[207] Smith, R. S., Guyomarcń, S., Mandel, T., Reinhardt, D., Kuhlemeier, C., and Prusinkiewicz, P. A plausible model of phyllotaxis. *Proceedings of the National Academy of Sciences of the United States of America 103*, 5 (2006), 1301–1306.

[208] Smith, R. S., Kuhlemeier, C., and Prz. Inhibition fields for phyllotactic pattern formation: a simulation study. *Candadian Journal of Botany 84* (2006), 1635–1649.

[209] Somerville, C., Bauer, S., Brininstool, G., Facette, M., Hamann, T., Milne, J., Osborne, E., Paredez, A., Persson, S., Raab, T., Vorwerk, S., and Youngs, H. Toward a systems approach to understanding plant cell walls. *Science 306*, 5705 (2004), 2206–2211.

[210] Spijker, M. N. Stiffness in numerical initial-value problems. *Journal of Computational and Applied Mathematics 72* (1996), 393–406.

[211] Stoma, S., Lucas, M., Chopard, J., Schaedel, M., Traas, J., and Godin, C. Flux-based transport enhancement as a plausible unifying mechanism for auxin transport in meristem development. *PLoS Computational Biology 4*, 10 (2008), e1000207.

[212] Sukhov, V., and Vodeneev, V. A mathematical model of action potential in cells of vascular plants. *Journal of Membrane Biology 232*, 1-3 (2009), 59–67.

[213] Swarup, K., Benková, E., Swarup, R., Casimiro, I., Péret, B., Yang, Y., Parry, G., Nielsen, E., Smet, I. D., Vanneste, S., Levesque, M. P., Carrier, D., James, N., Calvo, V., Ljung, K., Kramer, E., Roberts, R., Graham, N., Marillonnet, S., Patel, K., Jones, J. D. G., Taylor, C. G., Schachtman, D. P., May, S., Sandberg, G., Benfey, P., Friml, J., Kerr, I., Beeckman, T., Laplaze, L., and Bennett, M. J. The auxin influx carrier LAX3 promotes lateral root emergence. *Nature Cell Biology 10*, 8 (2008), 946–954.

[214] SWARUP, R., AND BENNETT, M. Auxin transport: the fountain of life in plants? *Developmental Cell 5*, 6 (2003), 824–826.

[215] SWARUP, R., FRIML, J., MARCHANT, A., LJUNG, K., SANDBERG, G., PALME, K., AND BENNETT, M. Localization of the auxin permease AUX1 suggests two functionally distinct hormone transport pathways operate in the *Arabidopsis* root apex. *Genes and Development 15*, 20 (2001), 2648–2653.

[216] SWARUP, R., KRAMER, E. M., PERRY, P., KNOX, K., LEYSER, O., HASELOFF, J., BEEMSTER, G. T. S., BHALERAO, R., AND BENNETT, M. J. Root gravitropism requires lateral root cap and epidermal cells for transport and response to a mobile auxin signal. *Nature Cell Biology 7*, 11 (2005), 1057–1065.

[217] SWARUP, R., PERRY, P., HAGENBEEK, D., STRAETEN, D. V. D., BEEMSTER, G. T. S., SANDBERG, G., BHALERAO, R., LJUNG, K., AND BENNETT, M. J. Ethylene upregulates auxin biosynthesis in *Arabidopsis* seedlings to enhance inhibition of root cell elongation. *The Plant Cell 19*, 7 (2007), 2186–2196.

[218] SWIETACH, P., ZANIBONI, M., STEWART, A. K., ROSSINI, A., SPITZER, K. W., AND VAUGHAN-JONES, R. D. Modelling intracellular H^+ ion diffusion. *Progress in Biophysics & Molecular Biology 83*, 2 (2003), 69–100.

[219] TAIZ, L. The plant vacuole. *Journal of Experimental Biology 172* (1992), 113–122.

[220] TAIZ, L., AND ZEIGER, E. *Plant Physiology*, 4 ed. Sinauer, Sunderland, Massachusetts, 2006.

[221] TANAKA, H., DHONUKSHE, P., BREWER, P. B., AND FRIML, J. Spatiotemporal asymmetric auxin distribution: a means to coordinate plant development. *Cellular and Molecular Life Sciences 63* (2006), 2738?2754.

[222] TANAKA, H., KITAKURA, S., DE RYCKE, R., DE GROODT, R., AND FRIML, J. Fluorescence imaging-based screen identifies ARF GEF component of early endosomal trafficking. *Current Biology 19*, 5 (2009), 391–397.

[223] TANAKA, Y., AND URITANI, I. Effect of auxin and other hormones on the metabolic response to wounding in sweet potato roots. *Plant & Cell Physiology 20*, 8 (1979), 1557–1564.

[224] TAO, Y., FERRER, J.-L., LJUNG, K., POJER, F., HONG, F., LONG, J. A., LI, L., MORENO, J. E., BOWMAN, M. E., IVANS, L. J., CHENG, Y., LIM, J., ZHAO, Y., BALLARÉ, C. L., SANDBERG, G., NOE, J. P., AND CHORY, J. Rapid synthesis of auxin via a new tryptophan-dependent pathway is required for shade avoidance in plants. *Cell 133*, 1 (2008), 164–176.

[225] THIMANN, K. V., AND SKOOG, F. Studies on the growth hormone of plants: III. the inhibiting action of the growth substance on bud development. *Proceedings of the National Academy of Sciences of the United States of America 19*, 7 (1933), 714–716.

[226] TITAPIWATANAKUN, B., BLAKESLEE, J. J., BANDYOPADHYAY, A., YANG, H., MRAVEC, J., SAUER, M., CHENG, Y., ADAMEC, J., NAGASHIMA, A., GEISLER, M., SAKAI, T., FRIML, J., PEER, W. A., AND MURPHY, A. S. ABCB19/PGP19 stabilises PIN1 in membrane microdomains in *Arabidopsis*. *The Plant Journal 57*, 1 (2009), 27–44.

[227] TITAPIWATANAKUN, B., AND MURPHY, A. S. Post-transcriptional regulation of auxin transport proteins: cellular trafficking, protein phosphorylation, protein maturation, ubiquitination, and membrane composition. *Journal of Experimental Botany 60*, 4 (2009), 1093–1107.

[228] TIWARI, S. B., HAGEN, G., AND GUILFOYLE, T. J. Aux/IAA proteins contain a potent transcriptional repression domain. *The Plant Cell 16*, 2 (2004), 533–543.

[229] Trainotti, L., Tadiello, A., and Casadoro, G. The involvement of auxin in the ripening of climacteric fruits comes of age: the hormone plays a role of its own and has an intense interplay with ethylene in ripening peaches. *Journal of Experimental Botany 58*, 12 (2007), 3299–3308.

[230] Tromas, A., Paponov, I., and Perrot-Rechenmann, C. AUXIN BINDING PROTEIN 1: functional and evolutionary aspects. *Trends in Plant Science 15*, 8 (2010), 436–446.

[231] Turing, A. The chemical basis of morphogenesis. *Philosophical Transactions of the Royal Society of London. Series B, Biological Sciences 237*, 641 (1952), 37–72.

[232] Twycross, J., Band, L. R., Bennett, M. J., King, J. R., and Krasnogor, N. Stochastic and deterministic multiscale models for systems biology: an auxin-transport case study. *BMC Systems Biology 4* (2010), 34.

[233] Umehara, M., Hanada, A., Yoshida, S., Akiyama, K., Arite, T., Takeda-Kamiya, N., Magome, H., Kamiya, Y., Shirasu, K., Yoneyama, K., Kyozuka, J., and Yamaguchi, S. Inhibition of shoot branching by new terpenoid plant hormones. *Nature 455*, 7210 (2008), 195–200.

[234] Urbansky, E. T., and Schock, M. R. Understanding, deriving, and computing buffer capacity. *Journal of Chemical Education 77* (2000), 1640–1644.

[235] Vernoux, T., Besnard, F., and Traas, J. Auxin at the shoot apical meristem. *Cold Spring Harbour Perspectives in Biology 2*, 4 (2010), a001487.

[236] Veylder, L. D., Beeckman, T., and Inzé, D. The ins and outs of the plant cell cycle. *Nature Reviews Molecular Cell Biology 8*, 8 (2007), 655–665.

[237] Vieten, A., Vanneste, S., Wiśniewska, J., Benková, E., Benjamins, R., Beeckman, T., Luschnig, C., and Friml, J. Functional redundancy of PIN proteins is accompanied by auxin-dependent cross-regulation of PIN expression. *Development 132*, 20 (2005), 4521–4531.

[238] Vogel, G. Auxin begins to give up its secrets. *Science 313* (2006), 1230–1231.

[239] Wabnik, K., Kleine-Vehn, J., Balla, J., Sauer, M., Naramoto, S., Reinöhl, V., Merks, R. M. H., Govaerts, W., and Friml, J. Emergence of tissue polarization from synergy of intracellular and extracellular auxin signaling. *Molecular Systems Biology 6* (2010), 447.

[240] Wabnik, K., Kleine-Vehn, J., Govaerts, W., and Friml, J. Prototype cell-to-cell auxin transport mechanism by intracellular auxin compartmentalization. *Trends in Plant Science in print* (2011).

[241] Wagner, A. Distributed robustness versus redundancy as causes of mutational robustness. *Bioessays 27*, 2 (2005), 176–188.

[242] Weijers, D., and Friml, J. Snapshot: Auxin signaling and transport. *Cell 136*, 6 (2009), 1172, 1172.

[243] Weijers, D., and Jürgens, G. Auxin and embryo axis formation: the ends in sight? *Current Opinion in Plant Biology 8*, 1 (2005), 32–37.

[244] Went, F. W. Reflections and speculations. *Annual Review of Plant Physiology 25* (1974), 1–27.

[245] Whalley, M. A. *A genetic dissection of auxin signal transduction in* Arabidopsis thaliana. PhD thesis, University of York, 1999.

[246] Wilson, J. W., Palni, L. M. S., and Wilson, P. M. W. Auxin concentrations in nodes and internodes of *Impatiens sultani*. *Annals of Botany 83* (1999), 285–292.

[247] WISNIEWSKA, J., XU, J., SEIFERTOVÁ, D., BREWER, P. B., RUZICKA, K., BLILOU, I., ROUQUIÉ, D., BENKOVÁ, E., SCHERES, B., AND FRIML, J. Polar PIN localization directs auxin flow in plants. *Science 312*, 5775 (2006), 883.

[248] WOODWARD, A. W., AND BARTEL, B. Auxin: regulation, action, and interaction. *Annals of Botany 95*, 5 (2005), 707–735.

[249] YAMAMOTO, Y., KAMIYA, N., MORINAKA, Y., MATSUOKA, M., AND SAZUKA, T. Auxin biosynthesis by the YUCCA genes in rice. *Plant Physiology 143* (2007), 1362–1371.

[250] YAN, F., ZHU, Y., MÜLLER, C., ZÖRB, C., AND SCHUBERT, S. Adaptation of H^+-pumping and plasma membrane H^+-ATPase activity in proteoid roots of white lupin under phosphate deficiency. *Plant Physiology 129*, 1 (2002), 50–63.

[251] YANG, Y., HAMMES, U. Z., TAYLOR, C. G., SCHACHTMAN, D. P., AND NIELSEN, E. High-affinity auxin transport by the AUX1 influx carrier protein. *Current Biology 16* (2006), 1123–1127.

[252] YANG, Z., AND MIDMORE, D. J. Self-organisation at the whole-plant level: a modelling study. *Functional Plant Biology 36* (2009), 56–65.

[253] YIP, K.-P., AND KURTZ, I. Confocal fluorescence microscopy measurements of pH and calcium in living cells. *Methods in Cell Biology 70* (2002), 417–427.

[254] ZAŽÍMALOVÁ, E., KŘEČEK, P., SKŮPA, P., HOYEROVÁ, K., AND PETRÁŽEK, J. Polar transport of the plant hormone auxin - the role of PIN-FORMED (PIN) proteins. *Cellular and Molecular Life Sciences 64*, 13 (2007), 1621–1637.

[255] ZAŽÍMALOVÁ, E., MURPHY, A. S., YANG, H., HOYEROVÁ, K., AND HOSEK, P. Auxin transporters - why so many? *Cold Spring Harbor Perspectives in Biology 2*, 3 (2010), a001552.

[256] ZIMMERMANN, M. R., MAISCHAK, H., MITHÖFER, A., BOLAND, W., AND FELLE, H. H. System potentials, a novel electrical long-distance apoplastic signal in plants, induced by wounding. *Plant Physiology 149*, 3 (2009), 1593–1600.

[257] ZIMMERMANN, S., EHRHARD, T., PLESCH, G., AND MÜLLER-RÖBER, B. Ion channels in plant signaling. *Cellular and Molecular Life Sciences 55* (1999), 183–203.